FABRICATION OF COLORIMETRIC pH INDICATOR FILMS BY ELECTROSPINNING

A Thesis Submitted to
the Graduate School of Engineering and Sciences of
İzmir Institute of Technology
in Partial Fulfilment of the Requirements for Degree of

MASTER OF SCIENCE

in Food Engineering

by
Elif EREZ

July 2022
İZMİR

ACKNOWLEDGEMENTS

This research was funded by the Scientific Research Council of Izmir Institute of Technology (Project No: 2020IYTE0077). I would like to thank to Scientific Research Council of Izmir Institute of Technology for giving me this opportunity which helped me a lot throughout my research.

This research was a life-changing experience for me which reminds me of the classical novel 'Jonathan Livingston Seagull' written by Richard Bach. Thanks to this thesis, I realized that I can go beyond my own limits every time I am subjected to difficulties as long as I want to fight for it the book emphasizes the same taught.

I would like to thank my advisor Assist. Prof. Dr. Beste Bayramoğlu and my co-advisor Prof. Dr. Ahmet Emin Eroğlu for their valuable support, motivation, inspiration, encouragement, and guidance no matter how challenging the circumstances throughout my studies. I am so grateful for their belief in me and lead me the way.

I would like to thank to all faculty members of the food engineering department who let me use the equipment in their laboratory. I would like to thank to Prof. Dr. Ahmet Emin Eroğlu, Prof. Dr. Durmuş Özdemir, and Prof. Dr. Metin Tanoğlu who let me use the equipment in their laboratory and Integrated Research Center in the same way. This facilitated me to complete my studies.

I would also thank to M.Sc. student Ömer Özyurt, studying in Prof. Dr. Ahmet Emin Eroğlu's Laboratory C-307, who plays an important role in my research. I learned everything I know about electrospinning from him. He always tirelessly answer my endless questions. His contribution to this thesis was undeniable.

My special thanks go to my lovely friends Menşure Elvan and Merve Özer. I would not complete this research without their heart-warming support in every aspect. During my studies, they listened all problems I've been going through by understanding and tried to help both informationally and psychologically. I am so lucky and glad to have you both. You have been an inseparableable part of my life.

I would also thank my office mate Berkay Berk. He helped me a lot at the most important times and make my life easier in tough times even if I know him for a short time. I am so grateful for his benevolence. Besides him, I would also mention Çağrı Çavdaroğlu whom I assisted with almost every semester, he helped me whenever I ask for help. Merve Hadimioğlu Özdemir is another person I specifically thank, she listened

all my problems every time I need and gave me suggestions which helped me a lot especially mentally. I would like to thank all my colleagues under the roof of the food engineering department at IZTECH during this semester for their support.

When I am approaching to the end, my deepest gratitude goes to my family to the most important and special people in my life; my mother Hatice EREZ, my father Bayram EREZ, my sisters Ebru and Esra EREZ for their unconditional love and encouragement. They have always had faith in me. It was impossible to finish this thesis without their support. I devoted and dedicated this thesis to my beloved family.

ABSTRACT

FABRICATION OF COLORIMETRIC pH INDICATOR FILMS BY ELECTROSPINNING

The trend in the food packaging industry evolves towards innovative packaging materials as biosensors, which record the status of the product and can warn the consumer. The logic behind the colorimetric pH biosensor is that they provide the essential information about food visually by detecting change in pH. Anthocyanins are natural color pigments susceptible to pH change. Purple basil is rich in anthocyanins. In this study, ultrasound-assisted extraction was used for the extraction of dry purple basil. The processing conditions were optimized by response surface methodology (RSM) in terms of the total monomeric anthocyanin content and the increase in green intensity with pH. Electrospinning is a nanofiber fabrication operation used to encapsulate sensitive bioactive compounds for the production of intelligent sensing system. Polycaprolactone (PCL) films incorporating different purple basil extract (PBE) concentrations were fabricated by electrospinning procedure for the usage of colorimetric pH-indicator films as intelligent packaging. The most beadles and uniform nanofibrous mats were obtained when the spinning conditions were V=20 kV and Q=0.4 mL h^{-1} for 10% (w v^{-1}) PCL solutions containing 0.4% and 0.6% (w v^{-1}) PBE. The average fiber diameters in these films were 178.59±52.92 nm and 235.39±92.46 nm, respectively. The films gave promising results with regards to their use as colorimetric pH-indicator films. The time required to observe a visible color change (ΔE) in these films was only 4-5 s. The ΔE values between all successive pH's were higher than 2, which is detectable by an inexperienced observer.

Keywords: *Anthocyanin, Purple Basil, Ultrasound-Assisted Extraction, Response Surface Methodology (RSM), Electrospinning, Colorimetric pH-indicator Films*

ÖZET

ELEKTROEĞİRME YÖNTEMİ İLE KOLORİMETRİK pH GÖSTERGESİ FİLMLERİN İMALATI

Gıda paketleme endüstrisindeki eğilim, ürünün durumunu kaydeden ve tüketiciyi ürünün tüketiminin güvenli olup olmadığı konusunda uyarabilen gelişmiş özelliklere sahip biyosensörler olarak yenilikçi ambalaj malzemelerine doğru evrilmektedir. Kolorimetrik pH biyosensörünün ardındaki mantık, pH değişimini tespit ederek gıda hakkında temel bilgileri görsel olarak sağlamalarıdır. Antosiyaninler, pH değişimine duyarlı doğal renk pigmentleridir. Ortam pH'ının değişmesi ile renk değişimi gösterirler. Mor reyhan antosiyaninler açısından zengindir. Bu çalışmada kuru mor reyhan özütü eldesi için ultrason destekli ekstraksiyon kullanılmıştır. Ekstraksiyon koşulları toplam monomerik antosiyanin miktarı ve pH'a bağlı yeşil renk yoğunluğundaki artış bazında yüzey yanıt metodolojisi kullanılarak optimize edilmiştir. Elektro-eğirme yöntemi, akıllı paketleme malzemelerinin üretimi için gerekli hassas biyoaktif bileşikleri enkapsüle etmek için kullanılan nanofiber üretim işlemidir. Bu çalışmada elektro-eğirme yöntemi kullanılarak kolorimetrik pH göstergesi filmler olarak kullanılabilecek farklı konsantrasyonlarda mor reyhan özü içeren polikaprolakton filmler üretilmiştir. En eşit dağılımlı ve boncuksuz morfolojiye sahip filmler %0.4 ve %0.6 (w v^{-1}) mor reyhan özütü içeren % 10 (w v^{-1}) polikaprolakton çözeltileri ile voltajın 20 kV ve akış hızının 0.4 mL h^{-1} olduğu koşullarda elde edilmiştir. Bu filmlerde ortalama fiber çapı, sırasıyla 178.59±52.92 nm and 235.39±92.46 nm olarak tespit edilmiştir. Elde edilen filmlerin kolorimetrik pH göstergesi olarak kullanımları açısından umut vaat edici sonuçlar elde edilmiştir. Bu filmlerle görünür bir renk değişikliğini (ΔE) gözlemlemek için gereken süre sadece 4-5 saniye olarak gözlemlenmiştir. Tüm ardışık pH'lar arasındaki ΔE değerleri, deneyimsiz bir gözlemci tarafından tespit edilebilecek şekilde 2'den yüksek bulunmuştur.

Anahtar Kelimeler: *Antosiyanin, Mor Reyhan, Ultrason-Destekli Ekstraksiyon, Yüzey Yanıt Methodolojisi, Elektro-eğirme, Kolorimetrik pH göstergesi filmler*

TABLE OF CONTENTS

LIST OF ABBREVIATIONS

A	absorbance
A_0	starting absorbance
A_f	final absorbance
ABTS	2,2′-Azino-bis (3-ethylbenzothiazoline-6-sulfonic acid)
Ac	acetic acid
AAE	ascorbic acid equivalent
ANOVA	analysis of variance
B	regression coefficients
β_0	intercept
β_i, β_1, β_2 and β_3;	linear regression coefficients
β_{ii}, β_{11}, β_{22} and β_{33}	quadratic coefficients
β_{ij}, β_{12}, β_{13} and β_{23}	cross(interaction) coefficients
cP	centipoise
^oC	centigrade
C3-G	cyanidin-3-glucoside equivalent
d	distance
DCM	dichloromethane
DF	dilution factor
DMF	N,N-dimethylformamide
DPPH	2,2-diphenyl-1-picylhydrazine
dw	dry weight
ε	molar absorptivity
EB	elongation at break
etc	et cetera
fw	fresh weight
g	gram
GAE	gallic acid equivalent
h	hour
HCl	hydrochloric acid
kHz	kilohertz

kV	kilovolt
k	consistency coefficient
$K_2S_2O_5$	potassium metabisulfite
L	liter
M	molar
m	number of the tested variable
mg	milligram
min	minute
mL	milliliter
mM	millimolar
MW	molecular weight
n	flow behavior index
nm	nanometer
µm	micrometer
µL	microliter
PBE	purple basil extract
PCL	Polycaprolactone
PEO	Polyethylene oxide
PPC	percent polymeric color
PVA	polyvinyl alcohol
Q	flow rate
RSM	response surface methodology
R^2	coefficient of determination
SS	sum of squares
Std. dev.	standart deviation
TE	trolox equivalent
TMA	total monomeric anthocyanin content
TPC	total phenolic content
TS	tensile strength
Trolox	6-hydrox-2,5,7,8-tetramethylchroman-2-carboxylic acid
UAE	ultrasound-assisted extraction
UV-Vis	ultraviolet visible
YM	Young’s modulus
v	volume

vs.	versus
V	voltage
W	watt
w	weight
X_1	ethanol concentration
X_2	solvent-to-solid ratio
X_3	time
3D	three-dimensional
τ	shear stress
$\dot{\gamma}$	shear rate
η	apparent viscosity
λ	wavelenght

LIST OF FIGURES

Figure **Page**

Figure **Page**

Figure **Page**

LIST OF TABLES

Table **Page**

Table **Page**

Table **Page**

Table **Page**

Table **Page**

CHAPTER 1

INTRODUCTION

1.1. Intelligent Packaging

The demand for fresh food product is gaining popularity day by day among consumers with the improvement of living standards. According to World Health Organization (WHO), almost 1 in 10 people in the world suffer from consuming contaminated food every year. Food-borne diseases based on food safety issues are one of the major public health concerns for consumers. Packaging material for maintaining the product quality is another factor that is undeniably important for the conscious consumer showing interest in high awareness about food safety issues.

The traditional food packages are fundamentally designed to protect food materials from outer effects to maintain the quality of food during distribution and storage. They isolate the product from environmental conditions serving in different sizes, volumes and shapes. Packages contain the necessary information about food such as ingredients, cooking instructions and best-before or expire dates, which makes them essential for food supply chain (Luo, Zaitoon, and Lim 2022). Food packaging sector consists of important portion for the packaging industry and is open to the new developments mainly driven by conscious consumer needs and satisfaction. Conventional food packages are no longer meet the needs of majority due to concerns in food safety, environmental causes generating both food and package waste, changing lifestyle of consumers. Consumers recently demand intelligent packaging material not only protect the food but also monitor the condition of the packaged food providing dynamically information about food quality (Topuz and Uyar 2020).

The logic in intelligent packaging is that they show differentiable properties related to changes in food in real time. Time-temperature, gas and freshness indicators, which give qualitative and quantitative information about the food are three types of intelligent packaging commercially available (Sohail, Sun, and Zhu 2018). As one of the evolutions of the idea in intelligent packaging, colorimetric pH indicator films detect and sense the conditions to show differentiable color change with pH change to warn consumers. Change in pH is a crucial indication for the microbial spoilage and

physiological deterioration of food. Metabolites generated by the growth of microorganisms result gradually in pH variation. A simultaneous color change response of the packaging material would enable consumers to monitor the freshness and quality of food material. pH indicator packaging materials mainly consist of two parts, i.e., a color dye, which is sensitive to pH changes, and a solid structure supporting the dye (Singh, Gaikwad, and Lee 2018). Some examples of colorimetric intelligent packages are illustrated in Figure 1.1.

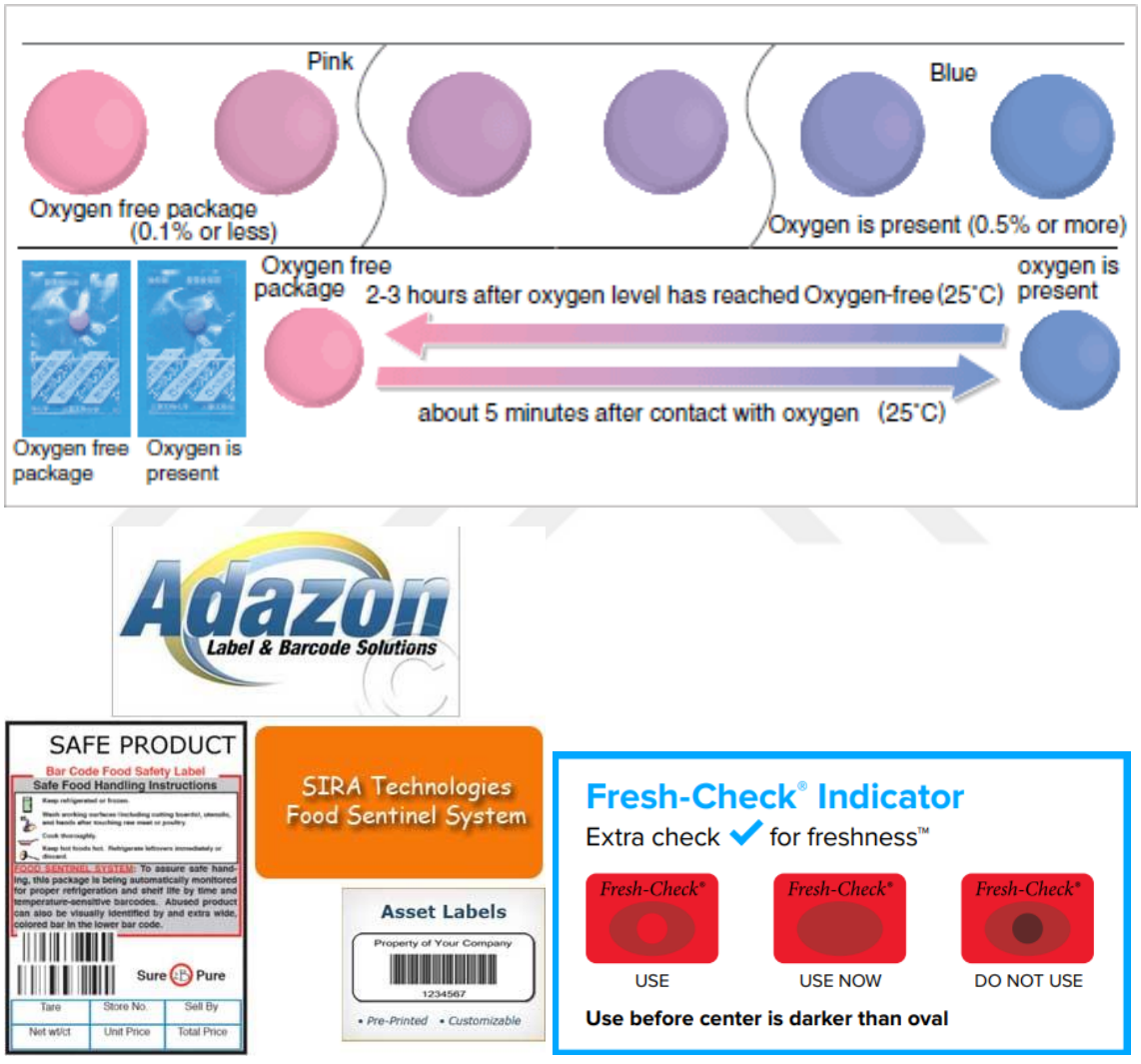

Figure 1.1 Some examples of intelligent packaging commercially available (*Ageless Eye, oxygen indicator: Products*, Technologies Food Sentinel System, *Zebra fresh check temperature indicator brochure V1*, nd)

Synthetic color dyes such as methyl red, bromocresol green, bromothymol blue have been used in pH-indicator film applications. However, synthetic color dyes create another

concern for high conscious consumers because of their toxic and carcinogenetic properties, which can cause serios problems to human health and environment. Their contact with food may cause migration and toxicity. As a consequence, trend of preference of natural color pigments over synthetic dyes is accelerated. Natural color pigments have various advantageous in terms of being generally recommended as safe (GRAS), environmentally friend, economically cheap and easily accessible (Roy and Rhim 2021).

1.2. Anthocyanin

The word of ‘anthocyanin’ is originated from the combination of Greek words *anthos* and *kianos*, meaning flower and blue, respectively (Sharif, Khoshnoudi-nia, and Mahdi 2020). Anthocyanins are phenolic compounds specifically belonging to the flavonoids plant kingdom. They naturally occur as glycosides and they are deposited within the vacuoles of cells in various tissues such as leaves, petals, bulbs, stems isolating from the interaction of enzymes and other delicate structures in the cytoplasm. Like the meaning implies, these molecules are known as natural color pigments, which are non-toxic and water-soluble dyes. They are responsible for attractive shiny colors such as pink, red, mauve, violet and blue. They are abundantly found in the flowers, fruits, vegetables, grains and tubers (Luiza Koop et al. 2022). Some anthocyanin sources are shown in Figure 1.2.

Figure 1.2 Flowers, fruits and vegetables that have high content of anthocyanins

Anthocyanidins are sugar free aglycones, which are the basic building blocks for the production of anthocyanins. When anthocyanidin bond one or more sugar moieties,

they form the anthocyanin molecule as a result of a wide range of glycosylation patterns. The number of anthocyanins identified in nature is more than 600 in plants (Tena, Martín, and Asuero 2020). Among these anthocyanins, glycoside forms of pelargonidin, cyanidin, peonidin, delphinidin, cyanidin, petunidin and malvidin are the six most abundant ones. The basic chemical structure of six different anthocyanidin found in nature can be seen from Figure 1.3. Among the anthocyanin pigments, cyanidin-4-glucoside is the major anthocyanin found in most of the plants with a distribution of 50 %. Delphinidin, pelargonidin, peonidin constitute the 12 %, whereas malvidin and petunidin constitute 7 % of the whole group (Khoo et al. 2017).

	R_1	R_2	λ_{max}*
Pelargonidin	-H	-H	503
Cyanidin	-OH	-H	517
Peonidin	$-OCH_3$	-H	517
Delphinidin	-OH	-OH	526
Petunidin	$-OCH_3$	-OH	526
Malvinidin	$-OCH_3$	$-OCH_3$	529

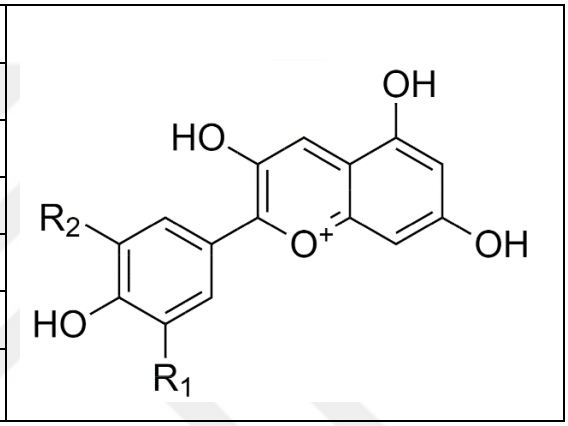

*The λ_{max} values shown are those of the corresponding 3-glucoside anthocyanins at pH 3.

Figure 1.3 Molecular structures of six most abundant anthocyanidins and the absorption maxima of anthocyanins

One of the significant characteristics of anthocyanins is their strong antioxidant activities. They have health benefits like anti-inflammatory and anti-carcinogenic properties fighting against free radicals for the prevention of some diseases such as cancer, diabetes and etc. There are several studies focused on the effect of anthocyanins in cancer treatment (Castañeda-Ovando et al. 2009; S. Silva et al. 2017).

Another important characteristic is unstable nature of these molecules to pH change. Anthocyanin pigments experience reversible structural transformations as a function of pH. Predominant structural forms of anthocyanins present at different pH values are given in Figure 1.4 (Becerril, 2021). Becerril et al. (2021) explains this mechanism at different pH values. Colored flavylium cation (oxonium form) predominates at pH 1. As pH increases, a proton is lost and a water molecule is gained.

As a result of this process, colorless carbinol pseudo-base (hemiketal form) is formed. Blue-colored quinonoidal base form predominates at neutral to alkaline pH range. In conclusion, anthocyanins are red in the form of flavylium cation at acidic environment whereas they are colorless in the form of carbinol pseudobase at less acidic environment. Increase in pH results in deprivation of color intensity. Anthocyanins are blue in the form of quinonoidal base at alkaline environments (Becerril et al., 2021; Castañeda-Ovando et al., 2009; Mistry & Kennedy, 2003).

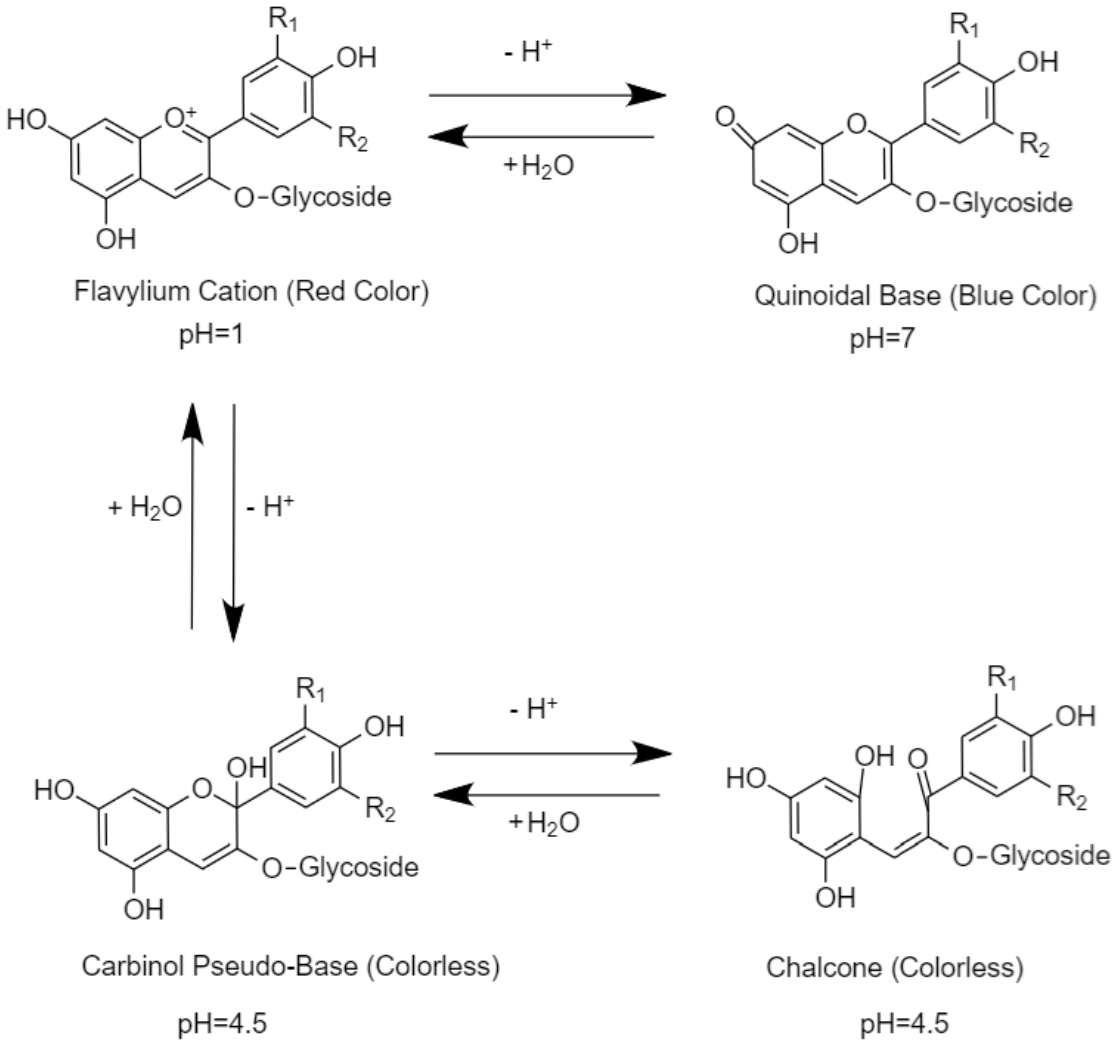

Figure 1.4 Structural forms of anthocyanins depending on the pH

The instability of anthocyanins has been considered as a disadvantage in the past, however the color changing property as a function of pH has been drawing attention recently for the application of colorimetric pH-indicator films. Anthocyanins as natural

dyeing agents have high potential as a food quality marker with no-toxicity to warn the consumer. Color change property with pH is visually important for consumers to understand the spoilage of food products.

1.3. Extraction

Extraction is a significant physical process used for separation of compounds from a solid matrix. Conventional methods are generally employed to extract bioactive compounds from natural food material. Conventional methods include maceration, Soxhlet extraction, cold compression etc. (Zia et al. 2020). Consumption of high amounts of hazardous organic solvents, long extraction times, and low extraction yield in conventional methods are not desirable in terms of time, economy and energy. Fyrthermore, sensitive compounds become more prone to destabilization with long extraction times. Therefore, food scientists find alternative extraction techniques to solve those problems. There is a globally new growing concept called ‘green extraction’. This concept can be a driving force to cross the challenges related with conventional methods enabling food industry to be more ecologic, economic and novel in order to protect both environment and health. Green extraction techniques alternative to conventional extraction methods can be listed as microwave assisted extraction, ultrasound assisted extraction, high pressure extraction, supercritical fluid extraction etc. These methods improve extraction yields with less solvent consumption and shorter process times, and are advantageous in terms of cost and energy efficiency, product or process safety, environmental issues (Chemat et al. 2017). Among these green extraction methods, ultrasound-assisted extraction (UAE) is a promising method for extraction of compounds. Recently, UAE has been reported to be used in the extraction of different compounds such as protein from Ganxet bean and cold pressed sesame cake (Lafarga et al. 2018; Yang et al. 2021), polysaccharides from purple glutinous rice bran (Oryza sativa L.) an cornus *officinalis* fruit (Surin et al. 2020; Tan, Cui, et al. 2022), oil from olives and pumpkin (Taticchi et al. 2019; Ferreira et al. 2019), phenolics from different food matrices like Thymus comosus Heuff. ex Griseb. et Schenk (wild thyme), pomegranate peel, aronia and grapes and flavonoids from Moringa oleifera Lam. Leaves and Moroccan Propolis (Babotă et al. 2022; Watrelot and Bouska 2022; Rashid et al. 2022)(L. M. P. Silva et al. 2022; Aboulghazi et al. 2022).

UAE has high potential as green extraction method for different compounds from food matrices. It requires minimal space, and is simple compared to other novel techonoliges. It requires less extraction solvent and time, and lower operating temperatures, which reduces operating costs and protect heat-sensitive bioactive molecules. UAE parameters should be optimized for different food materials in order to obtain desired molecule (Ojha et al. 2020).

1.3.1. Ultrasound-Assisted Extraction (UAE)

Ultrasounds are sound waves that can transfer through all phases of a susbtance by means of compression and expansion. Effect of energy produced by sound waves leads to cavitation. Bubbles are generated, they grow by absorbing energy until reaching an unstable structure, and then finally collapse. This collapse is known as cavitation in sonochemistry, which ensures complete extraction. Cavitation aids leaching from food matrix after breaking cell wall. The mass transfer is facilitated by UAE since it mechanically enables greater penetration of solvent into the solid matrix resulting in improved contact area between the solid and liquid phase (Pagano et al. 2021). UAE uses ultrasonic energy with frequencies between 20 kHz and 50 kHz for the creation of bubbles to improve extraction characteristics by shortening the time required for extraction. Schematic illustration is shown in Figure 1.5. This method is easy to operate, of low cost, time-efficient and causes low pollution to nature (Tan, Han, et al. 2022).

UAE has also been used for the extraction of anthocyanins. However, it is important to optimize the exraction conditions depending on the type of plant material used. Table 1.1 shows the current publications of the UAE for the optimal extraction conditions of anthocyanins from different natural matrices for the maximum yield. The parameters to be optimized are listed as, temperature, time, solvent type and concentration, solvent-to-solid ratio and ultrasound power, etc.

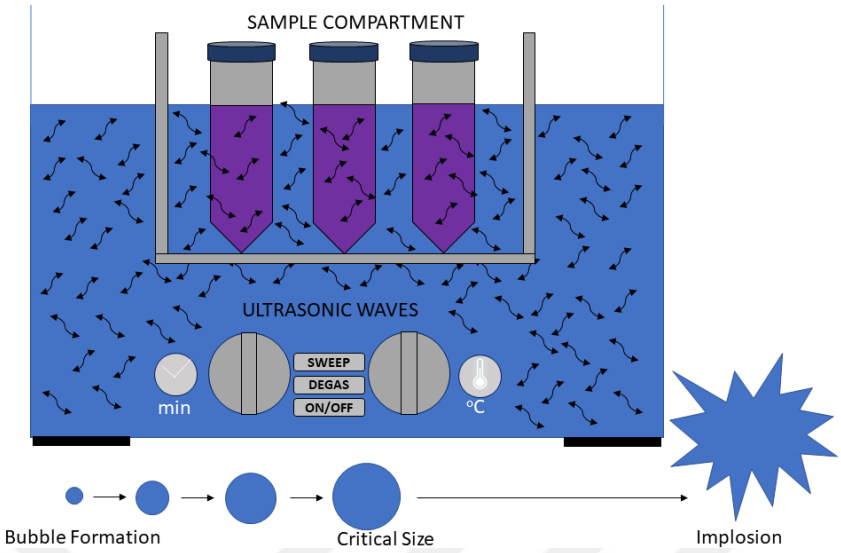

Figure 1.5 Schematic illustration of of UAE equipment, in which a fixed amount of crushed natural material is placed inside the sample compartment and cavitation mechanism in sonochemistry

Considering the law stating that "like dissolves like" in chemistry, the solvents generally used to extract anthocyanins are listed as methanol, ethanol, water, acetone, or their mixtures as anthocyanins has water soluble characteristics. Chemical structure of anthocyanin molecules is easily affected by pH. Anthocyanins are more stable under acidic environment, which increase the hydrolysis of the glycoside bond. This is why most of the extraction procedures require acidified conditions. pH of the environment determines the quality of extracted anthocyanin. Acidic solutions are added to extraction solvents to help stabilize the flavylium cation. The use of weak acids (e.g., formic acid, citric acid, or acetic acid) is recommended for this purpose since the use of strong concentrated acids may lead to destabilizing the anthocyanin molecule (S. Silva et al. 2017; Castañeda-Ovando et al. 2009). Hence, acidified solvent with two different acid types can be a good optimization base. Besides, organic solvents such as methanol are toxic and are not acceptable for foods. The use of ethanol has several advantages over the use of other solvents with extraction efficiency, lower toxicity and cost. Ethanol was selected as extraction solvent for experiments.

Table 1.1 Recent publications of the UAE for the optimal extraction conditions of anthocyanins from natural sources for the maximum yield

Food Matrix	**T (ºC**	**Solvent (v,v,%)**	**Solvent/ Solid (mL/g)**	**Time (min)**	**Yield**	**References**
Red araçá peel		90 % ethanol (0.1 % HCl) pH=1.5	10:1	90	121.85 ± 0.91 mg C3-G / 100 g of dw	(Meregalli et al. 2020)
Black Soybeans	20 ± 2	Distilled water	49.1:1	8.59	66.44 ± 4.84 mg C3-G / 100 g of dw	(Ryu and Koh 2019)
Reid Fruits	37	100% acidified ethanol	10:1	90	244 mg C3-G / 100 g of dw	(Blackhall et al. 2018)
Eggplant peel	55.1	54.4% methanol	10:1	44.85	2410.71 mg C3-G / kg dw	(Dranca and Oroian 2016)
Blueberry wine pomace	61	70% ethanol (0.01% HCl)	22:1	24	4.19 mg C3-G /g of dw	(He et al. 2016)
Purple Sweet Potato	60	90% ethanol (0.1% HCl)	10:1	60	214.92 ± 11.59 mg C3-G / 100 g of dw	(Cai et al. 2016)
Red Cabbage	40	42.39% ethanol	3:1	75	56.53 ± 2.25 mg C3-G / L extract	(Demirdöven, Özdoğan, and Erdoğan-Tokatlı 2015)
Purple majesty potato	33 ± 2	70% ethanol	40:1	5	364.3 ± 1.2 mg C3-G / kg fw	(Mane et al. 2015)
Haskap berries	35 ± 0.5	80% ethanol (0.5% formic acid	25:1	20	22.73mg C3-G /g of dw	(Celli, Ghanem, and Brooks 2015)
Jabuticaba peel	30 ± 1	46% ethanol solution acidified at pH 1	20:1	10	4.8 mg C3-G /g of dw	(Rodrigues et al. 2015)

C3-G: cyanidin-3-glucoside equivalent

Anthocyanin stability is also known to be greatly affected by the temperature. Roy and Rim recommend to use mild temperature in extraction process (Roy and Rhim 2021). In this study, 35 ^{o}C was chosen as extraction temperature to prevent anthocyanin degradation.

One of the most crucial parameter that should be optimized for the extraction is solvent-to-solid ratio, which depends on the anthocyanin content in the matrix and the solvents used. The optimization of solvent amount is important to minimize the use of solvent and also reduces the evoporation cost. Time is another factor that should be optimized. Some studies show that with increasing time, anthocyanin content increases while others show the opposite because of the degradation of anthocyanins. The effect of time may depend on the food material used in the study (Tena and Asuero 2022).

1.4. Purple Basil (*Ocimum basilicum L.*)

The genus Ocimum, Lamiaceae, collectively called basil, has long been acclaimed for its diversity in terms of morphological and chemical characteristics. Purple basil (*Ocimum basilicum L.*) is an ornamental plant with fragrant leaves cultivated in mostly Mediterranean countries. It is cultivaved by planting in fields in Arapgir region of Malatya province in Turkey. Purple basil is one of the most popular aromatic species commercially available as both form like fresh-produce and dried processed products used as a medicinal plant. Both forms of basil leaves are added to increase the aroma of food products such as salads, sauces, pasta and confectionary. Purple basil (*Ocimum basilicum L*) is demonstrated in Figure 1.6 (Díaz-Maroto et al. 2004).

Figure 1.6 Purple basil (*Ocimum basilicum L.*)

Phipppen and Simon (1998) isolated anthocyanins and characterized applying high-performance liquid chromatography, spectral data and plasma desorption mass spectrometry. Fourteen different anthocyanins were isolated, consisting of 11 cyanidin-based pigments and 3 peonidin-based pigments in their study. Results prove that purple basil *(Ocimum basilicum L.*) compared to other anthocyanin sources have intense purple color originating from abundant source of acylated and glycosylated anthocyanins providing unique source of stable color pigments for the food industry (Phippen and Simon 1998). The fact that purple basil is natural and do not cause residue problems increase its value for food industry to be used both as a colorant and as pH-indicator dye.

1.5. Electrospinning

Encapsulation technique has been known as entrapment of a bioactive component into the polymer matrix for protecting and delivering bioactive component to a targeted site. Several methods such as spray drying, freeze-drying, liposome preparation, emulsification, supercritical fluid have been used for the encapsulation. Spray drying is the most commonly used techniques among them. However, high working temperature may damage bioactive molecules and affect the stability and encapsulation efficiency (Wen et al. 2017).

The sensing power of biosensors can be improved by increasing the specific surface area of reacting molecule creating larger area of a sensing material in order to increase the ability to interact. Nanomaterials can be good candidates for increasing sensing ability (Mercante et al. 2017).

Electrospinning has recently attracted attentions as a promising nanotechnology-based nanofiber fabrication operation in order to encapsulate bioactive compound for the production of intelligent sensing system. Fundamental principle of this method relies on exposing a polymer solution into electrical forces, which result in elongated ultrathin fibers produced with submicron to nanoscale with high surface-to-volume ratio and porosity. The critical utility of electrospinning method is the absence of heat compared to conventional encapsulation methods, which facilitates the preservation of bioactive component. The parts of electrospinning equipment for laboratory scale are represented in Figure 1.7. The basic system is composed of 4 main parts including high-voltage power supply, syringe pump, syringe with a needle or spinneret and a collector. Horizontally

placing syringe filled with the polymer solution is connected to syringe pump, which allows precisely adjusting the flow rate of solution in a controllable manner. The polymer solution is being transferred from syringe to needle, the high voltage power supply is simultaneously operated in DC mode. Droplet of the polymer solution at the tip of the needle is deformed under the influence of high voltage. This leads to Taylor cone formation, which is explained as distort conical form at the tip of the needle when the electric forces equal to surface tension of the solution as voltage reaches the critical level. The electrically charged polymer jet is ejected from the Taylor cone. This jet is positioned through the grounded collector. As the jet gets closer to the collector, it is exposed to excess electric field which cause the bending of motion. As a result of this process, jet is elongated and the solvent is quickly evaporated. Finally, the electrospun polymer nanofibers as non-woven mat are randomly deposited on the rotating or stationary collector (Wongsasulak et al. 2010).

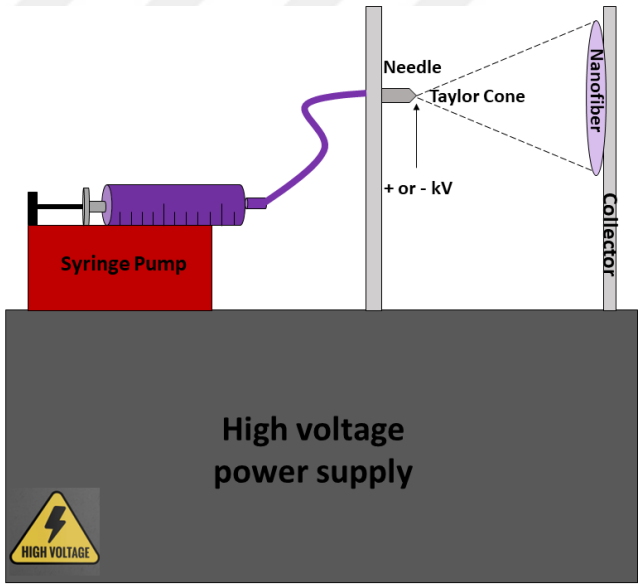

Figure 1.7 Laboratory Scale Electrospinning Setup

Nanofibers offer various attributes like larger surface area, controllable morphology with good mechanical properties. Electrospinning can be strongly affected by three main factors, which are solution conditions (type and concentration of polymer, viscosity, surface tension, solution conductivity), process conditions (voltage, flow rate, tip-to-collector distance) and environmental conditions (temperature and humidity). These factors may individually and synergestically influence the morphology of nanofiber (Leidy and Maria Ximena 2019; Li and Wang 2013).

1.6. Polymers

Different types of natural and synthetic polymers can be electrospun for different applications such as tissue engineering scaffolds, filtration membranes biomedical applications and intelligent film production. Natural polymers normally exhibit better biocompatibility compared to synthetic polymers. Despite their better biocompability, natural polymers are generally polyelectrolytes exposed to higher surface tension related with increasing charge carrying capacity of polymer jet during electrospinning process, which obstructs the nanofiber formation. Therefore, there are limited number of studies using natural polymers in the literature. Synthetic polymers are generally preferred for for the successfully production of nanofibers (Bhardwaj and Kundu 2010).

1.6.1. Polycaprolactone (PCL)

Polycaprolactone (PCL) is an aliphatic linear, semicrystalline, thermoplastic polyester, which has hydrophobic nature. Semicystallinity and hydrophobicity of PCL slows the degradation rate depending on its molecular weight, and it has good mechanical properties. It is biocompatible with low-cost, which has been approved for clinical use as slow release drug delivery material by Food and Drug Administration since 1980. These attributes make PCL a very good candidate for a variety of applications such as regenerative medicine and biomedical and tissue engineering. The chemical structure of PCL is presented in Figure 1.8 (Cipitria et al. 2011). The type of solvent should be taken into consideration when preparing the PCL solution, which directly affects the structure of nanofibers. PCL is reported to dissolve in chloform, toluene, benzene, carbon tetrachloride, cyclohexanone, tetrahydrofuran (THF), 2-nitropropane, dimethyl carbonate (DMC), and dioxane dichloromethane (DCM) (Azari et al. 2021).

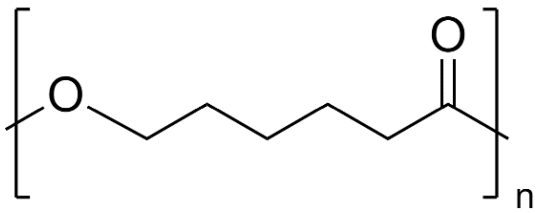

Figure 1.8 Chemical structure of PCL

1.7. Application of pH-indicator Films by Electrospinning in Food Science

The fabrication of electrospun nanofibers for intelligent packaging purposes is a new area in food industry. Overview of recent studies related with colorimetric indicator films fabricated by electrospinning method are summarized in Table 1.2.

Table 1.2 Overview of recent studies (2018-2022) related with colorimetric indicator films fabricated by electrospinning method

Polymer	Colorant	Food Material	Reference
PCL	*Clitoria ternatea Linn flower*	Shrimp	(Liu et al. 2022)
Chitosan/Gum Arabic	*Rosa damascena*	Chicken Fillets	(Shavisi and Shahbazi 2022)
PCL/PEO	*Hibiscus rosa sinensis*	Shrimp	(Jovanska, Chiu, Yeh, Chiang, et al. 2022)
Pullulan/Chitin	Curcumin /anthocyanin	*Plectorhynchus cinctus*	(Duan et al. 2021)
PCL/PEO	Curcumin/Spirulina microalga	-	(Terra et al., 2021)
Chitosan/PEO	Curcumin	Chicken Breast	(Yildiz, Sumnu, and Kahyaoglu 2021)
PLLA	Blueberry skin	*Mutton*	Sun et al., 2020
PVA	Red Cabbage (*Brassica oleracea L.*)	Fresh date fruit (Rutab)	(Maftoonazad and Ramaswamy 2019)
PCL/PEO	Acai *(Euterpe oleracea)*	-	(C. K. da Silva et al. 2019)
PLA/PEO	*Spirulina* microalga	-	(Moreira et al. 2018)
Zein	Red cabbage	-	(Prietto et al. 2018)

Most of the researches have evaluated the physical, structural, morphological, and color response properties of mats produced by electrospinning whereas other research groups have applied the electrospun intelligent nanofibers on real food systems and achieved valuable results on the efficiency of mats.

1.8. The Objectives of the Study

The trend in food packaging industry evolves towards innovative packaging materials as biosensors with improved attributes which record the status of the product and can warn the consumer whether the consumption of product is safe or not. The logic behind the colorimetric pH biosensor is that they provide the essential information visually about food by detecting change in pH. Change in pH is an indication for the microbial and physiological deterioration of food. Thus, pH-biosensors can be used to monitor the food quality. pH-biosensors contain a dye sensitive to pH changes and a structure that support the dye material. In general, the dyes that can be used for pH-biosensors are chemical and their contact with food may cause toxicity. Consumers recently have shown high awareness about food safety issues like usage of synthetically produced food colorants. Therefore, the trend in food industry is evolving towards use of dye stuff with natural-origin over synthetic-origin. Natural color pigments have various advantages such as being generally recommended as safe (GRAS), environmentally friend, economically preferrable and easily accessible.

Although anthocyanin content of purple basil is high, purple basil was not used as a pH indicator agent in film applications up to now. To date, the optimization of ultrasound assisted extraction of anthocyanins from dry purple basil by RSM has never been studied in literature. Therefore, the aim of the first part of this study is to determine the optimum process variables in terms of ethanol concentration, solvent-solid ratio and time for two different solvent systems (ethanol solution acidified with hydrochloric acid and acetic acid) for the extraction of dried purple basil that would give the maximum total monomeric anthocyanin content and maximum increase in green intensity with increasing pH. The main objective of the thesis is to fabricate electrospun polycaprolactone films incorporating purple basil extracts produced at optimum conditions, which can be integrated in food packaging materials to be potentially used as colorimetric pH-indicators.

CHAPTER 2

MATERIALS AND METHODS

2.1. Materials

Dried purple basil (*Ocimum basilicum. L.*) grown in the Arapgir region of Malatya (Turkey) was purchased from Arapgir Municipality. Acetic acid (glacial), hydrochloric acid (37%), sodium acetate, sodium carbonate, methanol, sodium chloride were purchased from Merck. Glycine, potassium chloride, potassium phosphate monobasic, potassium phosphate dibasic, sodium hydroxide, potassium metabisulfite, gallic acid, L-ascorbic acid, 2,2′-Azino-bis (3-ethylbenzothiazoline-6-sulfonic acid) diammonium salt,, potassium persulfate, 6-hydrox-2,5,7,8-tetramethylchroman-2-carboxylic acid)(trolox), sodium phosphate dibasic, chloroform and polycaprolactone (MW 80,000) were purchased from Sigma-Aldrich. Ethanol (99.9%) (Isolab), N,N-Dimethylformamid (Isolab), Folin-Ciocalteau reagent (Fluka) sodium phosphate monobasic (Riedelde Haen), 2,2-Diphenyl-1-picrylhydrazyl(DPPH) (Alfa-Aesar) were purchased from companies mentioned in brackets.

2.2. Methods

Firstly, the optimum extraction conditions of ultrasound-assisted extraction in dry purple basil were determined via Box Behnken design. After determination of optimum extraction condition of purple basil, colorimetric pH-indicator polycaprolactone films incorporating different concentrations of purple basil extracts obtained by the optimum extraction conditions were fabricated by electrospinnig procedure.

2.2.1. Experimental Design

Response Surface Methodology, specifically Box-Behnken design was applied to optimize the ultrasound-assisted extraction of dry purple basil (*Ocimum Basilicum L.*) in terms of total monomeric anthocyanin and the increase green intensity with increasing

pH. Minitab (2018, UK) was used to produce the experimental conditions via three-level Box-Behnken design that contains 15 experimental runs with 3 center points for two types of solvents (ethanol solution containing 0.1% acetic acid (Ac) and hydrochloric acid (HCl). The tested variables were X_1, X_2 and X_3 corresponding to ethanol concentration (v/v, %), solvent-to-solid ratio (mL/g), and time (min), respectively. X_1 ranged from 10 to 90 (v/v, %), X_2 ranged from 10 to 30 (mL/g), and X_3 ranged from 15 to 75 min. Uncoded forms of the variables were coded including three level -1,0 and +1 from lowest to highest value. Total monomeric anthocyanin content and the increase in green intensity with pH were aimed to maximized using experimental results. Experimental data were fitted to obtain a second-order polynomial equation to get the regression coeffients shown in Equation 2.1:

$$Y = \beta_0 + \sum_{i=1}^{m} \beta_i X_i + \sum_{i=1}^{m} \beta_{ii} X_i X_i + \sum_{i>j}^{m} \beta_{ij} X_i X_j \quad (2.1)$$

Y is the dependent response variable and is predictable using the independent process variables in the Equation 2.1, which are represented by X_1, X_2 and X_3, respectively. β_0 is the intercept, β_i as β_1, β_2 and β_3 represents linear regression coefficients, β_{ii} as β_{11}, β_{22} and β_{33} represents quadratic coefficients; β_{ij} as β_{12}, β_{13} and β_{23} represents cross (interaction) coefficients while m represents the number of tested variables, which is 3 in this study. Regression coefficients were analyzed with ANOVA with a 95% confidence interval. The model adequacy was checked by the coefficient of determination (R^2) values and comparison of predicted and experimental data. Three dimensional (3D) plots and the projection contour plots were generated using Equation 2.1 in MATLAB (R2022a) to interpret the correlation between dependent and independent variables in different levels. Optimized conditions were determined based on individual responses and multiple responses using desirability function. The validation experiments of the optimized conditions run with triplicate analysis of the optimized variables in the study. Error % was calculated for each case.

2.2.2. Ultrasound-Assisted Extraction (UAE) of Purple Basil

Ultrasound-assisted extraction of purple basil was performed using the method of Cai et al. (Cai et al., 2016) with a modification in an ultrasonic cleaning unit (Elmasonic S 40,Germany, 37 kHz, 140 W) with a volume of 4.25 L (internal dimensions: 240 mm x 137 mm x 150 mm). Extraction temperature was controlled in the ultrasonic bath at 30 ^{o}C ± 3 ^{o}C by circulating water at 30 ^{o}C from a water bath (Wisebath-WB22, South Korea) via a peristaltic pump (Shenchen-LabS3/UD15). The heated water (due to cavitation) was drained from the ultrasonic bath in order to keep temperature constant until the process was completed. Powdered purple basil was weighed into falcon tubes and required amounts of solvent was added. Falcon tube was immersed in ultrasonic bath. The extraction time was divided into three equal segments in order to increase mass transfer (yield) based on preliminary experiments. After first part of extraction was finished, the extract was separated (drained) from the solid part without any loss. This procedure was repeated two more times with required solvent and solvent-solid ratio without any loss. Drained extracts were filtrated using 0.45μm cellulose-acetate filters (Chromafil CA-45/25, Germany). Ethanol in the extracts was evaporated in a rotary evaporator (Heidolph Laborota-4000, Germany) under vacuum. Fresh extracts were analyzed for the total monomeric anthocyanin content and the increase in green intensity with pH. Unused extracts were stored at -18 ^{o}C for other analysis in refrigerator (Arcelik, Turkey).

2.2.3. Total Monomeric Anthocyanin Content (TMA)

Total monomeric anthocyanin content was determined by the pH-differential method (Mónica Giusti and Wrolstad 2005). 0.025 M potassium chloride (pH 1.0) and 0.4 M sodium acetate (pH 4.5) buffers were used. The purple basil extracts were diluted with appropriate dilution factor by pH 1.0 and pH 4.5 buffers. Dilutions were equilibrated for 15 min. The absorbance values were measured by ultraviolet-visible (UV-Vis) spectrophotometer (Perkin Elmer Lambda 25, USA) (in the range of 400-750 nm.) All measurements were done in triplicate. Total monomeric anthocyanin content of the extract was calculated with Equation 2.2.

$$\text{TMA (cyaniding-3-glucoside equivalents, mgL}^{-1}) = (A \times MW \times DF \times 1000) / (\varepsilon \times 1) \quad (2.2)$$

where $A = (A_{525\ nm} - A_{700\ nm})_{pH\ 1.0} - (A_{525\ nm} - A_{700\ nm})_{pH\ 4.5}$, MW is the molecular weight of cyanidin-3-glucoside (449.2 g mol^{-1}), DF is the dilution factor, and ε is the molar absorptivity of cyanidin-3-glucoside (26,900 L mol^{-1}). TMA was expressed as milligram of cyanidin-3-glucoside equivalent (mg C3-G) per 1 g of dried purple basil.

2.2.4. Increase in Green Intensity with pH by UV-Vis Spectroscopy

Color variations in purple basil extracts were analyzed to validate the use of the extract as a pH indicator dye from pH 1 to 10 based on the method by Choi et al. with some modifications (Choi et.al, 2017). Color of purple basil extracts was red when the environment was acidic. However, as the pH increased, the color of extracts turned pink, purple, blue and green color, respectively. This transformation is shown in Figure 2.1. UV-Vis spectra of extracts were taken using a UV-Vis spectrophotometer (Perkin Elmer Lambda 25, USA) in the range of 400-750 nm for pH range 1-10 (potassium chloride buffer, glycine-HCl buffer, sodium acetate buffer, sodium phosphate buffer, glycine-NaOH buffer). pH buffers were prepared using pH-meter (WTW-Inolab-ph7110, Germany). The maximum absorption peak moves to a higher wavelength with color change in extracts. The shift of the maximum absorption peak due to a pH increase is called a bathochromic shift, and commonly seen in anthocyanins. Generally, visible color absorbs light of wavelengths corresponding to its complementary color. Green color absorbs light of wavelengths 606–750 nm corresponding to its complementary color, red (Tewari & Vishnoi, 2009). In contrast, red color is a result of the compound absorbing the light of its complementary color, green. The maximum absorption peak was acquired at 525 nm at pH 1, and moved to higher wavelengths as pH increased. At pH 10 the absorption peak was obtained at 606 nm. In the method of Mónica Giusti & Wrolstad (2005), it was mentioned that samples to be measured should be clear as much as possible with no haze or sediments; however, some colloidal materials may be suspended in the sample, causing scattering of light and a cloudy appearance (haze). This scattering of light needs to be accounted for by reading at a wavelength (700 nm) where no absorbance of the sample occurs. Therefore, the increase in green intensity, which can be expressed as the difference in the absorbance ratios $((A_{606\ nm}-A_{700\ nm}) / (A_{525\ nm}-A_{700\ nm}))$ obtained when going from low to high pH, could be indication for the increase in green color compared

to red color. The curve for pH 1 to 10 showed exponential increase. Increase in green intensity in going from pH 1 to pH 10 was calculated using Equation 2.3.

Increase in green intensity $= (A_{606\ nm}-A_{700\ nm})/(A_{525\ nm}-A_{700\ nm})_{@pH\ 10} - (A_{606\ nm}-A_{700\ nm})/(A_{525\ nm}-A_{700\ nm})_{@pH\ 1}$ (2.3)

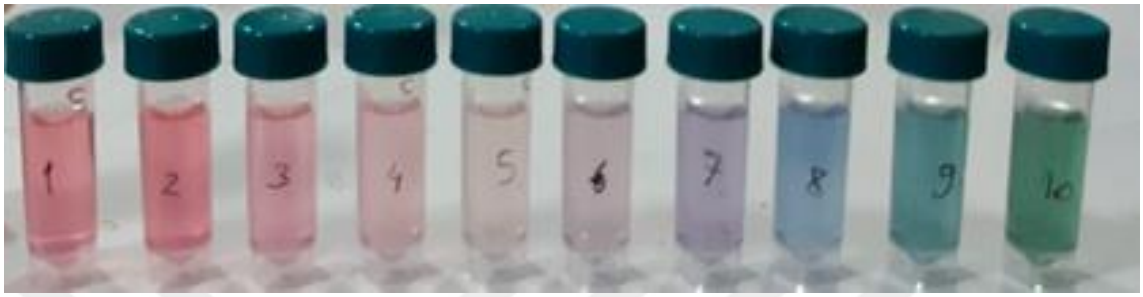

Figure 2.1 Color transformation of purple basil extract via pH alterations

2.2.5. Percent Polymeric Color (PPC)

Percent polymeric color (PPC) was determined for the purple basil extract obtained with optimized conditions by the method of Mónica Giusti & Wrolstad (2005). PPC gives idea about the proportion of polymeric anthocyanin compounds with more stable structure by forming complexes in comparison to the monomeric anthocyanins. Potassium metabisulfite ($K_2S_2O_5$) solution and 0.025 M potassium chloride buffer, pH 1.0 were used. The samples were allowed to equilibrate for 15 minutes. Absorbance values were measured at 420, 525 and 700 nm with a UV-Vis spectrophotometer (Perkin Elmer Lambda 25, USA). All measurements were done in triplicate. PPC (Equation 2.6) was calculated as the polymeric color (Equation 2.5) divided by color density (Equation 2.4), the ratio of polymerized anthocyanins in total.

$$\text{Color density} = [(A_{420\ nm} - A_{700\ nm}) + (A_{\mu vis\text{-}max} - A_{700\ nm})] \times DF \text{ (control sample)} \quad (2.4)$$

$$\text{Polymeric Color} = [(A_{420\ nm} - A_{700\ nm}) - (A_{\mu vis\text{-}max} - A_{700\ nm})] \times DF \text{ (bleached sample)} \quad (2.5)$$

$$\text{Percent Polymeric Color} = (\text{Polymeric Color}/\text{Color Density}) \times 100 \quad (2.6)$$

where DF is a dilution factor

2.2.6. Total Phenolic Content (TPC)

Total phenolic content was determined for the purple basil extract obtained at optimized conditions using the Folin-Ciocalteau's method (Singleton, 1965). This method was based on a reduction of Folin Ciocalteau reagent with phenolic compounds in basic conditions developing blue color enabling spectrophotometrically to measure total phenolic content. 0.5 mL diluted sample extract was transferred in tubes. Then, 2.5 mL diluted Folin-Ciocalteau reagent (1/10 aqueous dilution) was added. After 5 min, 2 mL sodium carbonate (Na_2CO_3) (7.5% w/v) was added and vortexed (Labnet-VX100). The tubes were kept in dark at room temperature for 2 h before the absorbance at 765 nm was measured against a blank UV-Vis spectrophotometer (Perkin Elmer Lambda 25, USA). Blank was prepared the same way as the sample except water was used instead. All measurements were done in triplicate. Gallic acid standarts ranging between 0-500 mg/L (0, 50, 100, 200, 250, 300, 400, 500 mg/L) were used to construct the gallic acid standart curve shown in Figure B.1 in Appendix B. TPC was expressed as gallic acid equivalent (GAE) in mg /g dry purple basil.

2.2.7. DPPH Radical Scavenging Activity

Scavenging activity of DPPH radical of purple basil extract was determined by the method of Benvenuti et al. (2006) for the optimized conditions. Different volumes of purple basil extracts (10-20-30-40-50 μL) were mixed with methanolic DPPH in a total volume of 3 mL. The mixtures were incubated at room temperature for 30 minutes in the dark. The absorbance was measured at 517 nm against a blank using UV-Vis spectrophotometer. % inhibition values were calculated using Equation 2.7.

$$\% \text{ Inhibition} = [(A_{DPPH} - A_{EXT})/A_{DPPH} \times 100] \quad (2.7)$$

A_{DPPH} represents the absorbance value of the blank whereas A_{EXT} represents the absorbance value of the sample to be tested. EC_{50} (concentrations that which 50 % radical scavenging occurs) values were determined from percent inhibition vs. microliter extract graphs by recording the percent decrease in absorbance for each different extract volume. All measurements were done in triplicate. 2.5 mM ascorbic acid solution was prepared as

standart stock solution and 5 different concentrations (0.5 mM, 1mM, 1.5 mM, 2 mM, 2.5 mM) were prepared by diluting the solution. Ascorbic acid standart curve was shown in Figure B.2 in Appendix B. DPPH radical activity results were expressed as mg ascorbic acid equivalent (AEE) in mg / g dry purple basil.

2.2.8. ABTS/TEAC Antioxidant Activity

ABTS antioxidant activty of purple basil extract was determined according to the method of Re et al. (1999). 7 mM ABTS solution containing 2.45 mM potassium persulfate was prepared. It was kept for 12-16 hours at room temperature for radical formation. Dilution was made with PBS so that the absorbance at 734 nm was 0.7±0.02. The initial absorbance values were recorded without any addition of extract. After adding the extracts, it was allowed to react at room temperature. At the end of 6 minutes, absorbance values at 734 nm were recorded against the blank with a UV-Vis spectrophotometer (Perkin Elmer Lambda 25, USA). % inhibition values were calculated with Equation 2.8.

$$\% \text{ Inhibition} = [(A_{ABTS\text{-}t=0} - A_{EXTt=6\ min})/A_{ABTS\text{-}t=0}\ x100] \quad (2.8)$$

$A_{ABTS\ -t=0}$ represents the absorbance value recorded before adding the extract, whereas $A_{EXTt=6\ min}$ represents the absorbance value recorded after 6 min of reaction with the extract. Percent inhibition vs. microliter extract graphs were plotted by recording the percent decrease in absorbance for each extract volume. All measurements were done in triplicate. 2.5 mM Trolox solution was prepared as standart stock solution with 5 different concentrations (0.5 mM, 1mM, 1.5 mM, 2 mM, 2.5 mM). Trolox standart curve was shown in Figure B.3 in Appendix B. ABTS results were expressed as mg Trolox equivalent (TE) in mg / g dry purple basil.

2.2.9. Preparation of PBE for Electrospinning

Dried purple basil was extracted by UAE at optimized conditions with 55.25% ethanol containing 0.1% acetic acid, 30 mL/g solvent/solid ratio and 39.24 min at 35 ^{o}C± 3 ^{o}C. Extracts were filtered using 0.45μm cellulose-acetate filters (Chromafil CA-45/25, Germany). Solvent in extract was evaporated in a rotary evaporator (Heidolph Laborota-

4000, Germany) under vacuum. After evaporation, purple basil extracts were lyophilized with a freeze-drier (Labconco, USA).

2.2.10. Preparation of Electrospinning Polymer Solutions

10% PCL (w v^{-1}) was prepared by dissolving in DMF:chloroform (v v^{-1}) 1:1 without extract as control with a magnetic stirrer (Ika-Werke, Germany) for 24 h (overnight) to make homogenous solution. Lyophilized purple basil extract was dissolved in DMF until no particulate matter was visible. Chloroform was added such that the DMF/chloroform (v v^{-1}) ratio of the solvent was 1:1. 10% PCL (w v^{-1}) was mixed with purple basil solution at 3 different concentrations (0.2%, 0.4% and 0.6% w v^{-1}) with a magnetic stirrer for 24 h (overnight) in order to study the effect of the concentration of PBE on nanofiber morphology, color response, mechanical properties etc.

2.2.11. Rheological Behavior of Polymer Solutions

Rheological properties of polymer solutions were measured by using a controlled AR 2000ex Rheometer (TA Instruments, USA) with a 20 mm parallel plate geometry whose gap is 1000 μm. Temperature was set to 25 ^{o}C ± 1. Shear rate was varied from 1 to100 s^{-1}. The shear stress (τ) and shear rate ($\dot{\gamma}$) data were obtained. Measurements were done in triplicate. The shear stress (τ) and shear rate ($\dot{\gamma}$) data collected from rheological experiments were fitted well to the power-law model (Equation 2.9),

$$\tau = k (\dot{\gamma})^{n} \quad (2.9)$$

where τ is the shear stress (Pa), $\dot{\gamma}$ is the shear rate (s^{-1}), k is the consistency coefficient ($Pa.s^{n}$) and n is the flow behavior index.

2.2.12. Electrospinning Procedure

The electrospinning process was applied by Nanospinner basic system (Inovenso, Turkey). Polycaprolactone solutions with and without PBE were placed in a 20 ml syringe having 22 mm inner diameter fitted with a metallic needle of 0.2 mm of inner diameter.

Syringe was horizontally placed. Square shaped stationary collector was covered with aluminum foil (Spon). Electrode was connected to the collector. The distance between the tip of the syringe and collector was 26 cm. Flow rate was adjusted with a syringe pump (NE-300, USA). Figure 2.2 shows the nanospinner basic system setup in laboratory. 10% PCL (w v^{-1}) solutions with different PBE concentrations (0%, 0.2%, 0.4%, 0.6% w v^{-1}) were electrospun. Electrospun films were fabricated with 20 kV and 25 kV with flow rates 0.4 ml h^{-1} and 0.5 mL h^{-1} in 3.5 h.

Figure 2.2 Nanospinner basic electrospinning unit (NanoSpinner 1 Electrospinning Equipment - Inovenso Inc. - PDF Catalogs | Technical Documentation | Brochure)

2.2.13. Morphology of Nanofibers

Morphological properties of nanofibers were determined with SEM (Quanta 250 FEG, USA). Nanofibroud films were stuck on metal stubs, and the surface images were taken. Diameters of randomly selected 60 fibers were measured with Image J software.

2.2.14. Film Thickness

The thickness of electrospun films were measured from five different locations chosen randomly with a digital micrometer (Chronos, UK).

2.2.15. Color Parameters

Electrospun films were cut in squares (1.5 cm x 1.5 cm) and immersed in buffer solutions ranging from pH 1 to 10. The films containing 0.2% (w v^{-1}) PBE were immersed in 5 min whereas the films containing 0.4 and 0.6% PBE (w v^{-1}) were immersed in 5 s. Afterwards, the color parameters (L*, a*, b*) were measured by a colorimeter (CR 400 Konica Minolta, Japan). The measured L*, a* and b* values were used to calculate the change in color (ΔE) according to Equation 2.10

$$\Delta E=[(\Delta L^*)^2+(\Delta a^*)^2+(\Delta b^*)^2]^{0.5} \quad (2.10)$$

where $\Delta L^*=L-L_0$, $\Delta a^*=a-a_0$, and $\Delta b^*= b-b_0$. Photographs of indicator membranes at different pH values were taken by Samsung Galaxy A21 smartphone (Korean) in pro mode (ISO=800 and WB)=10000K) under the same lighting conditions. Photoshop, version 6.0 (Adobe Systems Inc., San Jose, CA, USA) was used to analyze the photographs.

2.2.16. Mechanical Properties of Films

A texture analyzer TA-XT2 (Stable Microsystems,Godalming, UK) was used to determine the tensile strenght (TS), elongation at break (EB) and Young's Modulus (YM) of electrospun films according to the American Society for Testing and Materials (2002). The film strips (80 mm x10 mm) were initially fixed at an initial grip distance of 50 mm. The test speed was 50 mm/min, and the load was 5 kg. Each sample was measured with eight replicates.

2.2.17. Contact Angle Measurements

The hydrophilicty and hydrophobicity of films were determined by the contact angle analysis using Attention Theta Tensiometer. 5 microliter of distilled water was placed on the surface of the films. From the Surftens 3.0 software, three measurements of each image were applied using three measurement points arranged around the drop.

2.2.18. Fourier Transform Infrared (FT-IR) spectroscopy

FT-IR spectrophotometer (UATR-2 Perkin Elmer, UK) was used to analyze the characteristic intramolecular chemical bonds in PBE powder and 10% PCL % (w v^{-1}) electrospun mats with different PBE concentrations. Scans were performed in the 500-4000 cm^{-1} at 0.4 resolution.

2.2.19. Statistical Analysis

Statistical analysis was done by using ANOVA and Tukey's pairwise comparison test using Minitab (2018, UK) statistical software. The differences were considered significant for $p \leq 0.05$.

CHAPTER 3

RESULTS AND DISCUSSION

3.1. Optimization of UAE Conditions of Dry Purple Basil via RSM

Box-Behnken design was used to optimize the total monomeric anthocyanin content in purple basil extracts obtained by ultrasound-assisted extraction and the increase in the green intensity of the extracts due to pH change. Ethanol concentration (%), solvent/solid ratio (mL/g) and time (min) were three independent variables for the design. Two different solvent systems (acidified with HCl or Ac) were used. The design included 15 experimental runs with a total of 3 center points for each solvent system and consisted of three levels (-1, 0, 1). Tables 3.1 and 3.2 contain the experimental and predicted results extracted by ethanol acidified with 0.1% Ac and 0.1% HCl, respectively.

Table 3.1 Box-Behnken design and experimental results on total monomeric anthocyanin content and increase in green intensity of purple basil extracts extracted with Ac

Run	**Factors**			**Experimental (Predicted*) Results**	
	Ethanol Concentration(%)	**Solvent/Solid (mL/g)**	**Time (min)**	**TMA(mg C3-G/g dw)****	**Increase in Green Intensity**
1	90(1)	20(0)	15(-1)	0.26(-0.21)	2.37(2.31)
2	50(0)	20(0)	45(0)	4.54(4.44)	2.09(2.12)
3	90(1)	10(-1)	45(0)	0.25(0.20)	1.64(1.78)
4	50(0)	10(-1)	15(-1)	2.37(2.89)	1.98(1.90)
5	10(-1)	10(-1)	45(0)	0.73(0.59)	0.62(0.79)
6	50(0)	30(+1)	15(-1)	3.61(3.95)	2.17(2.40)
7	50(0)	30(+1)	75(+1)	5,47(4.95)	1.88(1.96)
8	10(-1)	20(0)	15(-1)	0.97(0.58)	0.87(0.78)
9	10(-1)	30(+1)	45(0)	2.13(2.19)	0.83(0.69)
10	50(0)	10(-1)	75(+1)	4.41(4.08)	2.26(2.04)

(cont. on next page)

Table 3.1 (cont.)

11	90(+1)	30(+1)	45(0)	0.40(0.54)	2.47(2.31)
12	90(+1)	20(0)	75(+1)	0.27(0.66)	1.86(1.94)
13	50(0)	20(0)	45(0)	4.58(4.44)	2.25(2.12)
14	50(0)	20(0)	45(0)	4.21(4.44)	2.01(2.12)
15	10(-1)	20(0)	75(+1)	1.43(1.90)	0.79(0.86)

*Given in the parantheses are the predicted values by the model.

**mg C3-G/g dw as milligram cyanidin-3-glucoside equivalent per gram dry weight

Table 3.2 Box-Behnken design and experimental results on total monomeric anthocyanin content and increase in green intensity of purple basil extracts extracted with HCl

Run	**Factors**			**Experimental (Predicted*) Results**	
	Ethanol Concentration(%)	**Solvent/Solid (mL/g)**	**Time (min)**	**TMA(mg C3-G/g dw)****	**Increase in Green Intensity**
1	10(-1)	10(-1)	45(0)	0.78(1.10)	0.57(0.78)
2	50(0)	30(+1)	75(+1)	4.34(4.41)	2.47(2.60)
3	50(0)	20(0)	45(0)	4.11(4.66)	2.30(2.17)
4	90(+1)	20(0)	75(+1)	0.91(1.16)	2.90(2.99)
5	90(+1)	30(+1)	45(0)	0.33(0.01)	3.37(3.15)
6	90(+1)	20(0)	15(-1)	0.17(-0.06)	2.91(2.98)
7	50(0)	30(+1)	15(-1)	0.16(0.46)	2.51(2.57)
8	90(+1)	10(-1)	45(0)	2.74(3.28)	2.44(2.58)
9	10(-1)	20(0)	75(+1)	2.59(2.82)	1.13(1.05)
10	50(0)	10(-1)	15(-1)	2.69(2.62)	2.29(2.16)
11	50(0)	20(0)	45(0)	4.18(4.66)	2.02(2.17)
12	50(0)	20(0)	45(0)	5.68(4.66)	2.18(2.17)
13	50(0)	10(-1)	75(+1)	4.58(4.03)	2.30(2.16)
14	10(-1)	30(+1)	45(0)	1.74(1.49)	1.12(1.04)
15	10(-1)	20(0)	15(-1)	2.87(2.58)	1.11(1.06)

*Given in the parantheses are the predicted values by the model.

**mg C3-G/g dw as milligram cyanidin-3-glucoside equivalent per gram dry weight

Phippen and Simon (1998) examined different basil varieties and found that anthocyanins varied from 6.49 mg cyanidin 3,5-diglucoside/ 100 g wet basis in purple bush to 18.78 mg cyanidin 3,5-diglucoside/ 100 g wet basis in purple ruffles. The authors identified a total of fourteen acylated and glycosylated anthocyanins. Specifically, eleven cyanidin-based pigments and three peonidin-based pigments were isolated from purple basil (Phippen and Simon 1998). Pedro et al. (2016), extracted 1 g fresh purple basil with 10 mL ethanol-citric acid (80:20) solution at different temperatures and time. In their study, 64.7 mg cyanidin-3-glucoside equivalent /100 g fresh purple basil was detected in the extraction at 30 ^{o}C and 60 min, while 47.10 mg cyanidin-3-glucoside equivalent /100 g fresh purple basil was detected at the same temperature and 20 min (Pedro et al. 2016). Flanigan and Niemeyer examined 8 different purple basil varieties of which the amount of anthocyanins varied between 7.55 mg kuromanin equivalent/g dry matter and 16.6 mg kuromanin equivalent/g dry matter (Flanigan and Niemeyer 2014). Although it is hard to make a direct comparison with the reported values (due to the large varience of process parameters such as extraction solvent, composition, time, method, etc., which highly affect extraction yields), the results obtained in this study seem to be in accordance with the literature.

Regression coefficients (β), determination coefficients (R^2), ANOVA results, and F values for dependent variables are shown in Table 3.3. The R^2 values for the TMA and the increase in the green intensity were 96.81% and 93.84%, respectively, for the experiments containing Ac, while they were 95.36% and 97.25% for the experiments containing HCl . These values indicate a high correlation between the experimental and predicted values. The ethanol concentration showed a strong significant effect on all models. The solvent/solid ratio showed a significant impact only on the increase in the green intensity in the experiments containing HCl . The time factor showed a significant effect on TMA results in the experiments containing Ac, and on the increase in the green intensity results in the experiments containing HCl. The p-values of the models for all responses were less than 0.05, indicating that these models reliably predicted the data. Non-significant lack of fit values for all responses also support that all models predict well. These models were applied to determine the experimental conditions that would optimize the increase in the green intensity and TMA.

Table 3.3 Regression coefficients (β) and ANOVA values for quadratic models obtained with RSM

Coefficient	TMA (mg C3-G/g dw) (Ac)	TMA (mg C3-G/g dw) (HCl)	Increase in Green Intensity(Ac)	Increase in Green Intensity(HCl)
β0	4.444**	4.658***	2.119**	2.165***
Lineer				
β_1	-0.510*	-0.802*	0.653***	0.970***
β_2	0.482	0.259	0.106	0.215***
β_3	0.548*	0.636	-0.074	0.004*
Quadratic Interactions				
β_{11}	-3.399***	-2.929***	-0.664**	-0.316*
β_{22}	-0.165	-0.692	-0.063	0.041
β_{33}	-0.313	-0.379	0.017	0.167
Cross Interactions				
β_{12}	-0.314	-0.481	0.154	0.077
β_{13}	-0.113	-0.029	-0.110	-0.003
β_{23}	-0.047	-0.070	-0.145	0.006
R^2	96.81%	93.84%	95.36%	97.25%
R^2_{adj}	91.07%	82.75%	87.00%	92.29%
R^2_{pred}	51.20%	49.53%	33.24%	62.41%
F_l	12.32	0.51	4.97	3.24
F_m	16.86	8.46	11.41	19.63
p_l	0.076	0.716	0.172	0.244
p_m	0.003**	0.015*	0.008**	0.002**

β_1, β_2, β_3 are the model coefficients of the variables ethanol concentration, solvent/solid ratio and time, respectively. β_{11}, β_{22}, β_{33} and β_{12}, β_{13}, β_{23} are the corresponding quadratic and cross interaction coefficients.

R^2, coefficient of multiple determination

R^2_{adj}, adjusted R^2

R^2_{pred}, predicted R^2

*Significant at $p \leq 0.1$,** Significant at $p \leq 0.05$ *** Significant at $p \leq 0.01$

Subscript l denotes lack of fit and subscript m denotes model

TMA mg C3-G /g dw as milligram cyanidin-3-glucoside equivalent per gram dry weight

3.1.1. Effect of Extraction Variables on Total Monomeric Anthocyanin Content

Multiple regression analysis was performed according to the experimental TMA results. The quadratic polynomial models including all interactions between the variables (X_1 : ethanol concentration (%), X_2 : solvent/solid (mL/g), X_3 :time (min)) are given below in Equations 3.1 and 3.2 for the experiments using ethanol acidified with 0.1% Ac, and 0.1% HCl, respectively.

$$\text{TMA (mg C3-G /g dw)} = 4.444 - 0.510\,X_1 + 0.482\,X_2 + 0.548\,X_3 - 3.399\,X_1^2 - 0.165\,X_2^2 - 0.313\,X_3^2 - 0.314\,X_1X_2 - 0.113\,X_1X_3 - 0.047\,X_2X_3 \quad (3.1)$$

$$\text{TMA(mg C3-G /g dw)} = 4.658 - 0.802\,X_1 + 0.259\,X_2 + 0.636\,X_3 - 2.929\,X_1^2 - 0.692\,X_2^2 - 0.379\,X_3^2 - 0.481\,X_1X_2 - 0.029\,X_1X_3 - 0.070\,X_2X_3 \quad (3.2)$$

The effects of each variable and the interaction of the variables on TMA can be analyzed with three-dimensional surface response plots of quadratic polynomial Equations 3.1 and 3.2. The two-dimensional contour plots are also included as the projection of the graphs. Two factors were taken into account while the other factor was kept constant at the medium level (0) in the following graphs.

In Figure 3.1a, ethanol concentration (acidified with 0.1 % Ac) was kept constant at 50% (0 at the coded level) and inserted into Equation 3.1. The obtained TMA values were reflected with a 3D surface graph. Based on this graph, while the amount of ethanol is constant, TMA values increase as time increases and the solvent/solid ratio increases. In Figure 3.1b, solvent/solid was kept constant at 20 mL/g (0 at the coded level) and inserted into Equation 3.1. According to the corresponding 3D graph, while solvent/solid is constant, TMA value is maximized as the time increases and the ethanol percentage approaches 50%. In Figure 3.1c , time was kept constant at 45 min (0 at the coded level) and inserted into Equation 3.1. The corresponding 3D graph indicates that, while the time is constant, TMA value is maximized as the solvent/solid increases and the ethanol percentage approaches 50%

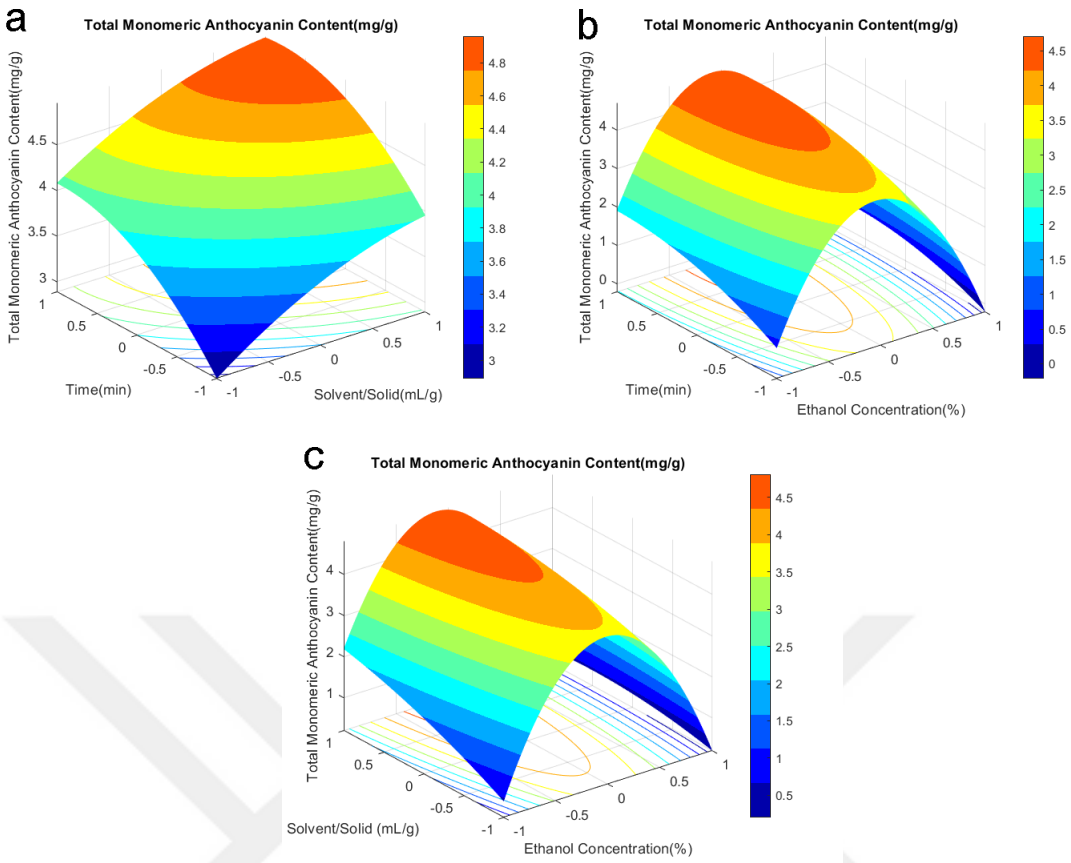

Figure 3.1 Response surface plot showing the effects of extraction variables on the TMA for experiment containing ethanol acidified with 0.1% Ac (a) X_1 kept at coded level 0 (b) X_2 kept at coded level 0 (c) X_3 kept at coded level 0

In Figure 3.2a, ethanol concentration (acidified with 0.1% HCl) was kept constant at 50% (0 at the coded level) and inserted into Equation 3.2. The obtained TMA values were reflected with a 3D surface graph. According to this graph, at constant ethanol concentration, TMA increases with time, while the maximum TMA is obtained at the solvent/solid ratio of 20-25. In Figure 3.2b, solvent/solid ratio was kept constant at 20 mL/g (0 at the coded level) and inserted into Equation 3.2. The corresponding TMA values were reflected with a 3D surface graph. According to this graph, while solvent/solid is constant, TMA value is maximized as the time increases and the ethanol percentage approaches 50%. In Figure 3.2c, time was kept constant at 45 min (0 at the coded level) and inserted into Equation 3.2. According to the corresponding 3D graph, while the time is constant, TMA value is maximized as the solvent/solid increases and the ethanol percentage approaches 45-50%.

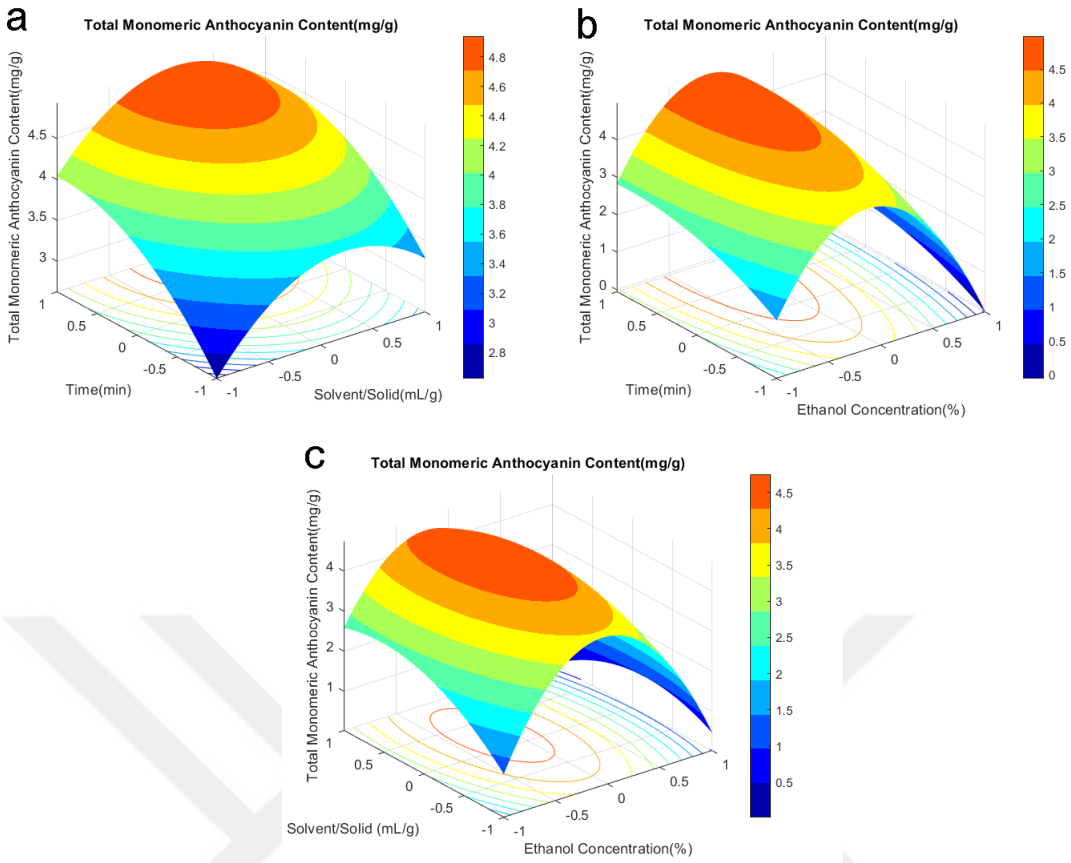

Figure 3.2 Response surface plot showing the effects of extraction variables on the TMA for experiment containing ethanol acidified with 0.1% HCl (a) X_1 kept at coded level 0 (b) X_2 kept at coded level 0 (c) X_3 kept at coded level 0

3.1.2. Effect of Extraction Variables on Increase in Green Intensity

Multiple regression analysis was performed according to the experimental results of increase in green intensity. The quadratic polynomial models including all interactions between the variables (X_1 : ethanol concentration (%), X_2 : solvent/solid (mL/g), X_3 :time (min)) are given below in Equations 3.3 and 3.4 for the experiments using ethanol acidified with 0.1% Ac, and 0.1% HCl, respectively.

$$\text{Increase in the Green Intensity} = 2.119 + 0.653\,X_1 + 0.106X_2 - 0.074\,X_3 - 0.664\,X_1^2 - 0.063\,X_2^2 + 0.017\,X_3^2 + 0.154\,X_1X_2 - 0.110\,X_{.1}X_3 - 0.145\,X_2X_3 \quad (3.3)$$

$$\text{Increase in the Green Intensity} = 2.165 + 0.970\ X_1 + 0.215\ X_2 + 0.004X_3 - 0.316\ X_1^2 + 0.041\ X_2^2 + 0.167X_3^2 + 0.077\ X_1\ X_2 - 0.003\ X_1\ X_3 + 0.006\ X_2\ X_3 \quad (3.4)$$

The effects of each variable and the interaction of the variables on the increase in green intensity can be analyzed with three-dimensional surface response plots of quadratic polynomial equations. The two-dimensional contour plots are also included as the projection of the graphs. Two factors were taken into account while the other factor was kept constant at the medium level (0) in the following graphs.

In Figure 3.3a, ethanol concentration (acidified with 0.1% Ac) was kept constant at 50% (0 at the coded level) and inserted into Equation 3.3. The obtained increase in the green intensity values were reflected with a 3D surface graph. Based on this graph, while the amount of ethanol is constant, increase in the green intensity values increase with time for lower solvent/solid ratios (10-15), while they decrease at higher solvent/solid ratios (15-30). In Figure 3.3b, solvent/solid was kept constant at 20 mL/g (0 at the coded level) and inserted into Equation 3.3. According to the corresponding graph, while solvent/solid is constant, increase in the green intensity value is maximized as time decreases and the ethanol percentage approaches 80%. In Figure 3.3c, time was kept constant at 45 min (0 at the coded level) and inserted into Equation 3.3. The corresponding 3D graph indicates that, while the time is constant, increase in the green intensity value is maximized as the solvent/solid increases and the ethanol percentage approaches 80%.

In Figure 3.4a, ethanol concentration (acidified with 0.1% HCl) was kept constant at 50% (0 at the coded level) and inserted into Equation 3.4. The obtained increase in the green intensity values were reflected with a 3D surface graph. Based on this graph, while the amount of ethanol is constant, increase in the green intensity values increase as time moves away from the 45 min level and the solvent/solid increases. In Figure 3.4b, solvent/solid was kept constant at 20 mL/g (0 at the coded level) and inserted into Equation 3.4. The corresponding increase in the green intensity values were reflected with a 3D surface graph. According to this graph, while solvent/solid is constant, increase in the green intensity value is maximized as the time moves away from 45 min and the ethanol percentage approaches 90%. In Figure 3.4c, time was kept constant at 45 min (0 at the coded level) and inserted into Equation 3.4 and obtained increase in the green intensity values were reflected with 3D surface graphs. According to the corresponding graph, while the time is constant, increase in the green intensity value is maximized as the solvent/solid increases and the ethanol percentage approaches 90%.

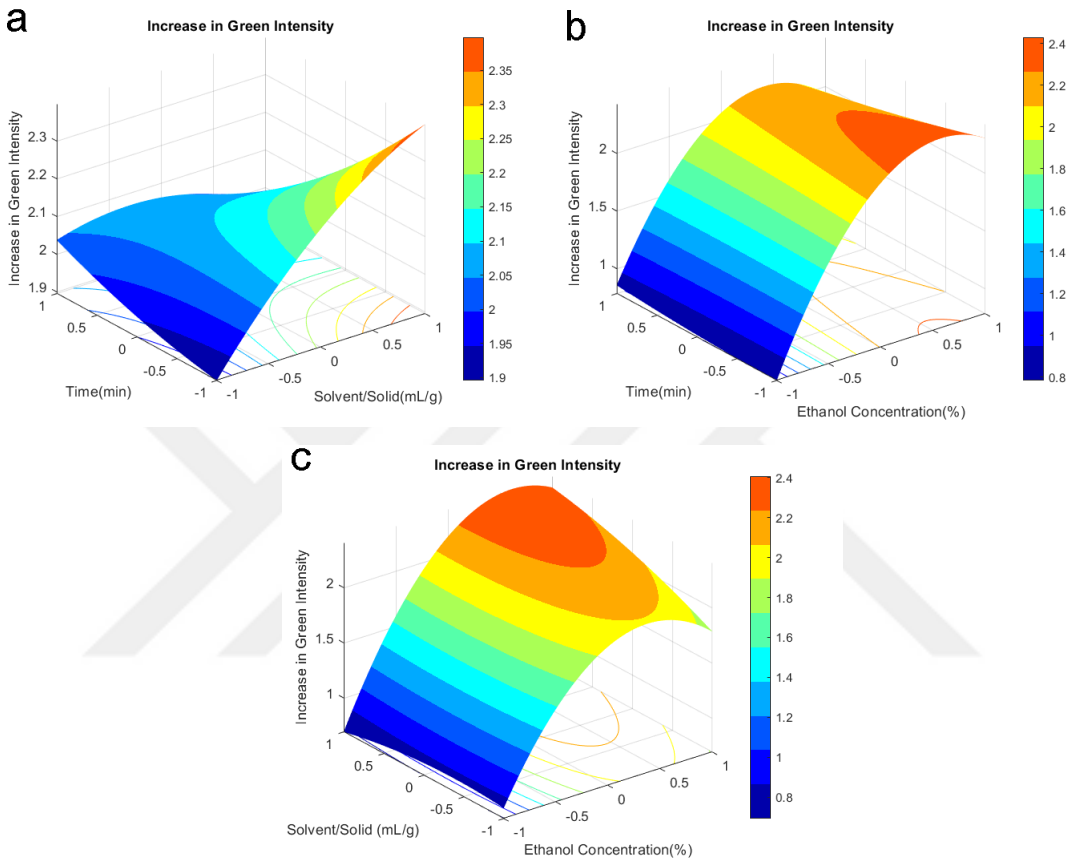

Figure 3.3 Response surface plot showing the effects of extraction variables on the increase in green intensity for experiments containing ethanol acidified with 0.1% Ac (a) X_1 kept at coded level 0 (b) X_2 kept at coded level 0 (c)X_3 kept at coded level 0

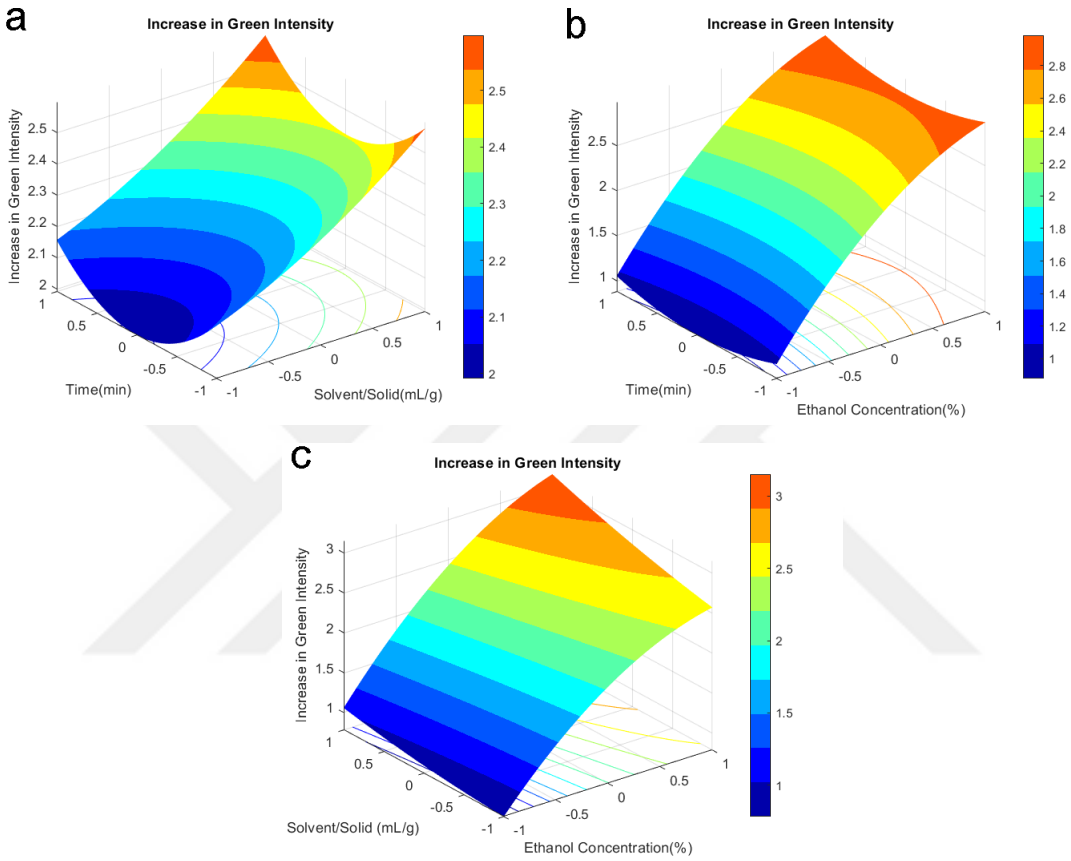

Figure 3.4 Response surface plot showing the effects of extraction variables on the increase in green intensity for experiments containing ethanol acidified with 0.1% HCl (a) X_1 kept at coded level 0 (b) X_2 kept at coded level 0 (c) X_3 kept at coded level 0

3.1.3. Optimum UAE Conditions of Dry Purple Basil and Experimental Validation of Models

The optimum conditions of the variables were determined for both single and multiple responses via the equations obtained with Minitab (2018) software using response optimizer tool. Validation experiments of the optimized conditions were carried out by triple analysis of the optimized variables in this study. Percentage of error was calculated for each case. Experimental results are shown in Table 3.4. The errors found in the experiments with ethanol containing 0.1% Ac conducted for the validation of the optimum conditions obtained for both single and multiple responses were below 10 %, which indicates that the models work correctly enough. The errors found in the experiments with ethanol containing 0.1% HCl conducted for the validation of the optimum conditions obtained for both single and multiple responses were mostly below 10%. Only in the case for multiple responses, the error was calculated as 18.70% for the increase in the green intensity response. Therefore, the corresponding multiple response model was not that successful in predicting the increase in the green intensity values under the optimized conditions for experiments with 0.1% HCl.

Table 3.4 Predicted optimum conditions and validation of experiments for single and multiple responses

Response variables	Optimized Extraction Conditions			Maximized Results			
	Ethanol Concentration (v/v, %)	Solvent/Solid (mL/g)	Time (min)	Predicted	Experimantal[e]	Error (%)[e]	Composite Desirability
Single Responses(0.1% Ac)							
TMA (mg C3-G /g dw)	44.75	30	69.55	5.02	5.50±0.14	9.50	0.91
Increase in Green Intensity	77.88	30	15	2.72	2.58±0.08	4.84	1.00

(cont. on next page)

Table 3.4 (cont.)

Multiple Responses(0.1% Ac)							
TMA(mg C3-G /g dw)	55.25	30	39.24	4.49	4.83±0.18	7.65	0.86
Increase in Green Intensity	55.25	30	39.24	2.30	2.29±0.05	0.47	0.86
Single Responses(0.1% HCl)							
TMA(mg C3-G /g dw	43.94	21.92	69.55	5.01	5.16±0.28	2.92	0.88
Increase in Green Intensity	90	30	75	3.33	3.45±0.30	3.63	0.99
Multiple Responses(0.1% HCl)							
TMA(mg C3-G /g dw)	56.06	25.15	75	4.60	4.47±0.28	2.78	0.77
Increase in Green Intensity	56.06	25.15	75	2.61	2.2±0.08	18.70	0.77

TMA mg C3-G /g dw as milligram cyanidin-3-glucoside equivalent per gram dry weight

[e]Mean(n=3)

It has been reported that purple basil has a high anthocyanin content in the literature (Flanigan and Niemeyer 2014). This study was designed for the first time to optimize the processing conditions of UAE of dry purple basil that would yield the maximum TMA content and pH-dependent increase in the green intensity of the extracts using response surface methodology.

The conditions to maximize only the anthocyanin content were determined as 44.75% ethanol, 30 mL/g solvent/solid ratio and 69.55 min for the case that the solvent contained 0.1% Ac , and the maximum TMA content was measured as 5.50±0.14 mg C3-G /g dw. Similarly, the conditions to maximize only the anthocyanin content were determined as 43.94% ethanol, 21.92 mL/g solvent/solid ratio and 69.55 min for the case that the solvent contained 0.1% HCl and the maximum TMA content was measured as 5.16±0.28 mg C3-G /g dw. On the other hand, the conditions to maximize only the increase in the green intensity were determined as 77.88% ethanol, 30 mL/g solvent/solid ratio and 15 min for the experiments containing ethanol with 0.1% acetic acid. The maximum increase in the green intensity was measured as 2.58±0.08. For the experiments ethanol with 0.1% HCl, the conditions to maximize only the increase in the green intensity were determined as 90% ethanol, 30 mL/g solvent/solid ratio and 75 min, and the maximum increase in the green intensity was measured as 3.45±0.30.

Speaking of multiple responses, the conditions to maximize both the TMA content and the increase in the green intensity were determined as 55.25% ethanol, 30 mL/g solvent/solid ratio and 39.24 min for the experiments containing ethanol with 0.1% Ac. The maximum TMA content and the increase in the green intensity were measured as 4.83±0.18 mg C3-G /g dw and 2.29±0.05, respectively. For the experiments containing ethanol with 0.1% HCl, the conditions to maximize both TMA content and the increase in the green intensity were determined as 56.06% ethanol, 25.15mL/g solvent/solid ratio and 75 min. The maximum TMA content and the increase in the green intensity were measured as 4.47±0.28 mg C3-G /g dw and 2.2±0.08, respectively.

Absorption spectra and color variation with pH change of PBE extracts extracted with 44.75% ethanol containing 0.1% acetic acid, 30 mL/g solvent/solid ratio and 69.55 min for maximum TMA were shown in Figure 3.5. Absorption spectra and color variation with pH change of PBE extracts extracted with 77.88% ethanol containing 0.1% acetic acid, 30 mL/g solvent/solid ratio and 15 min for the experiments for maximum increase in green intensity were illustrated in Figure 3.6. Absorption spectra and color variation with pH change of PBE extracts extracted with 55.25% ethanol containing 0.1% acetic acid, 30 mL/g solvent/solid ratio and 39.24 min for both maximum TMA and increase in green intensity were drawn in Figure 3.7. Absorption spectra and color variation with pH change of PBE extracts extracted with 43.94% ethanol containing 0.1% hydrochloric acid, 21.92 mL/g solvent/solid ratio and 69.55 min for maximum TMA were shown in Figure 3.8. Absorption spectra and color variation with pH change of PBE extracts

extracted with 90% ethanol containing 0.1% hydrochloric acid, 30 mL/g solvent/solid ratio and 75 min for the experiments for maximum increase in green intensity were illustrated in Figure 3.9. Absorption spectra and color variation with pH change of PBE extracts extracted with 56.06% ethanol containing 0.1% hydrochloric acid, 25.15 mL/g solvent/solid ratio and 75 min for both maximum TMA and increase in green intensity were drawn in Figure 3.10.

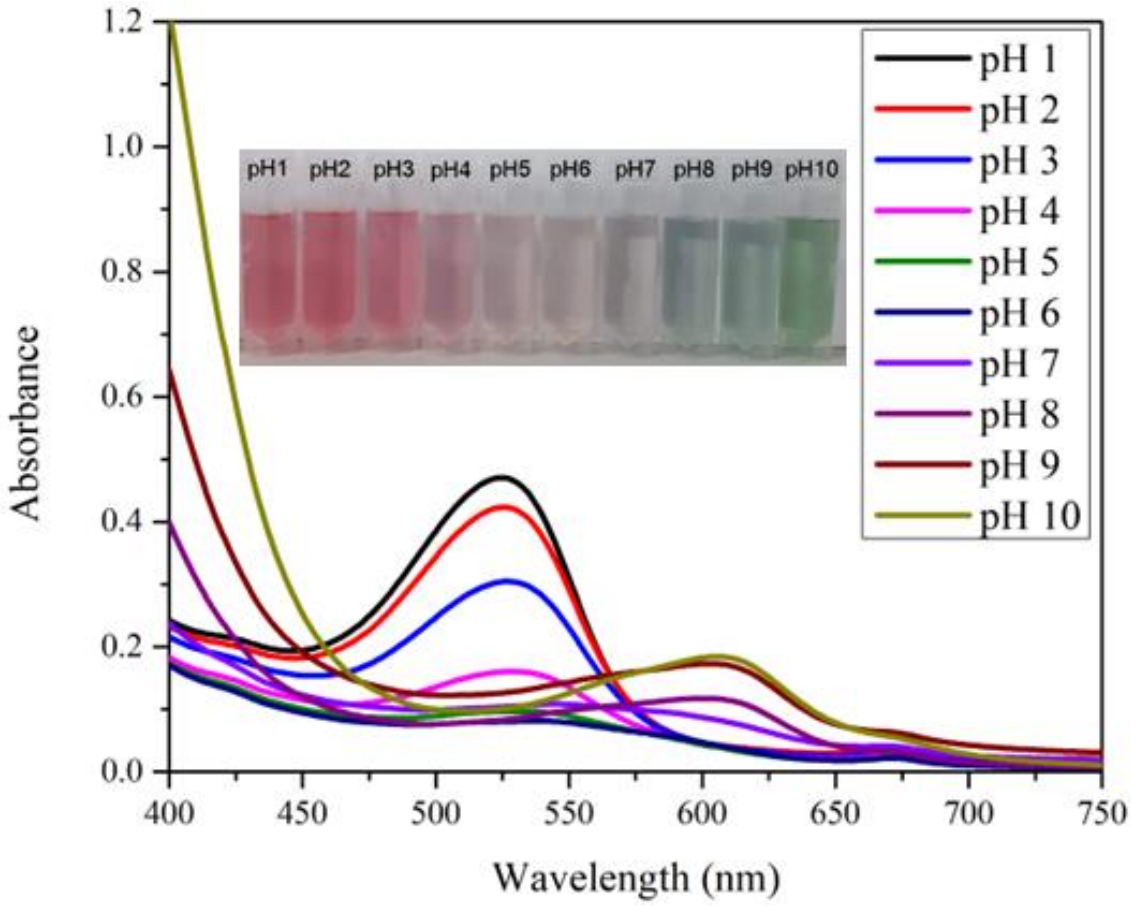

Figure 3.5 Absorption spectra and color variation with pH change of PBE extracts extracted with 44.75% ethanol containing 0.1% acetic acid, 30 mL/g solvent/solid ratio and 69.55 min for maximum TMA as mg C3-G /g dw content (extracts diluted to 1:20 with pH buffer solutions)

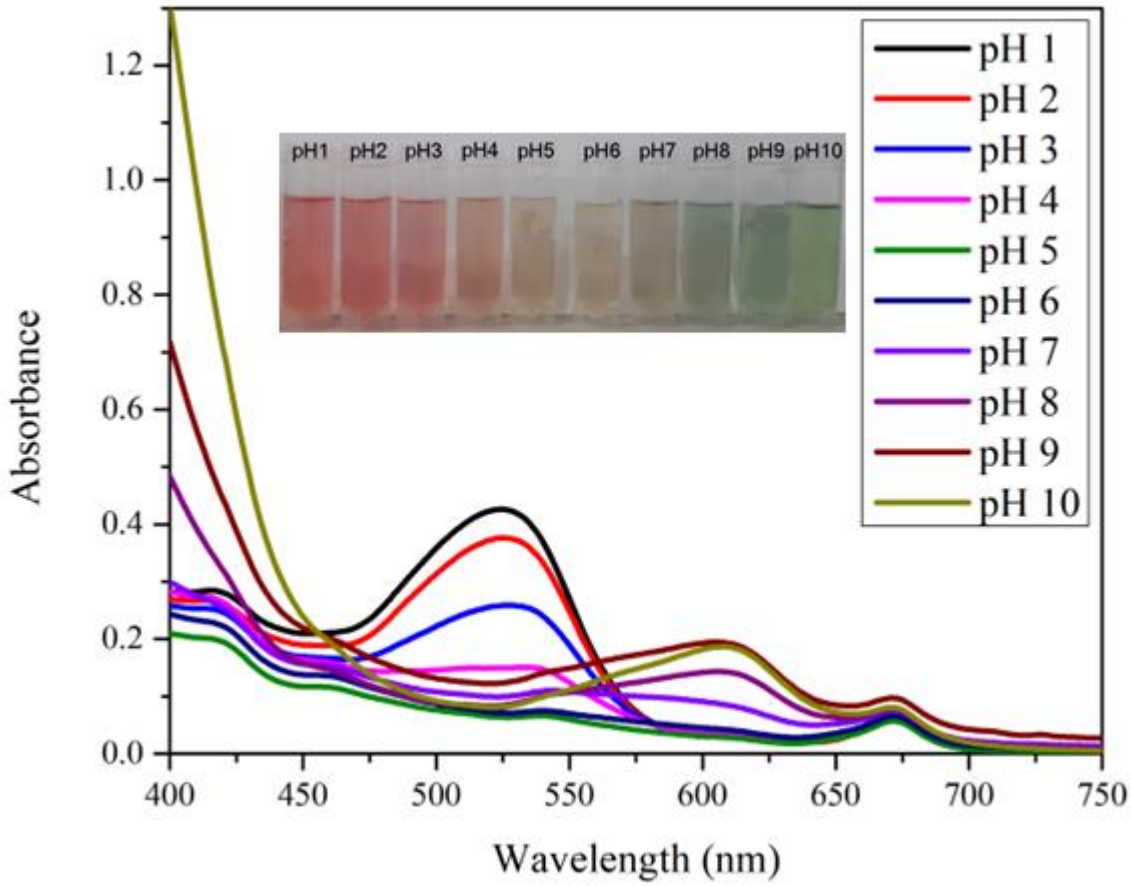

Figure 3.6 Absorption spectra and color variation with pH change of PBE extracts extracted with 77.88% ethanol containing 0.1% acetic acid, 30 mL/g solvent/solid ratio and 15 min for the experiments for maximum increase in green intensity (extracts diluted to 1:5 with pH buffer solutions)

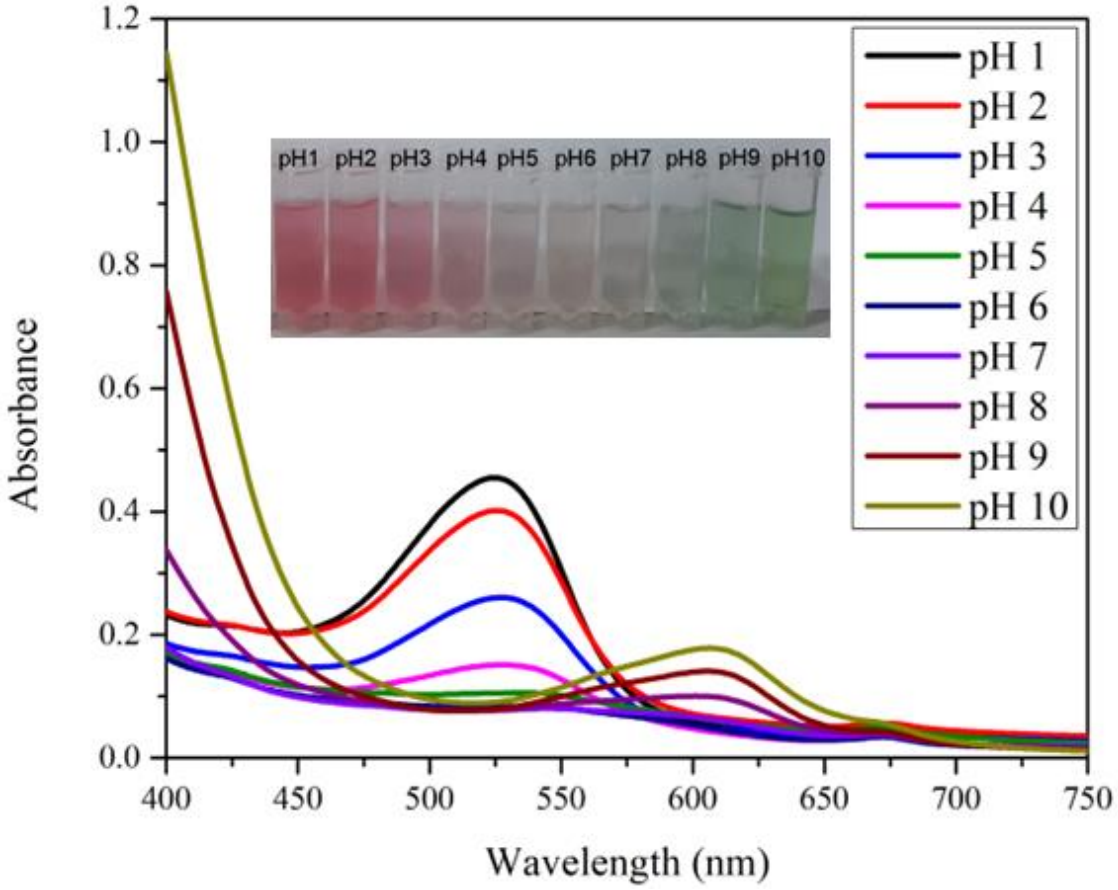

Figure 3.7 Absorption spectra and color variation with pH change of PBE extracts extracted with 55.25% ethanol containing 0.1% acetic acid, 30 mL/g solvent/solid ratio and 39.24 min for both maximum TMA as mg C3-G /g dw content and increase in green intensity (extracts diluted to 1:20 with pH buffer solutions)

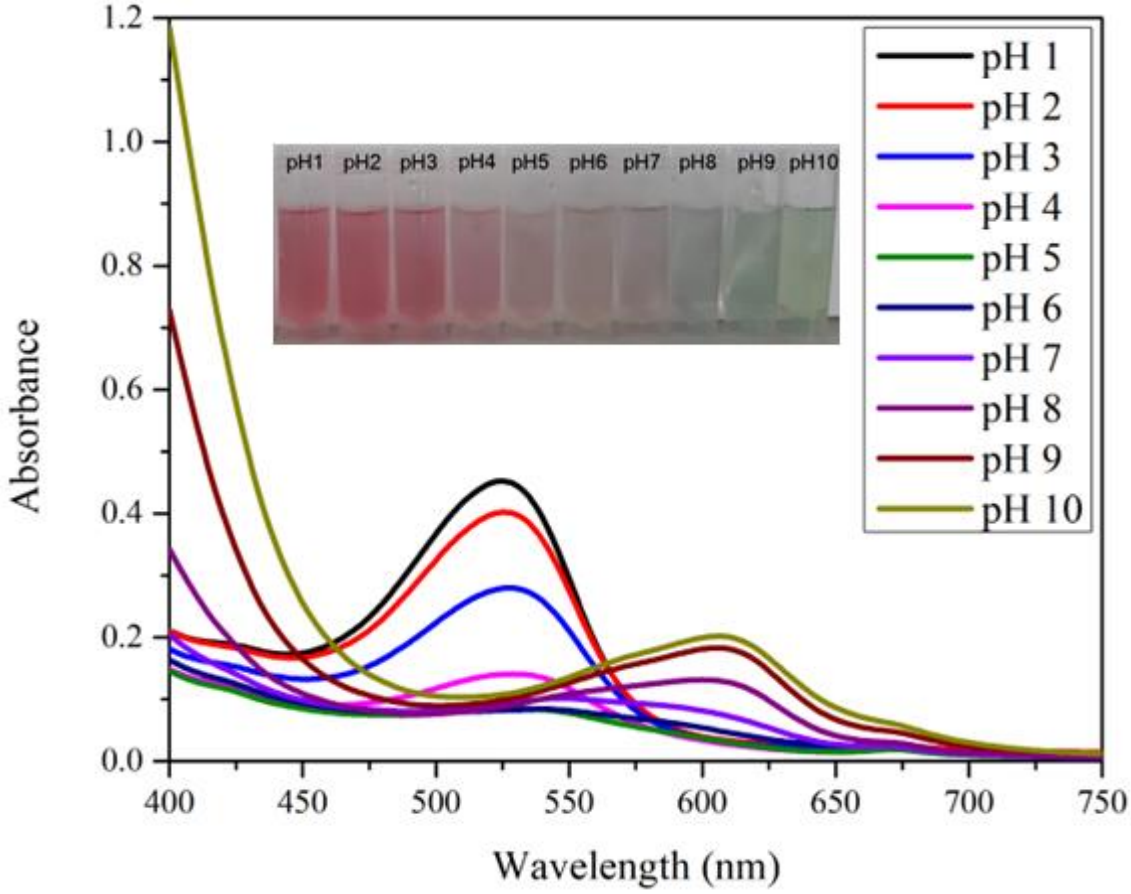

Figure 3.8 Absorption spectra and color variation with pH change of PBE extracts extracted with 43.94% ethanol containing 0.1% hydrochloric acid, 21.92 mL/g solvent/solid ratio and 69.55 min for maximum TMA as mg C3-G /g dw content (extracts diluted to 1:20 with pH buffer solutions)

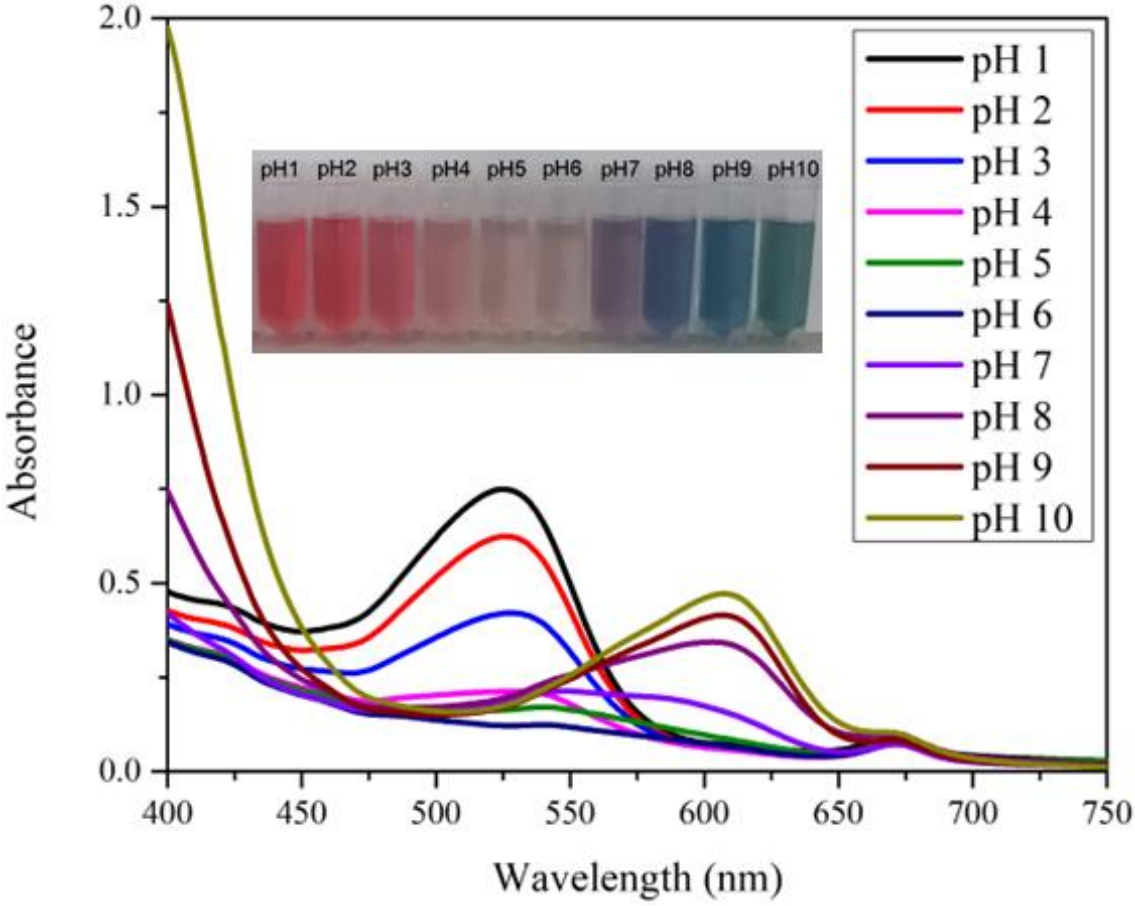

Figure 3.9 Absorption spectra and color variation with pH change of PBE extracts extracted with 90% ethanol containing 0.1% hydrochloric acid, 30 mL/g solvent/solid ratio and 75 min for the experiments for maximum increase in green intensity (extracts diluted to 1:5 with pH buffer solutions)

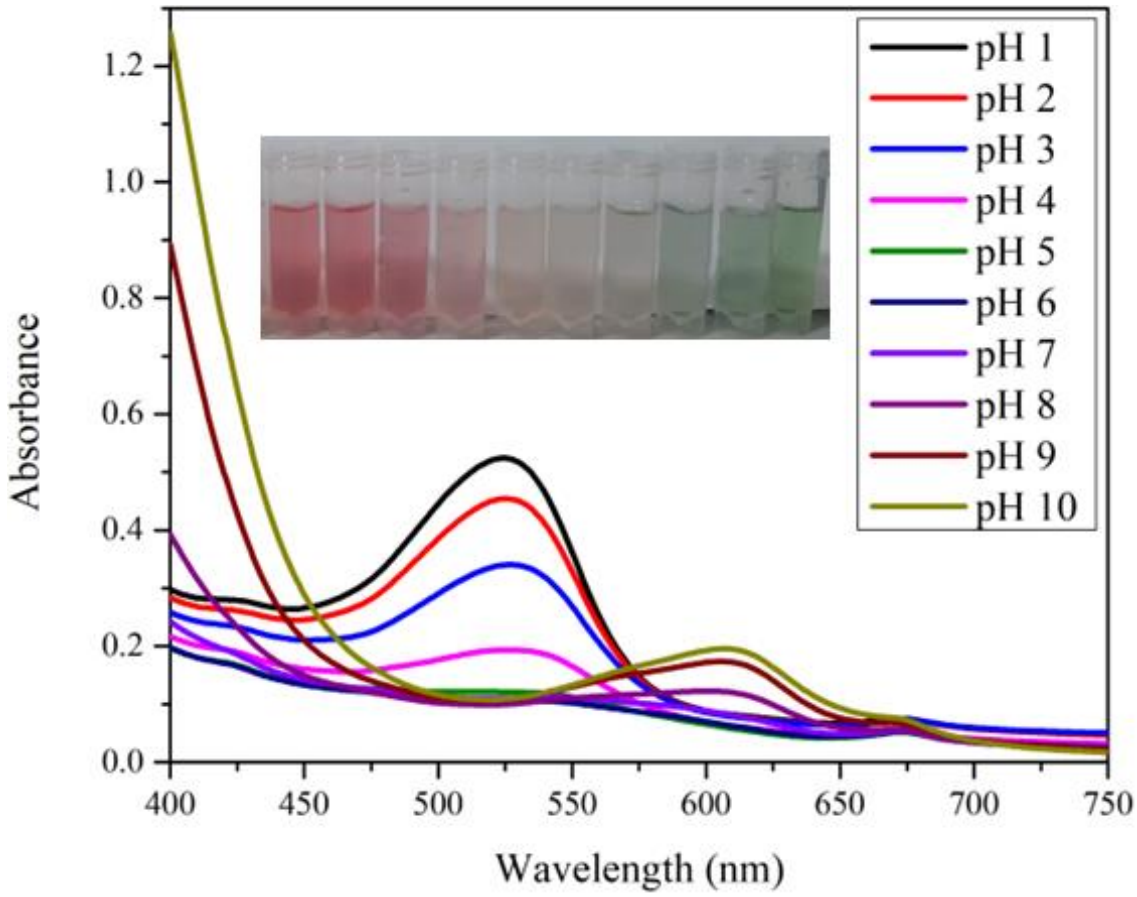

Figure 3.10 Absorption spectra and color variation with pH change of PBE extracts extracted with 56.06% ethanol containing 0.1% hydrochloric acid, 25.15 mL/g solvent/solid ratio and 75 min for both maximum TMA as mg C3-G /g dw content and increase in green intensity (extracts diluted to 1:20 with pH buffer solutions)

3.1.4. Characterization of the PBE Obtained Under Optimum UAE Conditions

TMA, PPC, TPC, ABTS and DPPH characterization tests were performed for the extracts of purple basil obtained as a result of experiments carried out under UDE-optimized conditions, and the results are shown in Table 3.5. Data were compared with One-Way ANOVA using Tukey's Test via the Minitab (2018) program for statistics. Significant differences were observed for the optimized values for single and multiple responses.

The highest TMA content was 5.50±0.14 mg C3-G /g dw in the extracts produced with 44.75% ethanol containing 0.1% Ac, 30 mL/g solvent/solid ratio and 69.55 min. This TMA value was followed by 5.16±0.28 mg C3-G /g dw for the extracts obtained with 43.94% ethanol containing 0.1% HCl, 21.92 mL/g solvent/solid ratio and 69.55 min extraction conditions, which was statistically significant (from the experiments containing ethanol with 0.1% Ac). The results showed that the experiments containing 0.1% Ac gave slightly higher results than the experiments containing 0.1% HCl in terms of TMA. TMA with multiple responses had lower TMA contents than single responses and differed statistically from both each other and single responses. In terms of PPC, only the extracts obtained with the extraction conditions of 55.25% ethanol containing 0.1% Ac, 30 mL/g solvent/solid ratio and 39.24 min significantly differed from the remaining extracts and were found to be higher.

The highest TPC content was 32.80±0.32 mg GAE /g dw in the extracts produced with 44.75% ethanol containing 0.1% Ac, 30 mL/g solvent/solid ratio and 69.55 min. This TPC value was followed by 31.77±0.66 mg GAE /g dw for the extracts obtained with the extraction conditions of 43.94% ethanol containing 0.1% HCl, 21.92 mL/g solvent/solid ratio and 69.55 min, which was statistically significant (from the experiments containing ethanol with 0.1% Ac). The results showed that the experiments containing 0.1% Ac gave slightly higher results than the experiments containing 0.1% HCl in terms of TPC which was also the case in TMA. This can be explained by that there was a correlation between TMA and TPC since anthocyanins and phenolics are both secondary plant metabolites known as antioxidants and they show similar properties. TPC with multiple responses exhibited lower TPC values than single responses and differed statistically from both each other and single responses. Pedro and colleagues (2016)

extracted 1 g fresh purple basil with 10 mL of ethanol-citric acid (80:20) at different temperatures and extraction times in their study. 688.22 mg GAE/ 100 g fresh basil was detected in the extraction performed at 30 ^{o}C and 60 min, while at the same temperature and 20 min, 464.30 mg GAE/100 g fresh basil was detected (Pedro et al. 2016). Flanigan and Niemeyer (2014) found that the amount of TPC in 8 different purple basil cultivars, which ranged from 15.12 mg GAE/ g dry matter to 22.01 mg GAE/g dry matter (Flanigan and Niemeyer 2014). Wangcharoen & Morasuk reported that the highest TPC of white and red holy basil were 12.60±1.02 and 19.46±1.97 mg gallic acid equivalent per gram of dry weight, respectively. The highest value of red holy basil in this recent study (19.46 mg gallic acid equivalent per gram of dry weight) was lower than the value (51.1 mg gallic acid equivalent per gram of dry weight) reported by Juliani and Simon (2002). These results were not doubtful because phenolic compounds in plant foods are largely influenced by genetic factors and environmental conditions (Bravo, 1998). The difference in phenolic content could affect the antioxidant capacity of plants, because many phenolic compounds in plants are good sources of natural antioxidants (Ho, 1992; Amiot et al., 1997).

The highest ABTS antioxidant activity was 69.59±3.27 mg TE /g dw in the extracts obtained with 44.75% ethanol containing 0.1% Ac, 30 mL/g solvent/solid ratio and 69.55 min. This ABTS value was followed by 68.01±4.68 mg TE /g dw for the extracts obtained with the extraction conditions of 43.94% ethanol containing 0.1% HCl, 21.92 mL/g solvent/solid ratio and 69.55 min, which was statistically significant (from the experiments containing ethanol with 0.1% Ac). The results showed that the experiments containing 0.1% Ac gave slightly higher results than the experiments containing 0.1% HCl in terms of ABTS. ABTS with multiple responses exhibited lower ABTS activities than single responses and differed statistically from both each other and single responses. ABTS value was reported as 65.82 mg TE/g dw in extracts of red holy basil extracted with 76% ethanol in the literature (Wangcharoen and Morasuk 2007)The ABTS activities determined in this study are similar to the values reportes in Wangchoren and Morasuk's (2007).

The DPPH content was 24.71±1.40 mg AAE /g dw in the extracts obtained with

43.94% ethanol containing 0.1% HCl, 21.92 mL/g solvent/solid ratio and 69.55 min. This ABTS value was followed by 19.98±0.85 mg AAE/g dw for the extracts obtained with the extraction conditions of 44.75% ethanol containing 0.1% Ac, 30 mL/g solvent/solid ratio and 69.55 min, which was statistically significant (from the

experiments containing ethanol with 0.1% Ac). The results showed that the experiments containing 0.1% HCl gave slightly higher results than the experiments containing 0.1% Ac in terms of DPPH. DPPH with multiple responses showed lower DPPH radical scavenging activities than single responses and differed statistically from both each other and single responses. DPPH value was reports as 5.28±0.16 mg AEE/g dw in extracts of red holy basil extracted with 57% ethanol in the literature (Wangcharoen, & Morasuk, 2014). DPPH values measured in this study by the extraction of UAE are approximately 3-4 times the DPPH values in 2007 by Wangcharoen & Morasuk (2007). Morasuk reported that ABTS and DPPH assays are methods for measuring the ability of antioxidant molecules to quench ABTS and DPPH free radicals, respectively. But ABTS and DPPH free radical are different. To explain why DPPH values were lower than ABTS values, Wang et al. (1998) showed that some compounds which have ABTS+ scavenging activity may not show DPPH scavenging activity, and Arts et al. (2004) found that some products of ABTS+ scavenging reaction may have a higher antioxidant capacity and can continually react with ABTS+.

Table 3.5 Total monomeric anthocyanin (TMA), percent polymeric color (PPC), total phenolic content (TPC), ABTS/TEAC antioxidant activity and DPPH radical scavenging activity of purple basil extracts obtained under optimized conditions with UAE

Optimized Extraction Conditions			**Experimental Results**				
Eth. Conc. (%)	**Solvent/ Solid (mL/g)**	**Time (min)**	**TMA***	**PPC**	**TPC****	**ABTS*****	**DPPH******
44.75 *(0.1% Ac)*	30	69.55	5.50±0.14[a]	52.72±4.76[b]	32.80±0.32[a]	69.59±3.27[a]	19.98±0.85[b]

(cont. on next page)

Table 3.5 (cont.)

55.25 *(0.1% Ac)*	30	39.24	4.83±0.18^{bc}	68.07±3.17^{a}	28.79±1.54^{bc}	55.85±1.71^{c}	16.80±1.08^{b}
43.94 *(0.1% HCl)*	21.92	69.55	5.16±0.28^{ab}	57.58±4.83^{b}	31.77±0,66^{ab}	68.01±4.68^{ab}	24.71±1.40^{a}
56.06 *(0.1% HCl)*	25.15	75	4.47±0.28^{c}	53.48±1.77^{b}	26.55±2.39^{c}	61.69±0.68^{bc}	19.27±2.04^{b}

Mean(n=3)

*TMA: mg C3-G /g dw as milligram cyanidin-3-glucoside equivalent per g dry weight

**TPC: mg GAEg dw as milligram gallic acid equivalent per g dry weight

***ABTS: mg TE/ g dw as milligram trolox equivalent per g dry weight

**** DPPH: mg AAE/g dw as milligram ascorbic acid equivalent per g dry weight

The difference between values with different letters in the same column is statistically significant.

3.2. Fabrication of pH-indicator Films by Electrospinning

10% PCL (w v^{-1}) solution including purple basil extract at 4 different concentrations (0%, 0.2%, 0.4% and 0.6% w v^{-1}) was electrospun. The electrospun films were fabricated with 20 kV and 25 kV with flow rates 0.4 ml h^{-1} and 0.5 mL h^{-1} in a controlled manner for 3.5 h where the distance between tip of the syringe and collector was 26 cm. These process parameters were determined by preliminary experiments using pure PCL solutions.

3.2.1. Effect of PBE Concentrations on Solution Viscosity

Viscosity of the polymer solution plays a significant role for creation of a stable jet of polymer solution forming a basis for spinnability. Solution viscosity is a function of both polymer concentration and solvent. If the viscosity is too low, the polymer solution does not properly get entangled causing bead or droplet formation (Mercante et al. 2017). On the contrary, high viscosity may cause hindering the flow of polymer

solution through the tip of the needle, which prevents formation of fibers (Aman Mohammadi, Hosseini, and Yousefi 2020). Therefore, an optimum viscosity, neither too high nor too low, is necessary in order to obtain bead-free fibers.

Flow behavior of the solutions obeyed 'Power Law Model'. The shear stress (τ) and shear rate (γ̇) data collected from rheological experiments were fitted well to the power-law model equation given below Equation 3.5, where τ is the shear stress (Pa), γ̇ is the shear rate (s^{-1}), k is the consistency coefficient ($Pa.s^n$) and n is the flow behavior index. The coefficient of determination (R^2) values ranged from 0.985 to 0.993.

$$\tau = k\,(\dot{\gamma})^{\,n} \tag{3.5}$$

Apparent viscosity ($\eta = k\,(\dot{\gamma})^{\,n-1}$) is a function of consistency coefficient (Sahin & Sumnu, 2006). The power-law parameters of 10% PCL (w v^{-1}) solution including purple basil extract at 3 different concentrations (0.2%, 0.4% and 0.6% w v^{-1}) are given in Table.3.6. It is clear that n values are lower than 1 for all electrospinning solutions, which means solutions showed shear-thinning behavior (also supported by Figure 3.11). As the shear rate increased, apparent viscosities of all spinning solutions decreased. The increase in k values and apparent viscosities of PCL solutions with increasing PBE concentrations was in accordance with literature. Prietto et al (2018) found that the viscosity of zein solutions was significantly increased by the addition of red cabbage (Brassica oleracea L.) anthocyanins. The apparent viscosity of zein solution without anthocyanin was measured as 124.8±1.6 cP whereas the apparent viscosities of zein solutions with 3%, 4% and 5% anthocyanin were measured as 238.7±1.3 cP, 304.3±0.3 and 346.2±0.9 cP, respectively (Prietto et al. 2018). Terra et al (2021) observed that the apparent viscosities of the PCL/ PEO solutions were increased with the addition of phycocyanin and curcumin (Terra et al., 2021). In a study by Moreira et al. (2019), the authors determined that the phycocyanin addition promoted an increase in the solution viscosity (Moreira et al., 2019). Similar to studies conducted by Prietto et al.(2018), Terra et al.(2021) and Moreira et al.(2018), addition of PBE increased the viscosity of 10% PCL (w v^{-1}) solution in this study, which resulted in morphological changes in nanofibers.

Table 3.6 Effects of PBE % (w v^{-1}) concentration on solution characteristics

Concentration	k(Pa s^n)	n	Apparent Viscosity at 50s^{-1}(η) (Pa.s) **	R^2
10% PCL (w v^{-1}) & 0% PBE (w v^{-1})	0.591±0.045^b	0.825±0.058^a	0.299±0.082^b	0.985
10% PCL(w v^{-1}) & 0.2% PBE (w v^{-1})	0.689±0.038^{ab}	0.869±0.038^a	0.411±0.071^{ab}	0.990
10% PCL (w v^{-1}) & 0.4% PBE (w v^{-1})	0.700±0.022^a	0.872±0.015^a	0.418±0.027^{ab}	0.991
10% PCL(w v^{-1}) & 0.6% PBE (w v^{-1})	0.775±0.054^a	0.888±0.004^a	0.494±0.029^a	0.993

Values represent the mean ± standard deviation; n = 3.
*Columns with different lowercase letters differ statistically (p≤0.05)

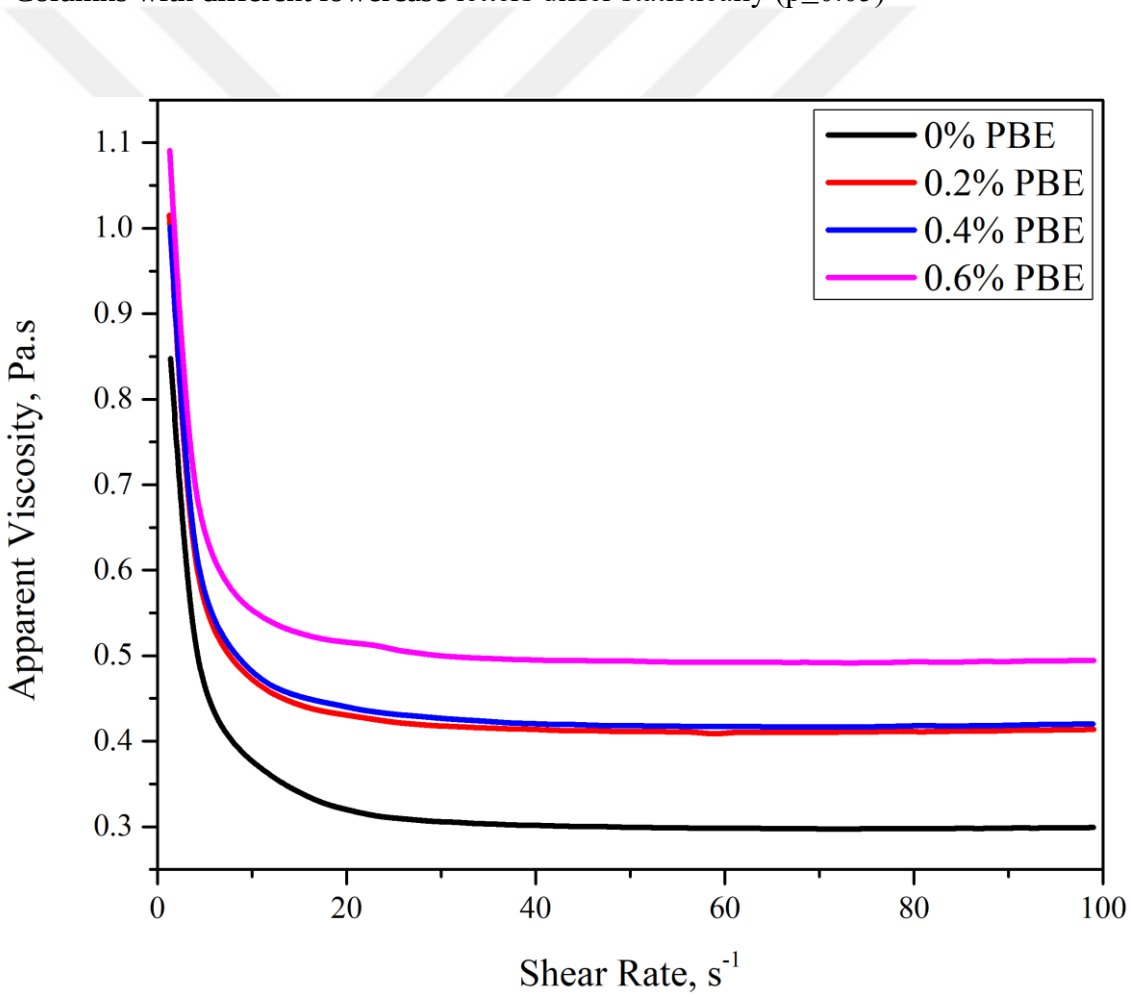

Figure 3.11 The effects of different PBE % (w v^{-1}) concentration in apparent viscosities

3.2.2. Morphologies of Nanofibrous Films

SEM images (5 000x) of 16 different electrospun films with two replicates were analyzed to examine the effects of electrospinning conditions and PBE concentrations on the morphology of nanofibers. Diameters of randomly selected 60 fibers were measured with Image J software for each film to interpret the results. Fiber diameter distributions were statistically analyzed and the results are summarized in Table 3.7. SEM images (5 000x) of the nanofibers obtained from solution with 10% (w v^{-1}) PCL and 0% PBE (w v^{-1}) for different electrospinning conditions are illustrated in Figure 3.12. The images indicate that electrospinning conditions highly impact the fibre morphologies. All 4 films without PBE had beads, however the film electrospun at V=20 kV and Q=0.4 mL h^{-1} had the least amount of beads and most uniform morphology compared to the rest. Columns with different lowercase letters differ statistically for electrospinning conditions in Table 3.7. For the films without PBE, the results indicate that fiber diameter increases as the voltage increases and flow rate decreases. According to Haider et al., the increase in the diameter and formation of beads or beaded nanofibers with an elevation in the applied voltage are connected to the decrease in the size of the Taylor cone and an increase in the jet velocity for the same flow rate (Haider, Haider, and Kang 2018).

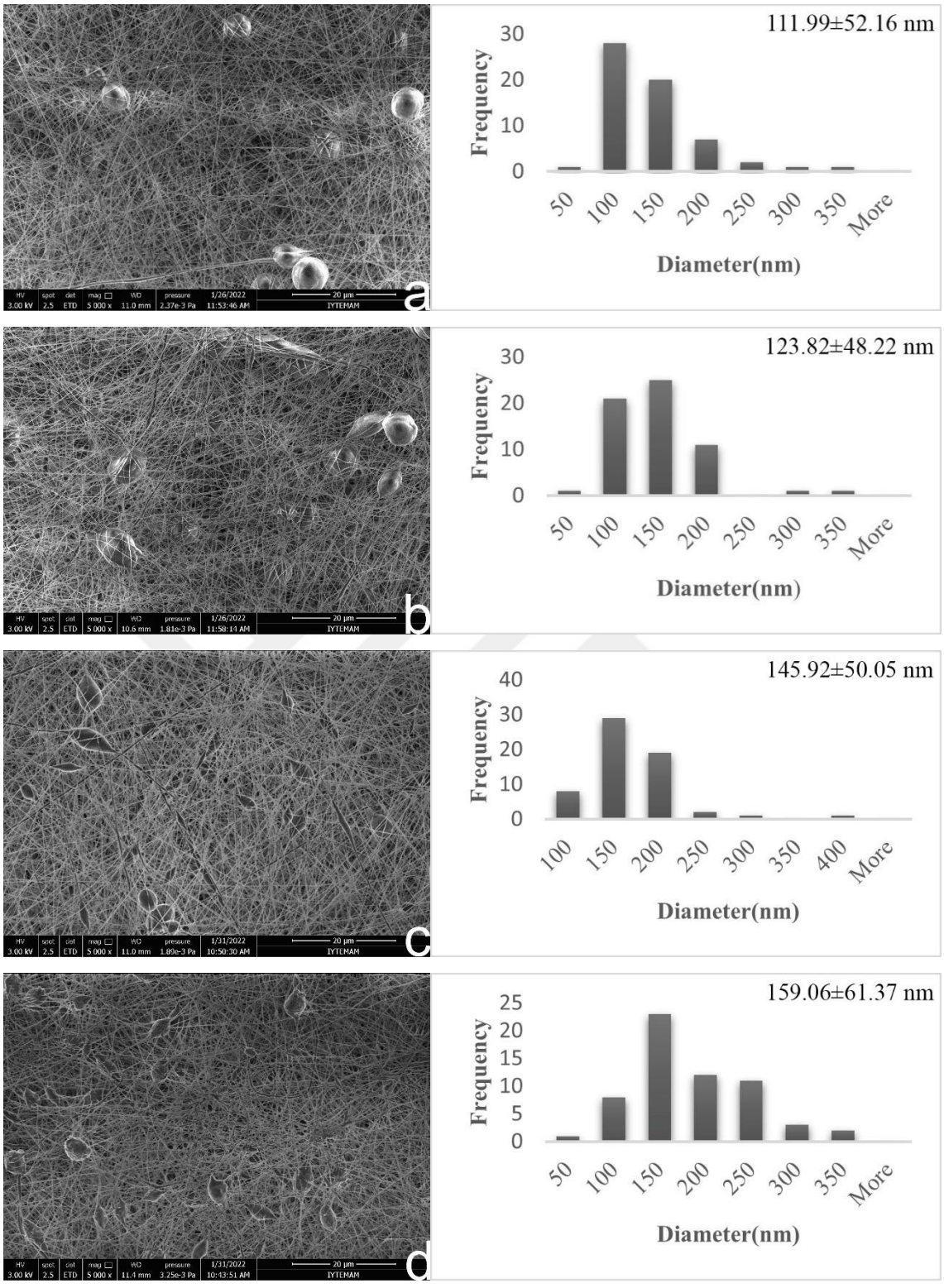

Figure 3.12 SEM images (5 000x) of the nanofibers, obtained from solution with 10% PCL (w v^{-1}) and 0% PBE (w v^{-1}) at (a) V=20 kV; Q=0.5 mL h^{-1}, (b) V=25 kV; Q=0.5 mL h^{-1}, (c) V=20 kV; Q=0.4 mL h^{-1} (d) V=25 kV; Q=0.4 mL h^{-1}

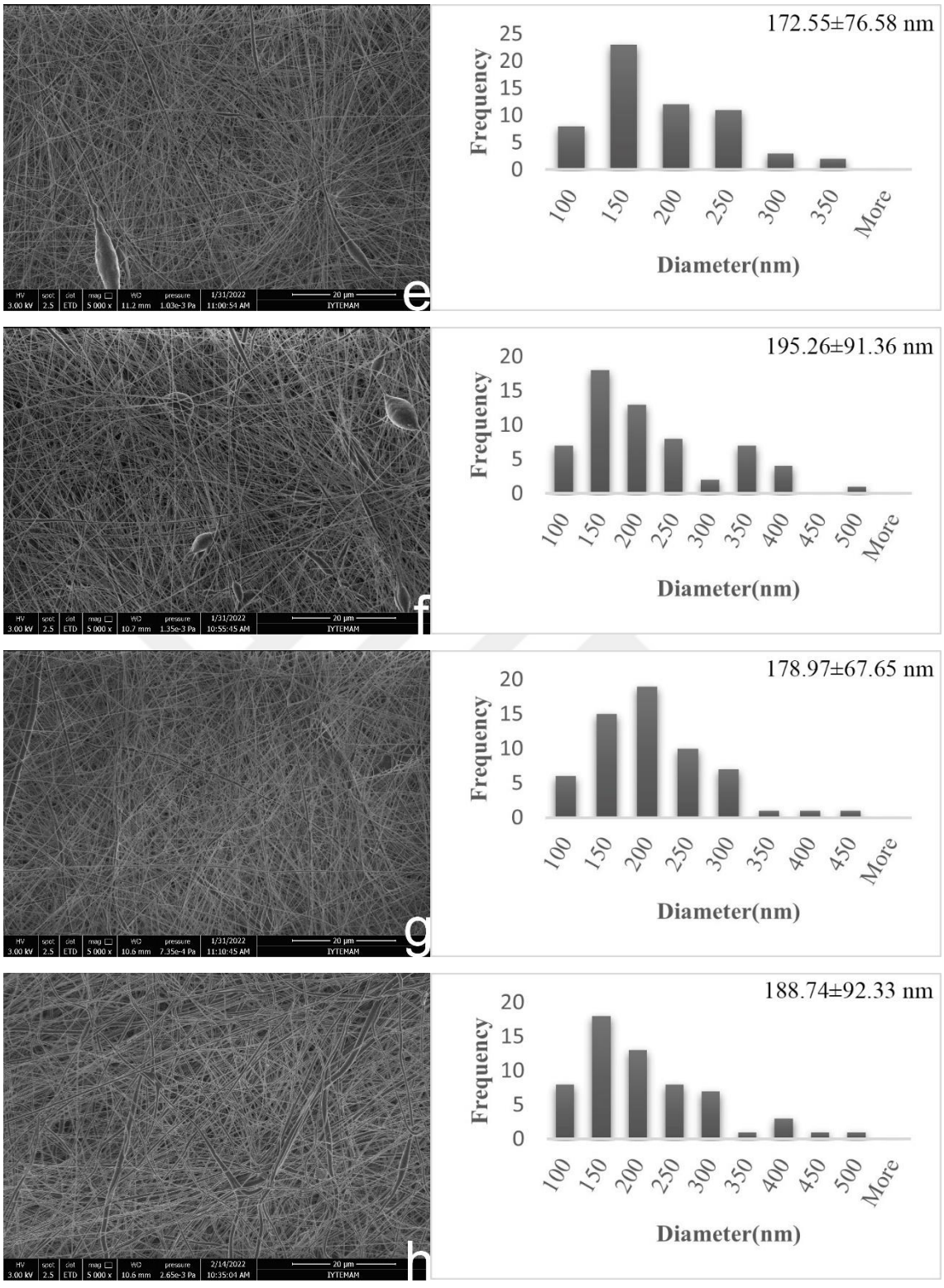

Figure 3.13 SEM images (5 000x) of the nanofibers, obtained from solution with 10% PCL (w v^{-1}) and 0.2% PBE(w v^{-1}) at (e) V=20 kV; Q=0.5 mL h^{-1}, (f) V=25 kV; Q=0.5 mL h^{-1}, (g) V=20 kV; Q=0.4 mL h^{-1} (h) V=25 kV; Q=0.4 mL h^{-1}

SEM images (5 000x) of the nanofibers obtained from the solution of 10% PCL (w v^{-1}) and 0.2% (w v^{-1}) PBE for different electrospinning conditions are illustrated in Figure 3.13. Compared to the films electrospun from plain PCL solutions, smaller and fewer beads were observed in films electrospun with a flow rate of 0.5 mL h^{-1} whereas there were no beads in films electrospun with a flow rate of 0.4 mL h^{-1}. While the electrospinning conditions affected the presence of bead within nanofibers, they did not have a significant effect on the fiber diameter in films containing 0.2% (w v^{-1}) PBE (Table 3.7).

SEM images (5 000x) of the nanofibrous films obtained from a solution with 10% PCL (w v^{-1}) and 0.4% PBE (w v^{-1}) for different electrospinning conditions are shown in Figure 3.14. Only the film containing 0.4% (w v^{-1}) PBE electrospun with a voltage of 20 kV and a flow rate of 0.4 mL h^{-1} had bead-free and uniform nanofibers. Similar to films containing 0.2% (w v^{-1}) PBE, electrospinning conditions had impact on the bead formation, but they did not have any statistically significant impact on the diameter of fibers in films including 0.4% (w v^{-1}) PBE (Table 3.7).

SEM images (5 000x) of the nanofibrous films obtained from a solution with 10% PCL (w v^{-1}) and 0.6% PBE (w v^{-1}) for different electrospinning conditions are shown in Figure 3.15. The electrospun films containing 0.6% PBE (w v^{-1}) electrospun with a voltage of 20 kV had bead-free and uniform morphologies. Similar to films without PBE, process conditions had an impact on the fiber diameter of films containing 0.6% (w v^{-1}) PBE. Films electrospun with a voltage of 20 kV and a flow rate of 0.4 mL h^{-1}, and films electrospun with a voltage of 25kV and a flow rate of 0.5 mL h^{-1} had similar and smaller fiber diameters compared to the other two films. Higher electrospinning voltages (25 kV) and lower flow rates (0.4 mL h^{-1}) gave the highest-fiber diameter for all films fabricated from solutions of different PBE concentrations.

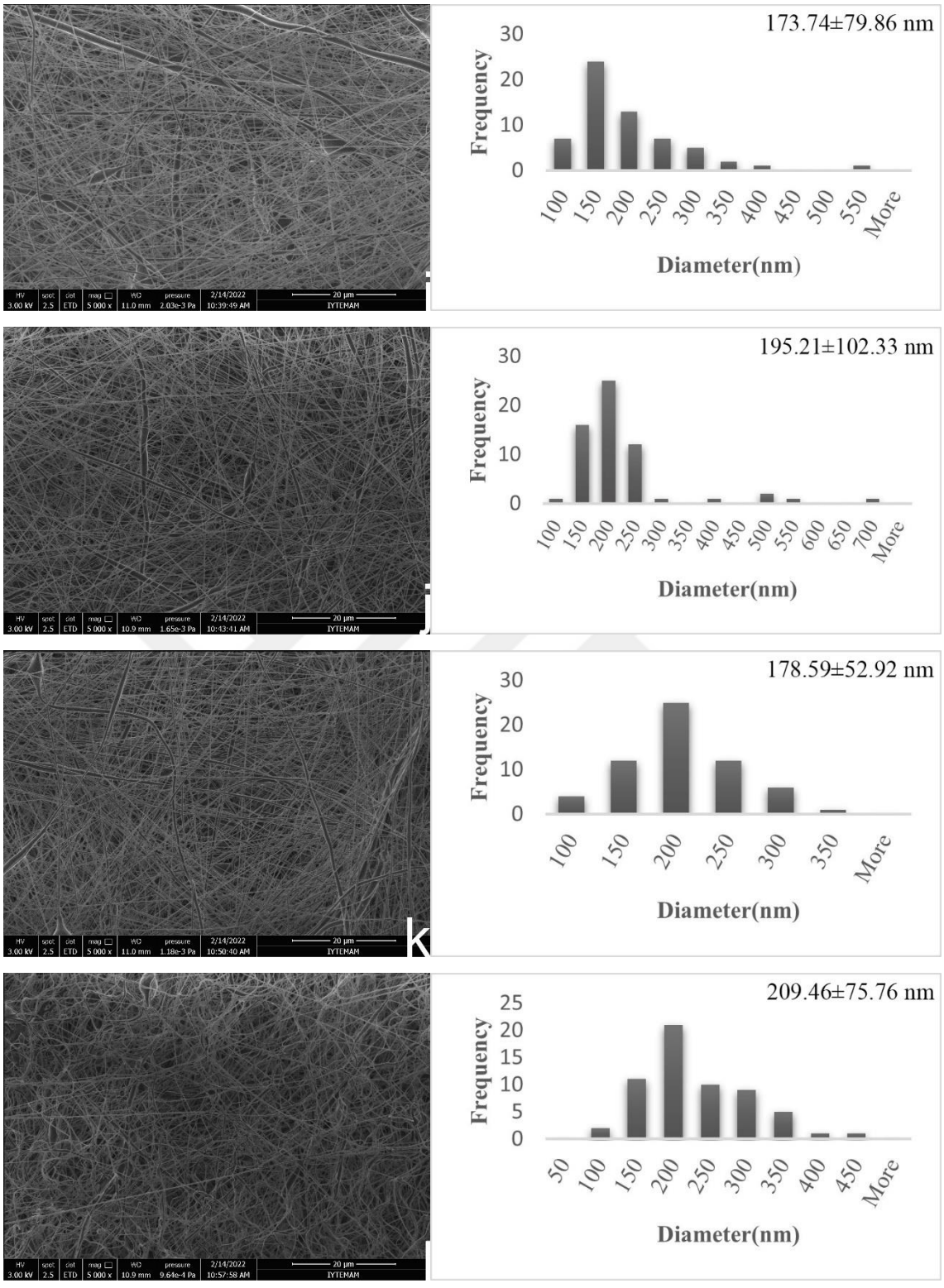

Figure 3.14 SEM images (5 000x) of the nanofibers, obtained from solution with 10% PCL (w v^{-1}) and 0.4% PBE (w v^{-1}) at (i) V=20 kV; Q=0.5 mL h^{-1}, (j) V=25 kV; Q=0.5 mL h^{-1}, (k) V=20 kV; Q=0.4 mL h^{-1} (l) V=25 kV; Q=0.4 mL h^{-1}

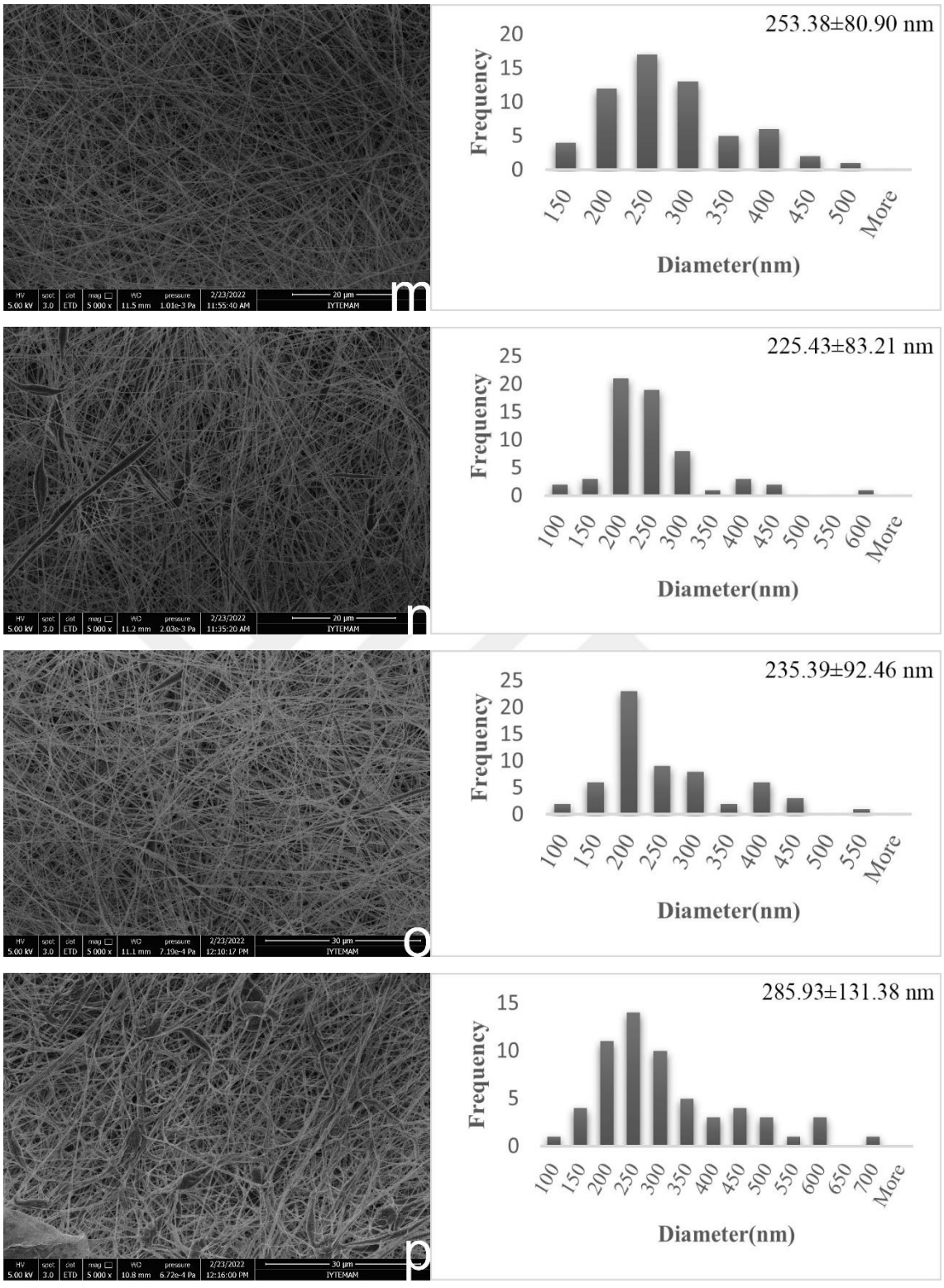

Figure 3.15 SEM images (5 000x) of the nanofibers, obtained from solution with 10% PCL (w v^{-1}) and 0.6% PBE(w v^{-1}) at (m) V=20 kV; Q=0.5 mL h^{-1}, (n) V=25 kV; Q=0.5 mL h^{-1}, (o) V=20 kV; Q=0.4 mL h^{-1} (p) V=25 kV; Q=0.4 mL h^{-1}

Table 3.7 Fiber Diameter (nm) Results by Image J analysis

Fiber Diameter(nm)				
(V(kV); Q(ml h^{-1})	**10% PCL (w v^{-1}) & 0% PBE (w v^{-1})**	**10% PCL (w v^{-1}) & 0.2% PBE (w v^{-1})**	**10% PCL (w v^{-1}) & 0.4% PBE (w v^{-1})**	**10% PCL (w v^{-1}) & 0.6% PBE (w v^{-1})**
20 kV; 0.5 ml h^{-1}	111.99 ± 52.16^{cC}	172.55 ± 76.58^{aB}	173.74 ± 79.86^{aB}	253.38 ± 80.90^{abA}
25 kV; 0.5 ml h^{-1}	123.82 ± 48.22^{bcB}	195.26 ± 91.36^{aA}	195.21 ± 102.33^{aA}	225.43 ± 83.21^{bA}
20 kV; 0.4 ml h^{-1}	145.92 ± 50.05^{abC}	178.97 ± 67.65^{aB}	178.59 ± 52.92^{aB}	235.39 ± 92.46^{bA}
25 kV; 0.4 ml h^{-1}	159.06 ± 61.37^{aC}	188.74 ± 92.33^{aBC}	209.46 ± 75.76^{aB}	285.93 ± 131.38^{aA}

Columns with different lowercase letters differ statistically for electrospinning conditions ($p\leq0.05$)

Rows with different uppercase letters differ statistically for PBE concentrations ($p\leq0.05$)

Overall, it can be concluded that as the PBE concentration increased, fiber morphology has become more bead-free and uniform for all electrospinning conditions. Films without PBE had the lowest fiber diameter whereas films with 0.6% (w v^{-1}) PBE had the highest fiber diameter for all electrospinning conditions, which can be attributed to the subsequent increase in solution viscosities. Films with 0.2% (w v^{-1}) PBE and 0.4% (w v^{-1}) PBE had similar nanofiber diameters for each electrospinning condition. Based on the fact that the apparent viscosities of these solutions were also statistically indifferent, it is interpreted that solution viscosity was the most important processing parameter administering the fibre diameter. According to Sun et al., the increase in the solution viscosity increases the viscoelasticity of the polymer jet, making the stretching of fibers more difficult, thereby increasing the diameter of the fibers (Sun et al. 2014). The results are in accordance with the literature. Duan et al. (2021) revealed that the surface of pullulan-chitin nanofibers with curcumin and anthocyanin was smoother and more uniform compared to pullulan-chitin nanofibers, and the diameter of the nanofibers increased with the addition of them. Pullulan-chitin nanofibers, pullulan-chitin nanofibers with curcumin, pullulan-chitin nanofibers with anthocyanin, pullulan-chitin nanofibers with both curcumin and anthocyanin had average diameters of 176.81±43.14, 284.19±69.61, 271.25±109.76, and 379.07±100.14 nm, respectively (Duan et al. 2021).

In addition, Prietto et al. (2018) produced pH-sensitive nanofibers based on zein (30 % w v^{-1}) and red cabbage anthocyanins (3, 4, and 5% w v^{-1}). SEM images demonstrated formation of continuous fibers with smooth surfaces. The average diameter of fibers increased by increasing anthocyanins concentration, ranged from 444 nm for neat zein fibers to 510 nm for fibers comprising 5% (w v^{-1}) anthocyanins (Prietto et al. 2018). Similar to these studies, Sun et al (2020) observed that the fiber diameter of poly-l-lactic acid nanofibers had an obvious beaded structure. However, when blueberry anthocyanin was added to poly-l-lactic acid, the beaded structure gradually disappeared (Sun et al., 2020). Terra et al. (2021) fabricated PCL/PEO nanofibers without dyes, which exhibited uniform morphology and an average fiber diameter of 316±27 nm (Terra et al., 2021). The average diameter obtained for the PCL/PEO nanofibers with 1% (w v^{-1}) phycocyanin was 899±145 nm. For the PCL/PEO nanofibers with 2% (w v^{-1}) phycocyanin, the diameter was measured as 850±123 nm, while for PCL/PEO nanofiber with 2% (w v^{-1}) of the curcumin was 550±117 nm. They used 2% (w v^{-1}) of curcumin with phycocyanin (0.5 and 1%, w v^{-1}), the nanofibers exhibited diameters of 570±127 nm and 587±101 nm, respectively. Similar behavior was found by Moreira et al., who developed nanofibers of concentrated microalgae protein and found that by increasing the concentration of this macromolecule, there was an increase in the diameter of the polymeric nanofiber (Moreira et al., 2019). In all of the abovementioned studies, the increase in fibre diameters with the incorporation of additives can be attributed to the subsequent increase in the viscosity of the electrospinning polymer solutions.

On the other hand, there are also studies that have reported reduction in fibre diameters with the addition of dyes/extracts in the literature, which was due to the subsequent decrease in solution viscosities. Haider and colleagues (2018) underlined that stretched droplets, elongated droplets, and spherical beads can be created by lowering the viscosity of the electrospinning fluid. Schoolaert et al. (2016) developed two types of halochromic nanofibers using a mixture of chitosan and poly(-caprolactone) with methyl red or rose bengal. The electrospinning was unaffected by the presence of dye in the polymer solution. In each case, the technique resulted in the creation of beadless and uniform strand nanofibers similar to this study. The nanofiber diameters in nanofibrous membranes containing Rose Bengal was determined using SEM images. The fiber diameters of nanofibrous membranes containing Rose Bengal (85±22 nm) were much smaller than the fiber diameters of membranes with the Methyl Red (250±27 nm) and the fiber diameters of membranes without dyes (258±74 nm). The difference can be explained

by increased solubility and reduced viscosity of chitosan after dye modification. Similar trend was observed in Pakolpakçıl et al. (2018). They used a 2:1 blend of 2% w w^{-1} PVA and 1% w w^{-1} sodium alginate (NaAlg) solution, as well as 2–3% red cabbage extract, to create pH-responsive electrospun nanofibers. The SEM pictures revealed that smooth, beadless, uniform, and continuous fiber mats with an average fibre diameter of 263 nm were produced without extract. The fibers with the extract have a beaded appearance whereas the average diameter of the fibres were reduced to 234 nm in nanofibrous mats electrospun from the solution containing the extracts due to the action of anthocyanins on the lowering of viscosity and conductivity of the solution. In conclusion, whether or not the fibre diameter will decrease upon the incorporation of extracts to the electrospinning solution seem to depend on the change in solution viscosity. If the interactions between the electrospinning polymers and the extracts cause a structure build-up in the solution resulting in elevated viscosities, then the fibre diameters tend to increase. In the opposite case structure break-down results in reduced viscosities, thus fibre diameters tend to decrease.

3.2.3. Film Thickness of Nanofiber Mats

Film thickness (μm) results for 10% PCL (w v^{-1}) films with different concentrations of PBE produced at different electrospinning conditions are displayed in Table 3.8. In general, the thicknesses of the nanofibrous mats ranged between 83 and 192 μm. Unfortunately, it was not possible to fabricate nanofibrous mats with uniform thicknesses (as indicated by the relatively large standard deviations) due to the limitations imposed by the instrument. Therefore, it is hard to make a clear and reliable interpretation about the effects of processing parameters on film thickness. Some improvements in the instrumental setup such as use of multiple ejection nozzles and maintenance of a more controlled environment (constant T and humidity) should be considered in order to obtain more homogeneous films in future studies

Table 3.8 Film thickness (μm) results for 10% PCL (w v^{-1}) films with different concentrations of PBE produced at different electrospinning conditions

Film thickness (μm)				
(V(kV); Q(ml h^{-1})	**10% PCL (w v^{-1}) & 0% PBE (w v^{-1})**	**10% PCL (w v^{-1}) & 0.2% PBE (w v^{-1})**	**10% PCL (w v^{-1}) & 0.4% PBE (w v^{-1})**	**10% PCL (w v^{-1}) & 0.6% PBE (w v^{-1})**
20 kV; 0.5 ml h^{-1}	117.40±26.91^{bA}	92.00±37.22^{aAB}	83.30±12.57^{bB}	92.80±12.68^{bAB}
25 kV; 0.5 mlh^{-1}	142.70±40.12^{abB}	121.90±18.22^{aB}	132.40±26.98^{aB}	192.50±57.78^{aA}
20 kV; 0.4 mlh^{-1}	122.10±14.40^{abA}	103.70±29.07^{aAB}	108.80±15.05^{aAB}	95.60±19.59^{bB}
25 kV; 0.4 ml h^{-1}	151.30±23.71^{aA}	117.50±5.68^{aAB}	114.40±21.61^{aB}	146.80±48.55^{aAB}

Columns with different lowercase letters differ statistically for electrospinning conditions ($p \leq 0.05$)

Rows with different uppercase letters differ statistically for PBE concentrations ($p \leq 0.05$)

3.2.4. Color Analysis of the Electrospun PCL Nanofibrous Mats to pH Change

The color change due to pH variation is the most critical criterion to assess whether the electrospun films can be used as a pH-indicator intelligent packaging material. Rapid color change with pH change and the ability to differentiate color change with naked eye are the most crucial attributes that are expected from intelligent packaging systems (Forghani, Almasi, and Moradi 2021). Color analyses of 16 different electrospun films (1.5 cm x 1.5 cm) with two replicates were performed in order to determine the effects of electrospinning conditions and PBE content on the color change response to pH variation. Each film was immersed in 2 mL pH buffer solutions ranging from pH 1 to 10. The color change of each film was measured without drying. The time required to observe a visible color change in films fabricated with 10% PCL (w v^{-1}) containing 0.2% PBE (w v^{-1}) was 5 min, whereas it took only 4-5 s to observe a color change in films fabricated with 10% PCL (w v^{-1}) containing 0.4% (w v^{-1}) and 0.6% PBE (w v^{-1}), which was similar to various studies in literature. For example, Zhang et al. (2011) fabricated pH indicator films using polyacrylonitrile (PAN), polyamide 66 (PA66), and phenolphthalein as dye

using a two-nozzle electrospinning process. The membranes responded to pH change over 5 s with a color variation from light yellow to violet in buffer solutions for pH ranging from 7 to 14 (Zhang et al. 2011). In a study conducted by Prietto et al. (2018), 3-5 s was required for a visible color change in zein films containing red cabbage extracts when immersed in pH buffers (Prietto et al. 2018). Agarwal et al. (2012) also reported that nylon 6 nanofibrous films encapsulating a mixture of synthetic dyes (phenol red, methyl red, bromothymol blue, phenolphthalein, and bromocresol green) gave a color response in 3 s from red to orange, yellow, green, and eventually to blue by increasing in pH values ranging from 1 to 10 (Agarwal et al. 2012).

Total color change (ΔE) response to pH is the most important criterion in order to assess the usage of nanofibrous films as pH-indicator packaging materials. In the literature, it has been reported that an observer cannot detect a color difference with naked eye for values of ΔE below 1; only trained observers can detect the difference for values between 1 and 2; inexperienced observers can notice a color difference between 2 and 3.5; the color difference is evident for ΔE between 3.5 and 5; and any observer can easily notice different colors for values of ΔE greater than 5 (Mokrzycki & Tatol, 2011). Similar to study of Mokryzci and Tatol, Barba et al. (2013) determined that the color difference was not noticeable for ΔE below 1.5; the difference was slightly noticeable for ΔE between 1.5–3.0; the difference was clearly visible for ΔE between 3–6; the color difference was great when ΔE was higher than 6 (Barba, Esteve, and Frigola 2013). The L* , a* and b* parameters were used to calculate ΔE values for each electrospun nanofibrous film undergoing color change at different pH values. This type of calculation guarantees perceptible changes from one pH to another. Silva et al., Moreira et al., and Prietto et al. calculated ΔE values using this approach (C. K. da Silva et al. 2019; Moreira et al. 2018; Prietto et al. 2018). As control groups, films fabricated using no PBE were also treated the same way as those fabricated with PBE.

Table 3.9 Photographs of pH-indicator nanofibrous films fabricated with 10% (w v^{-1}) PCL using different concentrations of PBE under various spinning conditions taken at constant lighting conditions (V as kV; Q as mL h^{-1}; PBE as % w v^{-1})

V	**Q**	**PBE**	**pH 1**	**pH 2**	**pH 3**	**pH 4**	**pH 5**	**pH 6**	**pH 7**	**pH 8**	**pH 9**	**pH 10**
20	0.5	0										
25	0.5	0										
20	0.4	0										
25	0.4	0										
20	0.5	0.2										
25	0.5	0.2										
20	0.4	0.2										
25	0.4	0.2										
20	0.5	0.4										
25	0.5	0.4										
20	0.4	0.4										
25	0.4	0.4										
20	0.5	0.6										
25	0.5	0.6										
20	0.4	0.6										
25	0.4	0.6										

Photographs of electrospun films dipped in different pH buffers ranging from 1 to 10 under the same lighting conditions are illustrated in Table 3.9. As expected, there is no noticeable color change with pH in the films belonging to the control groups (0% w v^{-1} PBE) (Appendix C, Table C1). Although there seems to be noticeable color differences between the pictures belonging to the lowest and highest pH's in films of 10% PCL (w v^{-1}) containing 0.2% PBE (w v^{-1}), the color change (ΔE) values between all successive pH's were not high enough to be considered in easily detectable regime (Appendix C). Besides, their response times (~5 min) were high. Therefore, the films with 0.2% PBE (w v^{-1}) cannot be considered as efficient pH-indicator films for which they were excluded from the rest of the analyses.

Color change (ΔE) values at pH 2-10 for electrospun films containing 0.6% PBE (w v^{-1}) (V=20 kV; Q=0.5 mL h^{-1}) are shown in Table 3.10. Since according to both Mokrzycki (2011) and Barba (2013) color changes of ΔE > 2 are considered as noticable by inexperienced observers, 10% PCL (w v^{-1}) films containing 0.6% PBE (w v^{-1}) fabricated with V=20 kV and Q=0.5 mL h^{-1} have the potential to be used as pH-indicator films (except for the pH range 1-2 at which (ΔE) value is below 1.5). Very good color changes were observed for the pH 5, 9 and 10. Additionally, untrained observers can easily notice the difference for all conditions (pH values) when the pH changes by two units. The color change (ΔE) values at pH 2-10 for electrospun films containing 0.4% PBE (w v^{-1}) (V=20 kV; Q=0.5 mL h^{-1}) are shown in Table 3.11. The results indicate that these nanofibrous mats also have the potential to be used as pH-indicator films except for the pH range 2-3 where ΔE was smaller than 1.5. Very good color changes were observed for the pH 4, 5 and 9. Similar to films containing 0.6% PBE (w v^{-1}) , untrained observers can easily notice the difference for all conditions (pH values) when the pH changes by two units with the films containing 0.4% PBE (w v^{-1}) .

Color change (ΔE) values at pH 2-10 for electrospun films containing 0.6% PBE (w v^{-1}) (V=25 kV; Q=0.5 mL h^{-1}) are shown in Table 3.12 whereas color change (ΔE) values at pH 2-10 for electrospun films containing 0.4% (w v^{-1}) PBE (V=25 kV; Q=0.5 mL h^{-1}) are shown in Table 3.13 Both of the films have the potential to be used as pH-indicators except for pH between 2-3. They have shown similar color change responses. Very good-to-excellent color change (ΔE) values which can easily be detected by any observer were determined for pH 5 and 9. Additionally, untrained observers can easily notice the difference very clearly for all conditions (pH values) when the pH changes by two units.

Color change (ΔE) values at pH 2-10 for electrospun films containing 0.6% PBE (w v^{-1}) (V=20 kV; Q=0.4 mL h^{-1}) are shown in Table 3.14. The films can be used as pH-indicators except for pH between 2-3. Excellent color change (ΔE) values were observed for pH 4 and 9. Additionally, untrained observers can easily notice the difference very clearly for all conditions (pH values) when the pH changes by two units. The color change (ΔE) values at pH 2-10 for electrospun films containing 0.4% PBE (w v^{-1})(V=20 kV; Q= 0.4 mL h^{-1}) are shown in Table 3.15. The results indicate that these films can be used as pH-indicators except for the pH range 2-3. Very good-to-excellent color change (ΔE) values were observed for the pH 5 and 9. Unexperienced observers can very easily notice the difference for all conditions (pH values) when the pH changes by two units with the films containing 0.4% PBE (w v^{-1}).

Table 3.10 Color change (ΔE) values at pH 2-10 for 10% PCL (w v^{-1}) films containing 0.6% (w v^{-1}) PBE (V=20 kV; Q=0.5 mL h^{-1})

pH	2	3	4	5	6	7	8	9	10
1	1.61± 0.35	3.62±0.77	7.30±2.27	12.79±0.85	14.25±0.96	15.30±0.33	17.71±0.22	21.95±0.10	23.08±0.36
2		2.41±0.27	6.22±1.68	11.89±1.55	13.14±0.42	14.02±0.87	16.49±0.83	20.82±0.74	22.14±0.97
3			3.86±1.46	9.59±1.79	10.87±0.24	11.80±1.03	14.25±0.97	18.73±0.74	19.97±1.12
4				5.77±3.23	7.10±1.24	8.27±2.41	10.58±2.35	15.20±1.92	16.24±2.53
5					3.29±0.27	5.29±1.11	6.35±0.04	10.50±1.04	10.83±0.42
6						2.77±0.25	3.91±0.61	8.43±0.30	9.41±1.51
7							2.74±0.30	7.72±0.01	9.86±0.67
8								5.33±0.57	7.42±0.12
9									4.50±1.48

Table 3.11 Color change (ΔE) values at pH 2-10 for 10% PCL (w v^{-1}) films containing 0.4% (w v^{-1}) PBE (V=20 kV; Q=0.5 mL h^{-1})

pH	2	3	4	5	6	7	8	9	10
1	3.18±1.56	2.63±1.13	6.59±1.48	11.39±3.75	13.43±2.94	16.39±5.02	17.51±4.32	21.37±3.73	21.80±5.65
2		1.33±0.35	5.21±2.55	10.08±0.15	12.00±0.89	14.82±1.42	15.91±0.82	19.99±0.04	20.58±1.91
3			5.33±1.01	10.24±1.49	12.03±0.63	14.89±3.04	15.86±2.27	19.98±1.51	20.65±3.44
4				5.00±2.45	6.95±1.46	10.09±3.36	11.29±2.58	15.08±2.26	15.60±4.37
5					2.78±0.04	5.53±0.64	7.26±0.56	10.49±0.26	10.78±2.14
6						3.70±1.51	4.81±0.66	8.22±0.79	8.99±2.92
7							2.76±1.29	6.05±0.96	7.00±0.10
8								4.89±1.24	6.95±0.46
9									3.14±0.83

Table 3.12 Color change (ΔE) values at pH 2-10 for 10% PCL (w v^{-1}) films containing 0.6% (w v^{-1}) PBE (V=25 kV; Q=0.5 mL h^{-1})

pH	2	3	4	5	6	7	8	9	10
1	3.30±1.88	4.58±1.94	7.87±2.70	13.59±1.02	17.54±0.35	17.86±3.17	19.98±2.53	25.68±3.60	28.17±3.37
2		1.41±0.20	4.86±0.97	10.82±0.88	14.65±1.44	14.78±1.33	16.89±0.57	22.76±1.71	25.49±1.58
3			3.50±0.71	9.55±1.25	13.32±1.70	13.43±1.16	15.58±0.43	21.46±1.51	24.22±1.31
4				6.12±2.03	9.86±2.38	10.04±0.44	12.25±0.13	18.12±0.81	20.90±0.59
5					4.28±1.02	5.80±0.38	7.41±1.12	12.77±2.07	15.22±2.19
6						3.27±0.23	3.67±2.36	8.72±2.80	11.49±2.52
7							2.76±0.26	8.62±0.24	12.12±0.02
8								6.65±1.14	10.43±1.38
9									4.39±0.25

Table 3.13. Color change (ΔE) values at pH 2-10 for 10% PCL (w v^{-1}) films containing 0.4% (w v^{-1}) PBE (V=25 kV; Q=0.5 mL h^{-1})

pH	2	3	4	5	6	7	8	9	10
1	2.76±1.44	3.23±0.26	5.96±0.12	11.14±0.38	15.19±1.14	17.24±1.35	19.24±0.96	24.83±0.57	27.09±0.08
2		1.54±0.15	3.39±1.47	8.69±1.34	12.74±0.47	14.68±0.19	16.72±0.49	22.45±0.99	24.80±1.48
3			3.06±0.07	8.38±0.15	12.34±0.93	14.24±1.20	16.18±0.74	21.98±0.28	24.43±0.13
4				5.38±0.10	9.39±0.99	11.33±1.23	13.39±0.89	19.14±0.42	21.60±0.11
5					4.20±0.74	6.53±0.51	8.76±0.35	14.02±0.22	16.50±0.41
6						2.76±0.39	4.94±0.28	9.86±0.56	12.46±1.19
7							2.57±0.25	8.34±1.01	11.27±1.48
8								6.69±0.89	10.01±0.82
9									3.85±0.23

Table 3.14 Color change (ΔE) values at pH 2-10 for 10% PCL (w v^{-1}) films containing 0.6% (w v^{-1}) PBE (V=20 kV; Q=0.4 mL h^{-1})

pH	2	3	4	5	6	7	8	9	10
1	3.92±3.11	4.43±1.39	10.02±1.40	11.95±1.41	16.06±0.44	16.20±1.15	18.69±1.80	22.80±1.83	24.23±1.91
2		1.85±0.87	6.89±2.71	8.81±2.41	12.99±3.45	13.12±2.17	15.44±1.77	20.07±1.45	21.33±1.80
3			6.12±0.52	7.93±0.32	12.10±1.36	12.07±0.31	14.50±0.26	19.01±0.34	20.49±0.22
4				2.54±0.25	6.25±0.78	7.38±0.07	9.34±0.07	13.86±1.36	14.83±0.65
5					4.25±1.13	5.01±0.16	6.97±0.25	11.55±1.29	12.65±0.61
6						3.78±0.74	4.27±0.64	7.98±2.31	8.85±1.36
7							2.89±1.20	7.53±0.41	9.79±0.69
8								6.24±0.76	7.59±0.48
9									4.59±3.18

Table 3.15 Color change (ΔE) values at pH 2-10 for 10% PCL (w v^{-1}) films containing 0.4% (w v^{-1}) PBE (V=20 kV; Q=0.4 mL h^{-1})

pH	2	3	4	5	6	7	8	9	10
1	2.33±0.17	4.04±0.35	7.84±2.20	12.65±1.53	16.11±1.72	17.81±1.22	19.49±1.54	24.06±2.69	25.19±3.13
2		1.80±0.26	5.72±2.24	10.63±1.59	14.07±1.79	15.70±1.23	17.39±1.55	22.12±2.81	23.36±3.30
3			4.00±1.90	8.94±1.23	12.33±1.47	13.92±0.97	15.62±1.31	20.40±2.54	21.72±2.96
4				4.97±0.65	8.45±0.37	10.20±0.83	12.04±0.38	16.65±0.75	17.90±1.23
5					3.64±0.24	5.89±0.34	7.89±0.15	11.88±1.29	12.98±1.93
6						2.72±0.44	4.65±0.00	8.32±1.06	9.74±1.58
7							2.07±0.54	7.16±1.65	9.48±1.60
8								6.10±1.39	8.95±1.10
9									3.56±0.92

Table 3.16 Color change (ΔE) values at pH 2-10 for 10% PCL (w v^{-1}) films containing 0.6 % (w v^{-1}) PBE (V=25 kV; Q=0.4 mL h^{-1})

pH	2	3	4	5	6	7	8	9	10
1	4.17±1.28	5.55±1.19	7.44±1.99	14.22±2.72	16.47±2.22	18.59±1.57	20.47±2.13	24.99±3.24	27.52±4.97
2		2.32±1.67	4.03±2.74	10.44±4.34	12.69±3.85	14.71±3.06	16.67±3.47	21.25±4.74	23.95±6.63
3			2.12±0.84	9.00±1.60	11.25±1.22	13.24±0.47	15.15±1.03	19.93±2.30	22.68±4.17
4				7.20±0.54	9.36±0.18	11.31±0.55	13.14±0.10	17.97±1.24	20.77±3.10
5					2.39±0.39	4.70±0.88	6.88±0.58	11.38±1.16	14.01±2.89
6						2.63±0.04	4.77±0.03	9.08±1.50	11.77±3.09
7							2.57±0.20	7.22±2.02	10.36±3.94
8								5.75±1.06	9.19±3.07
9									3.87±2.50

Table 3.17 Color change (ΔE) values at pH 2-10 for 10% PCL (w v^{-1}) films containing 0.4% (w v^{-1}) PBE (V=25 kV; Q=0.4 mL h^{-1})

pH	2	3	4	5	6	7	8	9	10
1	2.23±1.21	3.43±0.31	6.20±0.89	11.11±1.00	13.94±0.72	15.94±0.46	17.29±0.28	22.64±0.35	23.10±2.90
2		1.39±0.66	4.13±0.21	8.97±0.32	11.80±0.56	13.79±0.74	15.19±0.84	20.53±1.63	21.03±4.23
3			2.86±0.49	7.93±0.61	10.71±0.36	12.59±0.12	13.95±0.02	19.44±0.72	20.01±3.34
4				5.42±0.58	8.09±0.12	9.88±0.41	11.26±0.67	16.83±1.11	17.48±3.66
5					3.03±0.22	5.63±0.36	7.45±0.33	11.85±1.52	12.37±4.19
6						2.99±0.05	4.86±0.01	8.87±1.25	9.52±3.95
7							1.95±0.09	7.34±0.71	8.57±3.28
8								6.79±0.04	8.37±2.38
9									2.70±1.16

Color change (ΔE) values at pH 2-10 for electrospun films containing 0.6% PBE (w v^{-1}) (V=25 kV; Q=0.4 mL h^{-1}) are shown in Table 3.16. The films have the potential to be used as pH-indicators for all of the successive pH ranges, however the degree of noticability was found to be rather low as ΔE values ranged between 2-2.5 for a few pH's. Excellent color change (ΔE) values were observed for the pH 5 and 9. Additionally, untrained observers can very easily notice the difference for all conditions (pH values) when the pH changes by two units. The color change (ΔE) values at pH 2-10 for electrospun films containing 0.4% PBE (w v^{-1}) (V=25 kV; Q=0.4 mL h^{-1}) are shown in Table 3.17. The films can be used as pH-indicators except for the pH between 2-3 and 7-8. Excellent color change (ΔE) values were observed for the pH 5 and 9. Inexperienced observers can easily notice the difference for all conditions (pH values) when the pH changes by two units with the films containing 0.4% PBE (w v^{-1}).

Overall, the color response to pH change analyses for the films fabricated from 10% PCL (w v^{-1}) incorporating 0.4% and 0.6% PBE (w v^{-1}) showed similar results. Therefore, the choice of which films to continue the remaining analyses was based on the SEM results. SEM imaging gave the most beadles and uniform nanofibrous mats when the spinning conditions were V=20 kV and Q=0.4 mL h^{-1} for both types of solutions. Therefore, for the sake of reproducibility of the results, films electrospun at 20 kV and 0.4 mL h^{-1} from 10% PCL (w v^{-1}) containing 0.4% PBE (w v^{-1}) and 0.6 % PBE (w v^{-1}) were subjected to further analyses.

3.2.5. Mechanical Analysis of the Electrospun PCL Nanofibrous Films

Table 3.18 lists the mechanical properties of nanofibrous films electrospun from 10% PCL (w v^{-1}) solution containing different PBE concentrations % (w v^{-1}) using a voltage of 20 kV and a flow rate of 0.4 mL h^{-1}.

Table 3.18 The mechanical properties of nanofibrous films electrospun from 10 % PCL (w v^{-1}) solution containing different PBE concentrations % (w v^{-1}) at V=20 kV; Q=0.4 mL h^{-1}

10% PCL (w v^{-1})	**Film Thickness(µm)**	**Tensile Strength (TS)(MPa)**	**Elongation At Break (%) (EB)**	**Young's Modulus (MPa) (YM)**
0% PBE (w v^{-1})	122.10±14.40^{a}	4.90±2.67^{a}	55.46±11.29^{b}	0.11±0.05^{a}
0.4% PBE (w v^{-1})	108.80±15.05^{ab}	3.80±0.99^{ab}	82.26±21.79^{a}	0.09±0.01^{a}
0.6% PBE (w v^{-1})	95.60±19.59^{b}	2.47±0.34^{b}	85.15±19.36^{a}	0.08±0.01^{a}

Columns with different lowercase letters differ statistically for electrospinning conditions ($p \leq 0.05$) (n=8)

Hu et al. (2018) studied mechanical properties of electrospun zein/poly(e-caprolactone) composites. TS, EB and YM values were found as 12.36 MPa, 49.29 % and 0.152±0.074 GPa, respectively for the films with a zein/PCL ratio of 0/100 (w w^{-1}) (Hu et al. 2018). These values were close to this study except for TS value. This can be originated from the solvent used in their study which were DMF, acetic acid and DCM, while the solvents used in this study were DMF and chloroform. In addition, the applied voltage was fixed at 15-20 kV; solution flow rate was 0.3-1 mL h^{-1}; needle diameter was 1.0 mm; and the collecting distance was 6-10 cm. These electrospinning conditions were also different from this study. Hence, it was quite normal to have changes in mechanical properties. Similar to this study, Montenegro-Nicolini et al (2018) reported that electrospun PCL films (11-18% w v^{-1}) had EB as 59.323±9.569 which was very close to in this study 10% PCL (w v^{-1}) without PBE, but TS value was recorded as 0.433±0.076 MPa which was nearly 1/10 of this study. Besides, they found YM as 0.043±0.006 Mpa which was approximately 1/2 of this study (Montenegro-nicolini et al. 2018). These changes can be related with differences in electrospinning conditions. Liu and colleagues (2022) created bilayer colorimetric film incorporating polycaprolactone (PCL) with clitoria ternatea Linn anthocyanin via electrospinning. They found that film (without anthocyanin) thickness was 0.058±0.015mm; TS was 7.935±2.043 MPa and EB % was 215.036±10.781, whereas film without anthocyanin thickness was 0.122±0.014mm; TS

was 4.90±2.67 MPa and EB % was 55.46±11.29 in this study. Based on these results, film thickness can influence the mechanical properties (Liu et al. 2022)

It was clear that film thickness and TS values were decreased and EB values were increased significantly as the PBE content increased in the film, whereas YM values were similar for each film according to Table 3.18. This behavior was supported by the study conducted by Duan et al (2021). The TS values of the pullulan-chitin nanofibers, pullulan-chitin nanofibers with curcumin , pullulan-chitin nanofibers with anthocyanin, a pullulan-chitin nanofibers with curcumin and anthocyanin nanofibers were 5.36 ± 3.82, 4.48 ± 4.77, 1.74 ± 0.15, and 4.3 ± 4.11 MPa, while the EB of nanofibrous mats were 7.45% ± 2.66%, 8.12% ± 4.65%, 24.55% ± 1.72%, and 10.05% ± 6.83%, respectively. The results showed that the addition of curcumin and anthocyanin decreased the TS value and increased the EB value of the nanofibers. The pullulan-chitin nanofibers with anthocyanin had a lower TS value and higher EB value than the other nanofibers (Duan et al. 2021). In addition, findings of Shavisi et al (2022) agrred with the results of this study. They produced chitosan-gum arabic nanofiber membranes which presented a significant decrease in TS (6.71 MPa to 3.77 MPa as the Rosa damascena extract content was elevated in nanofibers). A significant reduction in the TS of nanofibrous films was linked to the interactions of phenolic compounds by hydrogen bonds and/or hydrophobic interactions that prevent the polymer chain's interactions and make greater inter-chain distances in the chitosan- gum arabic network. EB (7.68% to 111.43%) values were significantly increased with the amount of Rosa damascena extract within the films. They explained that the extract have acted as a plasticizer that enhanced the mobility of the polysaccharide chains (Shavisi and Shahbazi 2022).

3.2.6. Contact Angle Analysis of the Electrospun PCL Nanofibrous Films

Contact angle measurements give information about the hydrophilicity or hydrophobicity of a surface. PCL is a hydrophobic polymer and is commonly utilized to fabricate water-resistant mats. PCL can be a base material in order to protect the pH indicator films from collapsing upon contact with liquid sample. Contact angle larger than 90° indicates that the mat is hydrophobic; therefore, water will form droplets on its surface, while complete wetting occurs on mats with a water contact angle of 0° in (Yuan

& Lee, 2013). Previous studies have suggested that hydrophilicity is favored for pH-indicator films because a hydrophilic mat allows liquid sample to spread across the surface and enable them to work as indicator.

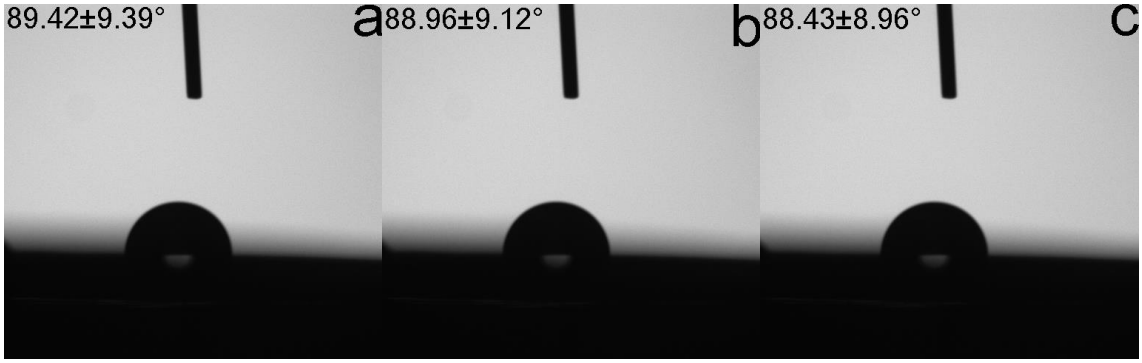

Figure 3.16 Contact angle of 10% PCL (w v^{-1}) films containing 0% PBE (w v^{-1}) fabricated (V=20 kV; Q=0.4 mL h^{-1}) (a) after 2 s (b) after 8 s (c) after 14 s

Contact angle of 10% PCL (w v^{-1}) films without PBE are shown in Figure 3.16 for different time intervals and water formed droplets on their surfaces. The film showed hydrophobic characteristics since water did not spread with time on the surface and the contact angle value was around 90°. Contact angle of 10% PCL (w v^{-1}) films containing 0.4 and 0.6% PBE (w v^{-1}) are illustrated in Figure 3.17 and Figure 3.18 for different time intervals.

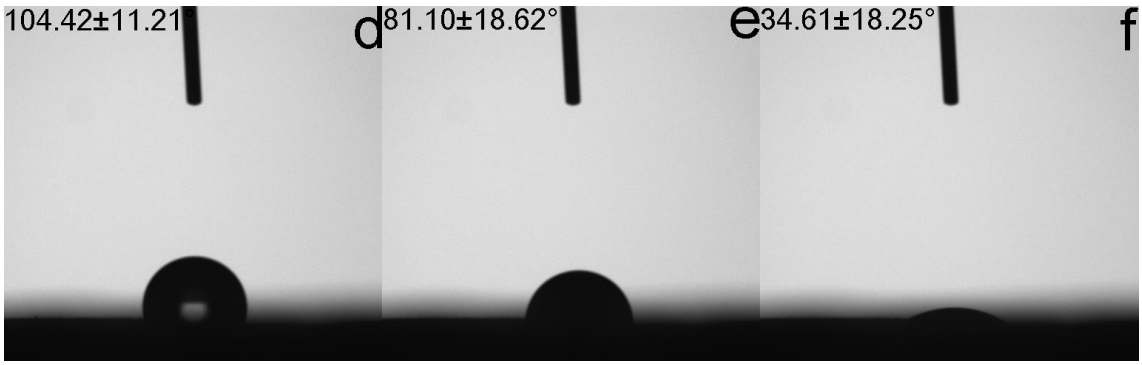

Figure 3.17 Contact angle of 10% PCL (w v^{-1}) films containing 0.4% PBE (w v^{-1}) fabricated (V=20 kV; Q=0.4 mL h^{-1}) (d) after 2 s (e) after 8 s (f) after 14 s

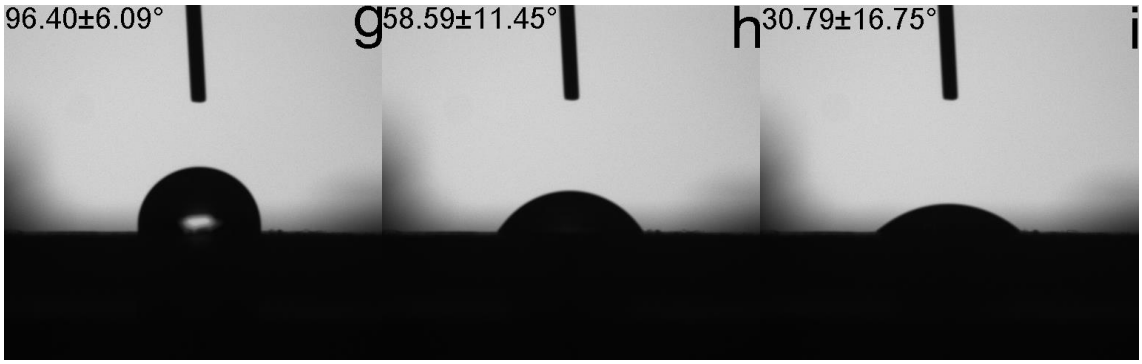

Figure 3.18 Contact angle of 10% PCL (w v^{-1}) films containing 0.6% PBE (w v^{-1}) fabricated (V=20 kV; Q=0.4 mL h^{-1}) (g) after 0.72 s (h) after 1.92 s (i) after 2.88 s

Both films showed hydrophilic behavior since the water spread as the time passes and complete wetting occurred. According to the figures, 10% PCL (w v^{-1}) films containing 0.6% PBE (w v^{-1}) was more hydrophilic than 10% PCL (w v^{-1}) films containing 0.4% PBE (w v^{-1}) as the spreading was faster.

This findings are in agreement with numerous studies in literature. In a study conducted by Jowanska and Parın (2022), thermoplastic polyurethane and polycaprolactone were used as hydrophobic based polymers. The authors found that increase of spirulina amount resulted in a further decrease in water contact angle value of the samples. The amount of 1 wt % spirulina significantly enhanced the hydrophilicity of composite fibers (the contact angle value reduced to around 36° (Nur and Parın 2022)). Study conducted by Jovanska et al (2022) showed a similar results. They added PEO into PCL solution to increase the hydrophilicity of membrane enabling spreading water to allow the samples to contact hibiscus rosa sinensis extract embedded in the fiber to show pH indicator property. Water contact angle for all samples was less than 90°, indicating that all mats tend to be hydrophilic and allow the spread of the water in their study (Jovanska, Chiu, Yeh, and Chiang 2022). Silva et al (2019) also proved that nanofibers produced using PCL and PEO blends had hydrophilic characteristics (30.25 ± 4.32°) contrary to fibers produced with only PCL had hydrophilic characteristics 122.34 ± 1.72° (C. K. da Silva et al. 2019).

In another study reported by Moreira et al. (2018), the contact angle was determined as 92.2 ± 2.6° for the PLA/PEO ultrafine fibers fabricated without the addition of phycocyanin. When added the phycocyanin was added to the spinning solutions, the

corresponding values obtained were 84.7 ± 1.8°; 81.3 ± 2.5°; 66.4 ± 1.4°; 43.6 ± 0.7° and 20.1 ± 1.3° for the samples with 2, 3, 4, 5 and 6% (w v^{-1}) of the pigment, respectively. Therefore, the higher the concentration of phycocyanin the higher was the wettability of the membrane (Moreira et al. 2018). Prietto et al (2018) reported that the times for distilled water to recede to zero contact angle for the the membranes of pure zein, zein with 3% anthocyanins (w v^{-1}), zein with 4% anthocyanins (w v^{-1}), and zein with 5% anthocyanins (w v^{-1}) were 10, 5, 4 and 2 s. The membranes were highly hydrophilic. The hydrophilicity of the membranes can be attributed to surface morphology, porosity, the size of the ultrafine fibers, and capillary action of the electrospun membrane. The increased wettability facilitate the diffusion of H+ or OH– into the membrane, allowing these ions to interact with anthocyanins, thereby giving a rapid color response as a function of pH (Prietto et al. 2018)

As a result, with increasing PBE concentration in PCL films, water contact angle decreased which allowed reaction with antocyanins and gave color change response to pH variation. 10% PCL (w v^{-1}) films containing 0.4% and 0.6% PBE (w v^{-1}) can be potentially used as pH-indicator films with rapid color response.

3.2.7. FTIR Spectroscopy of the Electrospun PCL Nanofiber

The FTIR spectra obtained for PCL nanofibers with different PBE concentration and plain PBE powder are shown in Figure 3.19. The spectrum of the films illustrated peaks at approximately 2900 and 2800 cm^{-1} since PCL have C-H stretching vibration. The peak at 1750 cm^{-1} corresponds to C=O stretching band and 1100 cm^{-1} to C-O stretching band. The peak at 1250 cm^{-1} contains the C-O stretching vibration in PCL films. The differences in the peak intensities can be related to PBE concentration. All characteristic peaks of PBE decreased after being incorporated in PCL mats, because the PBE concentration within films was very low. The FTIR spectrum was very similar to study conducted by (Liu et al. 2022; Jovanska, Chiu, Yeh, and Chiang 2022)

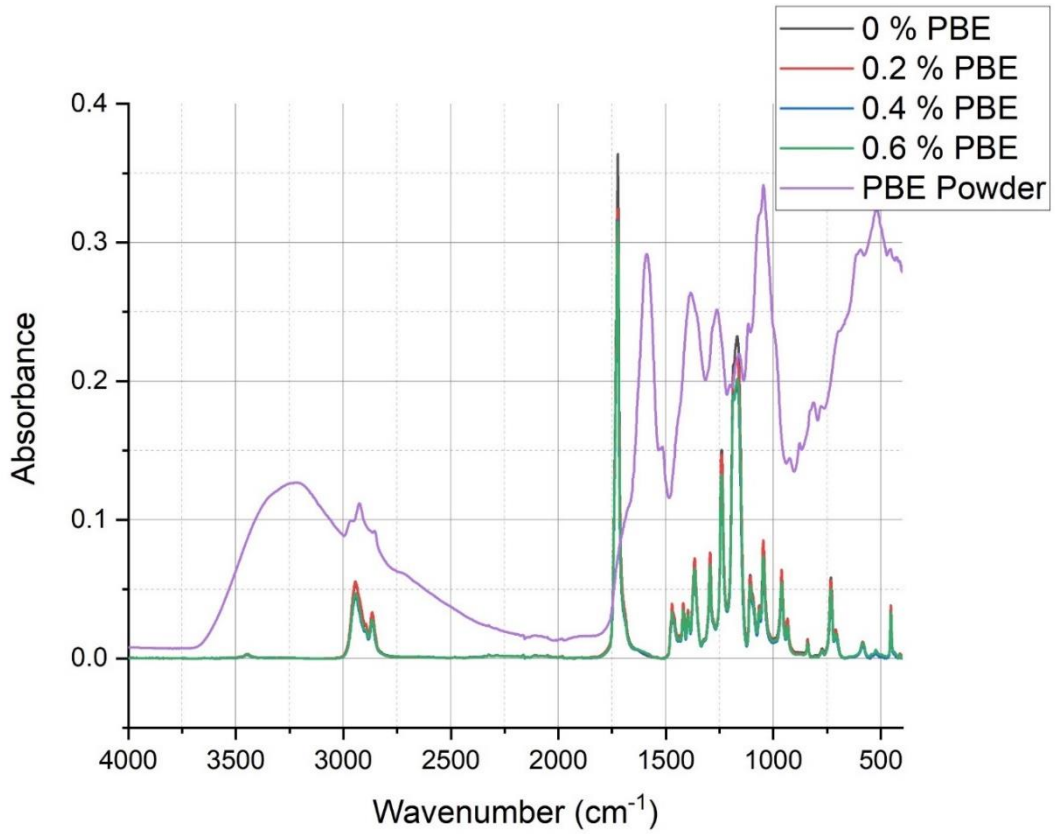

Figure 3.19 FTIR spectra of 10% PCL (w v^{-1}) electrospun films containing different PBE concentrations and PBE powder

CONCLUSIONS

As the first objective of this study, optimum processing conditions for the ultrasound assisted extraction of dried purple basil were determined as 55.25% ethanol containing 0.1% acetic acid, 30 mL/g solvent/solid ratio and 39.24 min based on both the total monomeric anthocyanin content and the increase green intensity with pH change. After determination of the optimum extraction condions, polycaprolactone films incorporating different purple basil extract (produced at optimum conditions) concentrations (0.2, 0.4 and 0.6% w v^{-1}) were fabricated with the electrospinning technique as the main objective of this research for the usage of pH indicator films in packaging material. It was found that as the purple basil extract content increases the viscosity of polycaprolactone solution increases, which directly affects the fiber morphology. Besides the concentration of purple basil extract, electrospinning process conditions were also found effective on fiber morphology. The color change due to pH variation is the most important parameter to decide whether the electrospun films can be used as a pH-indicator intelligent packaging material. The time required to observe a visible color change in films fabricated with 10% PCL (w v^{-1}) containing 0.2% PBE (w v^{-1}) was 5 min, however films fabricated with 10% PCL (w v^{-1}) containing 0.4% and 0.6% PBE (w v^{-1}) color change was observed only in 4-5 s. The color response to pH change analyses for the films fabricated from 10% PCL(w v^{-1}) incorporating 0.4% and 0.6% PBE (w v^{-1}) showed similar promising results. SEM images gave the most beadles and uniform nanofibrous mats when the spinning conditions were V=20 kV and Q=0.4 mL h^{-1} for both types of solutions. Therefore, for the sake of reproducibility of the results, films electrospun at 20 kV and 0.4 mL h^{-1} from 10% PCL (w v^{-1}) containing 0.4% and 0.6% PBE (w v^{-1}) were produced for the remaining analyses. Water contact angle decreased with increasing PBE concentration in PCL films, which accelerated the reaction between anthocyanins and gave quick color change response to pH variation. This study showed that electrospinning was a promising method for the fabrication of pH indicator films with rapid color response from 10% PCL (w v^{-1}) films containing 0.4% and 0.6% PBE (w v^{-1}). The applicability of these nanofibrous mats as colorimetric pH-indicator films to visually detect food spoilage should be tested on real food systems in future studies.

REFERENCES

Aboulghazi, Abderrazak, Meryem Bakour, Mouhcine Fadil, and Badiaa Lyoussi. 2022. "Simultaneous Optimization of Extraction Yield, Phenolic Compounds and Antioxidant Activity of Moroccan Propolis Extracts: Improvement of Ultrasound-Assisted Technique Using Response Surface Methodology." *Processes* 10 (2). https://doi.org/10.3390/pr10020297.

Agarwal, Anshika, Anant Raheja, T S Natarajan, and T S Chandra. 2012. "Sensors and Actuators B : Chemical Development of Universal PH Sensing Electrospun Nanofibers." *Sensors & Actuators: B. Chemical* 161 (1): 1097–1101. https://doi.org/10.1016/j.snb.2011.12.027.

"Ageless Eye, Oxygen Indicator: Products." Mitsubishi Gas Chemical Company, Inc. Accessed May 19, 2022. https://www.mgc.co.jp/eng/products/sc/ageless-eye.html.

Aman Mohammadi, Masoud, Seyede Marzieh Hosseini, and Mohammad Yousefi. 2020. "Application of Electrospinning Technique in Development of Intelligent Food Packaging: A Short Review of Recent Trends." *Food Science and Nutrition* 8 (9): 4656–65. https://doi.org/10.1002/fsn3.1781.

American Society for Testing and Materials, ASTM. 2002. "American Society for Testing and Materials. D 882-02: Standard Test Method for Tensile Properties of Thin Plastic Sheeting." *D882-12* 14: 1–10.

Amiot, M.J., Fleuriet, A., Cheynier, V. and Nicolas, J. 1997. Phenolic compounds and oxidative mechanisms in fruit and vegetables. In TomasBarberan, F.A. and Robins, R.J. (eds.). Phytochemistry of fruit and vegetables. Clarendon Press, Oxford. p 51-85

Arts, M.J.T.J., Haenen, G.R.M.M., Voss, H.P. and Bast A. 2004. Antioxidant capacity of reaction products limits the applicability of the Trolox equivalent antioxidant capacity (TEAC) assay. Food Chem. Toxical., 42: 45-49.

Azari, Arezo, Ali Golchin, Maryam Mahmoodinia Maymand, Fatemeh Mansouri, and Abdolreza Ardeshirylajimi. 2021. "Electrospun Polycaprolactone Nanofibers: Current Research and Applications in Biomedical Application." *Advanced Pharmaceutical Bulletin*, no. December 2021. https://doi.org/10.34172/apb.2022.070.

Babotă, Mihai, Oleg Frumuzachi, Alexandru Gâvan, Cristian Iacoviță, José Pinela, Lillian Barros, Isabel C.F.R. Ferreira, et al. 2022. "Optimized Ultrasound-Assisted Extraction of Phenolic Compounds from Thymus Comosus Heuff. Ex Griseb. et Schenk (Wild Thyme) and Their Bioactive Potential." *Ultrasonics Sonochemistry* 84 (January): 1–10. https://doi.org/10.1016/j.ultsonch.2022.105954.

Barba, Francisco J, Maria J Esteve, and Ana Frigola. 2013. "Physicochemical and Nutritional Characteristics of Blueberry Juice after High Pressure Processing." *FRIN* 50 (2): 545–49. https://doi.org/10.1016/j.foodres.2011.02.038.

Becerril, Raquel, Cristina Nerín, and Filomena Silva. 2021."Bring Some Colour to Your Package: Freshness Indicators Based on Anthocyanin Extracts." *Trends in Food Science & Technology* 111: 495–505. https://doi.org/10.1016/j.tifs.2021.02.042.

Benvenuti, S., F. Pellati, M. Melegari, And D. Bertelli. 2006. "Polyphenols, Anthocyanins, Ascorbic Acid, and Radical Scavenging Activity of Rubus, Ribes, and Aronia." *Journal of Food Science* 69, no. 3 (2006). https://doi.org/10.1111/j.1365-2621.2004.tb13352.x.

Bhardwaj, Nandana, and Subhas C. Kundu. 2010. "Electrospinning: A Fascinating Fiber Fabrication Technique." *Biotechnology Advances* 28 (3): 325–47. https://doi.org/10.1016/j.biotechadv.2010.01.004.

Blackhall, Melanie L., Rachael Berry, Noel W. Davies, and Justin T. Walls. 2018. "Optimized Extraction of Anthocyanins from Reid Fruits' Prunus Avium 'Lapins' Cherries." *Food Chemistry* 256 (February): 280–85. https://doi.org/10.1016/j.foodchem.2018.02.137.

Bravo, L. 1998. Polyphenols: chemistry, dietary sources, metabolism, and nutritional significance. Nutr. Rev., 56(11): 317-333.

Cai, Zhan, Ziqian Qu, Yu Lan, Shujuan Zhao, Xiaohua Ma, Qiang Wan, Pu Jing, and Pingfan Li. 2016. "Conventional, Ultrasound-Assisted, and Accelerated-Solvent Extractions of Anthocyanins from Purple Sweet Potatoes." *Food Chemistry* 197: 266–72. https://doi.org/10.1016/j.foodchem.2015.10.110.

Castañeda-Ovando, Araceli, Ma de Lourdes Pacheco-Hernández, Ma Elena Páez-Hernández, José A. Rodríguez, and Carlos Andrés Galán-Vidal. 2009. "Chemical Studies of Anthocyanins: A Review." *Food Chemistry* 113 (4): 859–71. https://doi.org/10.1016/j.foodchem.2008.09.001.

Celli, Giovana Bonat, Amyl Ghanem, and Marianne Su Ling Brooks. 2015. "Optimization of Ultrasound-Assisted Extraction of Anthocyanins from Haskap Berries (Lonicera Caerulea L.) Using Response Surface Methodology." *Ultrasonics Sonochemistry* 27: 449–55. https://doi.org/10.1016/j.ultsonch.2015.06.014.

Chemat, Farid, Natacha Rombaut, Anne Gaëlle Sicaire, Alice Meullemiestre, Anne Sylvie Fabiano-Tixier, and Maryline Abert-Vian. 2017. "Ultrasound Assisted Extraction of Food and Natural Products. Mechanisms, Techniques, Combinations, Protocols and Applications. A Review." *Ultrasonics Sonochemistry* 34: 540–60. https://doi.org/10.1016/j.ultsonch.2016.06.035.

Choi, Inyoung, Jun Young Lee, Monique Lacroix, and Jaejoon Han. 2017."Intelligent pH Indicator Film Composed of Agar/Potato Starch and Anthocyanin Extracts from Purple Sweet Potato." *Food Chemistry* 218: 122–28. https://doi.org/10.1016/j.foodchem.2016.09.050.

Cipitria, A., A. Skelton, T. R. Dargaville, P. D. Dalton, and D. W. Hutmacher. 2011. "Design, Fabrication and Characterization of PCL Electrospun Scaffolds - A Review." *Journal of Materials Chemistry* 21 (26): 9419–53. https://doi.org/10.1039/c0jm04502k.

Demirdöven, Aslihan, Kenan Özdoğan, and Kader Erdoğan-Tokatli. 2015. "Extraction of Anthocyanins from Red Cabbage by Ultrasonic and Conventional Methods: Optimization and Evaluation." *Journal of Food Biochemistry* 39 (5): 491–500. https://doi.org/10.1111/jfbc.12153.

Díaz-Maroto, M. Consuelo, Eva Sánchez Palomo, Lucia Castro, M. A. González Viñas, and M. Soledad Pérez-Coello. 2004. "Changes Produced in the Aroma Compounds and Structural Integrity of Basil (Ocimum Basilicum L) during Drying." *Journal of the Science of Food and Agriculture* 84 (15): 2070–76. https://doi.org/10.1002/jsfa.1921.

Dranca, Florina, and Mircea Oroian. 2016. "Optimization of Ultrasound-Assisted Extraction of Total Monomeric Anthocyanin (TMA) and Total Phenolic Content (TPC) from Eggplant (Solanum Melongena L.) Peel." *Ultrasonics Sonochemistry* 31: 637–46. https://doi.org/10.1016/j.ultsonch.2015.11.008.

Duan, Mengxia, Shan Yu, Jishuai Sun, Haixin Jiang, Jianbo Zhao, Cailing Tong, Yaqin Hu, Jie Pang, and Chunhua Wu. 2021. "Development and Characterization of Electrospun Nanofibers Based on Pullulan/Chitin

Nanofibers Containing Curcumin and Anthocyanins for Active-Intelligent Food Packaging." *International Journal of Biological Macromolecules* 187 (June): 332–40. https://doi.org/10.1016/j.ijbiomac.2021.07.140.

Ferreira, Daniele F., Juliano S. Barin, Arianna Binello, Valery V. Veselov, and Giancarlo Cravotto. 2019. "Highly Efficient Pumpkin-Seed Extraction with the Simultaneous Recovery of Lipophilic and Hydrophilic Compounds." *Food and Bioproducts Processing* 117: 224–30. https://doi.org/10.1016/j.fbp.2019.07.014.

"Food Safety." World Health Organization. World Health Organization. Accessed May 19, 2022. https://www.who.int/en/news-room/fact-sheets/detail/food-safety.

Flanigan, Patrick M., and Emily D. Niemeyer. 2014. "Effect of Cultivar on Phenolic Levels, Anthocyanin Composition, and Antioxidant Properties in Purple Basil (Ocimum Basilicum L.)." *Food Chemistry* 164: 518–26. https://doi.org/10.1016/j.foodchem.2014.05.061.

Forghani, Samira, Hadi Almasi, and Mehran Moradi. 2021. "Electrospun Nanofibers as Food Freshness and Time-Temperature Indicators: A New Approach in Food Intelligent Packaging." *Innovative Food Science and Emerging Technologies* 73 (June): 102804. https://doi.org/10.1016/j.ifset.2021.102804.

Haider, Adnan, Sajjad Haider, and Inn Kyu Kang. 2018. "A Comprehensive Review Summarizing the Effect of Electrospinning Parameters and Potential Applications of Nanofibers in Biomedical and Biotechnology." *Arabian Journal of Chemistry* 11 (8): 1165–88. https://doi.org/10.1016/j.arabjc.2015.11.015.

He, Bo, Ling Li Zhang, Xue Yang Yue, Jin Liang, Jun Jiang, Xue Ling Gao, and Peng Xiang Yue. 2016. "Optimization of Ultrasound-Assisted Extraction of Phenolic Compounds and Anthocyanins from Blueberry (Vaccinium Ashei) Wine Pomace." *Food Chemistry* 204: 70–76. https://doi.org/10.1016/j.foodchem.2016.02.094.

Ho, Chi-Tang. 1992."Phenolic Compounds in Food." *ACS Symposium Series*: 2–7. https://doi.org/10.1021/bk-1992-0507.ch001.

Hu, Xiyu, Liang Yang, Kaijun Wang, and Yanli Zixuan Wei. 2018. "Studies of Mechanical Properties of Electrospun Zein / Poly (e -Caprolactone) Composites and Antibacterial Properties against Listeria Monocytogenes

Strains of Zein / Poly (e -Caprolactone)/ Poly (e -Lysine) Films." https://doi.org/10.1177/0040517517732083.

John Barth Article Author July 25, Article Author, and Maria April 29. Sira Technologies Food Sentinel System. Accessed May 19, 2022. https://www.adazonusa.com/blog/barcode-industry/sira-technologies-food-sentinel-system.

Jovanska, Lavernchy, Chun-hui Chiu, Yi-cheun Yeh, and Wen-dee Chiang. 2022. "Development of a PCL-PEO Double Network Colorimetric PH Sensor Using Electrospun Fibers Containing Hibiscus Rosa Sinensis Extract and Silver Nanoparticles for Food Monitoring." *Food Chemistry* 368 (July 2021): 130813. https://doi.org/10.1016/j.foodchem.2021.130813.

Jovanska, Lavernchy, Chun Hui Chiu, Yi Cheun Yeh, Wen Dee Chiang, Chang Chi Hsieh, and Reuben Wang. 2022. "Development of a PCL-PEO Double Network Colorimetric PH Sensor Using Electrospun Fibers Containing Hibiscus Rosa Sinensis Extract and Silver Nanoparticles for Food Monitoring." *Food Chemistry* 368 (July 2021): 130813. https://doi.org/10.1016/j.foodchem.2021.130813.

Juliani, H.R. and Simon, J.E. 2002. Antioxidant of basil. In Janick, J. and Whipkey, A. (eds.). Trends in new crops and new uses. ASHS Press, Alexandra, VA. p 575-579

Khoo, Hock Eng, Azrina Azlan, Sou Teng Tang, and See Meng Lim. 2017. "Anthocyanidins and Anthocyanins: Colored Pigments as Food, Pharmaceutical Ingredients, and the Potential Health Benefits." *Food & Nutrition Research* 61 (1): 1361779. https://doi.org/10.1080/16546628.2017.1361779.

Lafarga, Tomás, Carlos Álvarez, Gloria Bobo, and Ingrid Aguiló-Aguayo. 2018. "Characterization of Functional Properties of Proteins from Ganxet Beans (Phaseolus Vulgaris L. Var. Ganxet) Isolated Using an Ultrasound-Assisted Methodology." *Lwt* 98 (July): 106–12. https://doi.org/10.1016/j.lwt.2018.08.033.

Leidy, Ricaurte, and Quintanilla Carvajal Maria Ximena. 2019. "Use of Electrospinning Technique to Produce Nanofibres for Food Industries: A Perspective from Regulations to Characterisations." *Trends in Food Science and Technology* 85 (May 2018): 92–106.

https://doi.org/10.1016/j.tifs.2019.01.006.

Li, Zhenyu, and Ce Wang. 2013. “Effects of Working Parameters on Electrospinning.” *SpringerBriefs in Materials*, 15–28. https://doi.org/10.1007/978-3-642-36427-3_2.

Liu, Li, Junjun Zhang, Xiaobo Zou, Muhammad Arslan, Jiyong Shi, Xiaodong Zhai, Jianbo Xiao, et al. 2022. “A High-Stable and Sensitive Colorimetric Nanofiber Sensor Based on PCL Incorporating Anthocyanins for Shrimp Freshness.” *Food Chemistry* 377 (July 2021): 131909. https://doi.org/10.1016/j.foodchem.2021.131909.

Luiza Koop, Betina, Milena Nascimento da Silva, Fabíola Diniz da Silva, Kennya Thayres dos Santos Lima, Lenilton Santos Soares, Cristiano José de Andrade, Germán Ayala Valencia, and Alcilene Rodrigues Monteiro. 2022. “Flavonoids, Anthocyanins, Betalains, Curcumin, and Carotenoids: Sources, Classification and Enhanced Stabilization by Encapsulation and Adsorption.” *Food Research International* 153 (September 2021). https://doi.org/10.1016/j.foodres.2021.110929.

Luo, Xiaoyu, Amr Zaitoon, and Loong Tak Lim. 2022. “A Review on Colorimetric Indicators for Monitoring Product Freshness in Intelligent Food Packaging: Indicator Dyes, Preparation Methods, and Applications.” *Comprehensive Reviews in Food Science and Food Safety*, no. February. https://doi.org/10.1111/1541-4337.12942.

Maftoonazad, Neda, and Hosahalli Ramaswamy. 2019. “Design and Testing of an Electrospun Nanofiber Mat as a PH Biosensor and Monitor the PH Associated Quality in Fresh Date Fruit (Rutab).” *Polymer Testing* 75 (September 2018): 76–84. https://doi.org/10.1016/j.polymertesting.2019.01.011.

Mane, Shon, David H. Bremner, Athina Tziboula-Clarke, and M. Adília Lemos. 2015. “Effect of Ultrasound on the Extraction of Total Anthocyanins from Purple Majesty Potato.” *Ultrasonics Sonochemistry* 27: 509–14. https://doi.org/10.1016/j.ultsonch.2015.06.021.

Mercante, Luiza A., Vanessa P. Scagion, Fernanda L. Migliorini, Luiz H.C. Mattoso, and Daniel S. Correa. 2017. “Electrospinning-Based (Bio)Sensors for Food and Agricultural Applications: A Review.” *TrAC - Trends in Analytical Chemistry* 91: 91–103. https://doi.org/10.1016/j.trac.2017.04.004.

Meregalli, Monalise Marcante, Bruna Maria Saorin Puton, Fernanda Dal Maso Camera, Alexandre Umpierrez Amaral, Jamile Zeni, Rogério Luis Cansian, Marcelo Luis Mignoni, and Geciane Toniazzo Backes. 2020. "Conventional and Ultrasound-Assisted Methods for Extraction of Bioactive Compounds from Red Araçá Peel (Psidium Cattleianum Sabine)." *Arabian Journal of Chemistry* 13 (6): 5800–5809. https://doi.org/10.1016/j.arabjc.2020.04.017.

Mistry, Jamie, and John F Kennedy. 2003. "Food: The Chemistry of Its Components (4th Edition)." *Carbohydrate Polymers* 54 (3): 394. https://doi.org/10.1016/s0144-8617(03)00116-4.

Mónica Giusti, M., and Ronald E. Wrolstad. 2005. "Characterization and Measurement of Anthocyanins by UV-Visible Spectroscopy." *Handbook of Food Analytical Chemistry* 2–2: 19–31. https://doi.org/10.1002/0471709085.ch18.

Mokrzycki, W. S., and Tatol, M. 2011 ."Color difference delta E- A survey." *Machine Graphics and Vision*, 20, 383-411

Montenegro-nicolini, Miguel, Patricio E Reyes, Miguel O Jara, Parameswara R Vuddanda, Andrónico Neira-carrillo, Nicole Butto, Sitaram Velaga, and Javier O Morales. 2018. "The Effect of Inkjet Printing over Polymeric Films as Potential Buccal Biologics Delivery Systems" 19 (8): 3376–87. https://doi.org/10.1208/s12249-018-1105-1.

Moreira, Juliana Botelho, Loong-Tak Lim, Elessandra da Zavareze, Alvaro Renato Dias, Jorge Alberto Costa, and Michele Greque Morais. 2019. "Antioxidant Ultrafine Fibers Developed with Microalga Compounds Using a Free Surface Electrospinning." *Food Hydrocolloids* 93: 131–36. https://doi.org/10.1016/j.foodhyd.2019.02.015.

Moreira, Juliana Botelho, Ana Luiza Machado Terra, Jorge Alberto Vieira Costa, and Michele Greque de Morais. 2018. "Development of PH Indicator from PLA/PEO Ultrafine Fibers Containing Pigment of Microalgae Origin." *International Journal of Biological Macromolecules* 118: 1855–62. https://doi.org/10.1016/j.ijbiomac.2018.07.028.

Nur, Fatma, and Uğur Parın. 2022. "Spirulina Biomass-Loaded Thermoplastic Polyurethane / Polycaprolacton (TPU / PCL) Nanofibrous Mats : Fabrication , Characterization , and Antibacterial Activity as Potential Wound Healing" 202104148: 1–8. https://doi.org/10.1002/slct.202104148.

Ojha, K. Shikha, Ramón Aznar, Colm O'Donnell, and Brijesh K. Tiwari. 2020.

"Ultrasound Technology for the Extraction of Biologically Active Molecules from Plant, Animal and Marine Sources." *TrAC - Trends in Analytical Chemistry* 122. https://doi.org/10.1016/j.trac.2019.115663.

Pagano, Imma, Luca Campone, Rita Celano, Anna Lisa Piccinelli, and Luca Rastrelli. 2021. "Green Non-Conventional Techniques for the Extraction of Polyphenols from Agricultural Food by-Products: A Review." *Journal of Chromatography A* 1651: 462295. https://doi.org/10.1016/j.chroma.2021.462295.

Pakolpakçıl, A., E. Karaca, and B. Becerir. 2018 ."Investigation of a Natural PH-Indicator Dye for Nanofibrous Wound Dressings." *IOP Conference Series: Materials Science and Engineering* 460: 012020. https://doi.org/10.1088/1757-899x/460/1/012020.

Pedro, Alessandra C., Fernanda Moreira, Daniel Granato, and Neiva Deliberali Rosso. 2016. "Extraction of Bioactive Compounds and Free Radical Scavenging Activity of Purple Basil (Ocimum Basilicum L.) Leaf Extracts as Affected by Temperature and Time." *Anais Da Academia Brasileira de Ciencias* 88 (2): 1055–68. https://doi.org/10.1590/0001-3765201620150197.

Phippen, Winthrop B., and James E. Simon. 1998. "Anthocyanins in Basil (Ocimum Basilicum L.)." *Journal of Agricultural and Food Chemistry* 46 (5): 1734–38. https://doi.org/10.1021/jf970887r.

Prietto, Luciana, Vania Zanella Pinto, Shanise Lisie Mello El Halal, Michele Greque de Morais, Jorge Alberto Vieira Costa, Loong Tak Lim, Alvaro Renato Guerra Dias, and Elessandra da Rosa Zavareze. 2018. "Ultrafine Fibers of Zein and Anthocyanins as Natural PH Indicator." *Journal of the Science of Food and Agriculture* 98 (7): 2735–41. https://doi.org/10.1002/jsfa.8769.

Rashid, Rubiya, F. A. Masoodi, Sajad Mohd Wani, Shaziya Manzoor, and Amir Gull. 2022. "Ultrasound Assisted Extraction of Bioactive Compounds from Pomegranate Peel, Their Nanoencapsulation and Application for Improvement in Shelf Life Extension of Edible Oils." *Food Chemistry* 385 (March): 132608. https://doi.org/10.1016/j.foodchem.2022.132608.

Re, Roberta, Nicoletta Pellegrini, Anna Proteggente, Ananth Pannala, Min Yang, and Catherine Rice-Evans. 1999 . "Antioxidant Activity Applying an Improved ABTS Radical Cation Decolorization Assay." *Free Radical Biology and Medicine* 26, no. 9-10: 1231–37. https://doi.org/10.1016/s0891-5849(98)00315-3.

Rodrigues, Sueli, Fabiano A.N. Fernandes, Edy Sousa de Brito, Adriana Dutra Sousa, and Narendra Narain. 2015. “Ultrasound Extraction of Phenolics and Anthocyanins from Jabuticaba Peel.” *Industrial Crops and Products* 69: 400–407. https://doi.org/10.1016/j.indcrop.2015.02.059.

Roy, Swarup, and Jong Whan Rhim. 2021. “Anthocyanin Food Colorant and Its Application in PH-Responsive Color Change Indicator Films.” *Critical Reviews in Food Science and Nutrition* 61 (14): 2297–2325. https://doi.org/10.1080/10408398.2020.1776211.

Ryu, Dayeon, and Eunmi Koh. 2019. “Optimization of Ultrasound-Assisted Extraction of Anthocyanins and Phenolic Compounds from Black Soybeans (Glycine Max L.).” *Food Analytical Methods* 12 (6): 1382–89. https://doi.org/10.1007/s12161-019-01462-2.

Sahin, Serpil, and Servet Gulum Sumnu. 2006 . *Physical Properties of Foods*. New York: Springer.

Schoolaert, Ella, Iline Steyaert, Gertjan Vancoillie, Jozefien Geltmeyer, Kathleen Lava, Richard Hoogenboom, and Karen De Clerck. 2016 . “Blend Electrospinning of Dye-Functionalized Chitosan and Poly(ε-Caprolactone): Towards Biocompatible pH-Sensors.” *Journal of Materials Chemistry B* 4, no. 26: 4507–16. https://doi.org/10.1039/c6tb00639f.

Sharif, Niloufar, Sara Khoshnoudi-nia, and Seid Mahdi. 2020. “Nano / Microencapsulation of Anthocyanins ; a Systematic Review and Meta-Analysis.” *Food Research International* 132 (October 2019): 109077. https://doi.org/10.1016/j.foodres.2020.109077.

Shavisi, Nassim, and Yasser Shahbazi. 2022. “Chitosan-Gum Arabic Nanofiber Mats Encapsulated with PH-Sensitive Rosa Damascena Anthocyanins for Freshness Monitoring of Chicken Fillets.” *Food Packaging and Shelf Life* 32 (December 2021): 100827. https://doi.org/10.1016/j.fpsl.2022.100827.

Silva, Cleber Klasener da, Duna Joanol da Silveira Mastrantonio, Jorge Alberto Vieira Costa, and Michele Greque de Morais. 2019. “Innovative PH Sensors Developed from Ultrafine Fibers Containing Açaí (Euterpe Oleracea) Extract.” *Food Chemistry* 294 (July 2018): 397–404. https://doi.org/10.1016/j.foodchem.2019.05.059.

Silva, Larissa Marina Pereira, Maria Raquel Cavalcanti Inácio, Gualter Guenter Costa da Silva, Jucier Magson de Souza e Silva, Jefferson Romáryo Duarte da Luz,

Maria das Graças Almeida, Edgar Perin Moraes, Debora Esposito, Leandro De Santis Ferreira, and Silvana Maria Zucolotto. 2022. “The First Optimization Process from Cultivation to Flavonoid-Rich Extract from Moringa Oleifera Lam. Leaves in Brazil.” *Foods* 11 (10): 1452. https://doi.org/10.3390/foods11101452.

Silva, S., E. M. Costa, C. Calhau, R. M. Morais, and M. E. Pintado. 2017. “Anthocyanin Extraction from Plant Tissues: A Review.” *Critical Reviews in Food Science and Nutrition* 57 (14): 3072–83. https://doi.org/10.1080/10408398.2015.1087963.

Singh, Suman, Kirtiraj K. Gaikwad, and Youn Suk Lee. 2018. “Anthocyanin – A Natural Dye for Smart Food Packaging Systems.” *Korean Journal of Packaging Science and Technology* 24 (3): 167–80. https://doi.org/10.20909/kopast.2018.24.3.167.

Singleton, V. L and Rossi, Joseph. A. Jr, J. 1965. “*COLORIMETRY OF TOTAL PHENOLICS W I T H A C I D REAGENTS*.”

Sohail, Muhammad, Da Wen Sun, and Zhiwei Zhu. 2018. “Recent Developments in Intelligent Packaging for Enhancing Food Quality and Safety.” *Critical Reviews in Food Science and Nutrition* 58 (15): 2650–62. https://doi.org/10.1080/10408398.2018.1449731.

Sun, B, Y Z Long, H D Zhang, M M Li, J L Duvail, X Y Jiang, and H L Yin. 2014. “Progress in Polymer Science Advances in Three-Dimensional Nanofibrous Macrostructures via Electrospinning” 39: 862–90. https://doi.org/10.1016/j.progpolymsci.2013.06.002.

Sun, Wuliang, Yilin Liu, Lu Jia, Marleny D. Saldaña, Tungalag Dong, Ye Jin, and Wenxiu Sun. 2020. “A Smart Nanofibre Sensor Based on Anthocyanin/Poly-l-Lactic Acid for Mutton Freshness Monitoring.” *International Journal of Food Science & Technology* 56, no. 1 (2020): 342–51. https://doi.org/10.1111/ijfs.14648.

Surin, Siriluck, Sang Guan You, Phisit Seesuriyachan, Rattana Muangrat, Sutee Wangtueai, Anet Režek Jambrak, Suphat Phongthai, Kittisak Jantanasakulwong, Thanongsak Chaiyaso, and Yuthana Phimolsiripol. 2020. “Optimization of Ultrasonic-Assisted Extraction of Polysaccharides from Purple Glutinous Rice Bran (Oryza Sativa L.) and Their Antioxidant Activities.” *Scientific Reports* 10 (1): 1–10. https://doi.org/10.1038/s41598-

020-67266-1.

Tan, Jiaqi, Pengshan Cui, Shaoqin Ge, Xu Cai, Qian Li, and Hongkun Xue. 2022. "Ultrasound Assisted Aqueous Two-Phase Extraction of Polysaccharides from Cornus Officinalis Fruit: Modeling, Optimization, Purification, and Characterization." *Ultrasonics Sonochemistry* 84 (January): 105966. https://doi.org/10.1016/j.ultsonch.2022.105966.

Tan, Jiaqi, Yanmei Han, Bo Han, Xiangmei Qi, Xu Cai, Shaoqin Ge, and Hongkun Xue. 2022. "Extraction and Purification of Anthocyanins: A Review." *Journal of Agriculture and Food Research* 8 (April): 100306. https://doi.org/10.1016/j.jafr.2022.100306.

Taticchi, Agnese, Roberto Selvaggini, Sonia Esposto, Beatrice Sordini, Gianluca Veneziani, and Maurizio Servili. 2019. "Physicochemical Characterization of Virgin Olive Oil Obtained Using an Ultrasound-Assisted Extraction at an Industrial Scale: Influence of Olive Maturity Index and Malaxation Time." *Food Chemistry* 289 (November 2018): 7–15. https://doi.org/10.1016/j.foodchem.2019.03.041.

Tena, Noelia, and Agustin G. Asuero. 2022. "Up-To-Date Analysis of the Extraction Methods for Anthocyanins: Principles of the Techniques, Optimization, Technical Progress, and Industrial Application." *Antioxidants* 11 (2). https://doi.org/10.3390/antiox11020286.

Tena, Noelia, Julia Martín, and Agustín G. Asuero. 2020. "State of the Art of Anthocyanins: Antioxidant Activity, Sources, Bioavailability, and Therapeutic Effect in Human Health." *Antioxidants* 9 (5). https://doi.org/10.3390/antiox9050451.

Terra, Ana Luiza, Juliana Botelho Moreira, Jorge Alberto Costa, and Michele Greque Morais. 2021 . "Development of Time-pH Indicator Nanofibers from Natural Pigments: An Emerging Processing Technology to Monitor the Quality of Foods." *LWT* 142 : 111020. https://doi.org/10.1016/j.lwt.2021.111020.

Topuz, Fuat, and Tamer Uyar. 2020. "Antioxidant, Antibacterial and Antifungal Electrospun Nanofibers for Food Packaging Applications." *Food Research International* 130 (August 2019): 108927. https://doi.org/10.1016/j.foodres.2019.108927.

Wang, Mingfu, Jiangang Li, Meera Rangarajan, Yu Shao, Edmond J. LaVoie, Tzou-Chi Huang, and Chi-Tang Ho. 1998. "Antioxidative Phenolic Compounds from

Sage (*Salvia Officinalis*).” *Journal of Agricultural and Food Chemistry* 46, no. 12 : 4869–73. https://doi.org/10.1021/jf980614b.

Wangcharoen, Wiwat, and Wallaya Morasuk. 2007. “Antioxidant Capacity and Phenolic Content of Holy Basil.” *Songklanakarin Journal of Science and Technology* 29 (5): 1407–15.

Watrelot, Aude A., and Lindsey Bouska. 2022. “Optimization of the Ultrasound-Assisted Extraction of Polyphenols from Aronia and Grapes.” *Food Chemistry* 386 (March): 132703. https://doi.org/10.1016/j.foodchem.2022.132703.

Wen, Peng, Min Hua Zong, Robert J. Linhardt, Kun Feng, and Hong Wu. 2017. “Electrospinning: A Novel Nano-Encapsulation Approach for Bioactive Compounds.” *Trends in Food Science and Technology* 70 (May): 56–68. https://doi.org/10.1016/j.tifs.2017.10.009.

Wongsasulak, Saowakon, Manashuen Patapeejumruswong, Jochen Weiss, Pitt Supaphol, and Tipaporn Yoovidhya. 2010. “Electrospinning of Food-Grade Nanofibers from Cellulose Acetate and Egg Albumen Blends.” *Journal of Food Engineering* 98 (3): 370–76. https://doi.org/10.1016/j.jfoodeng.2010.01.014.

Yang, Kai, Tian Rui Xu, Yan Hong Fu, Ming Cai, Qi Le Xia, Rong Fa Guan, Xian Guo Zou, and Pei Long Sun. 2021. “Effects of Ultrasonic Pre-Treatment on Physicochemical Properties of Proteins Extracted from Cold-Pressed Sesame Cake.” *Food Research International* 139 (November 2020): 109907. https://doi.org/10.1016/j.foodres.2020.109907.

Yildiz, Eda, Gulum Sumnu, and Leyla Nesrin Kahyaoglu. 2021. “International Journal of Biological Macromolecules Monitoring Freshness of Chicken Breast by Using Natural Halochromic Curcumin Loaded Chitosan / PEO Nano Fi Bers as an Intelligent Package.” *International Journal of Biological Macromolecules* 170: 437–46. https://doi.org/10.1016/j.ijbiomac.2020.12.160.

Yuan, Yuehua, and T. Randall Lee. 2013 . “Contact Angle and Wetting Properties.” *Surface Science Techniques*, 2013, 3–34. https://doi.org/10.1007/978-3-642-34243-1_1.

“Zebra Fresh Check Temperature Indicator Brochure V1.” Accessed May 19, 2022. https://www.zebra.com/content/dam/zebra_new_ia/en-us/solutions-verticals/product/monitoring-sensing/food-temp-indicators/freshcheck/brochure/fresh-check-brochure-comz-en-us.pdf.

Zhang, Chaoqun, Yapeng Li, Wei Wang, Naiqian Zhan, Ning Xiao, Shuai Wang, Yaoxian Li, and Qingbiao Yang. 2011. “A Novel Two-Nozzle Electrospinning Process for Preparing Microfiber Reinforced PH-Sensitive Nano-Membrane with Enhanced Mechanical Property.” *European Polymer Journal* 47 (12): 2228–33. https://doi.org/10.1016/j.eurpolymj.2011.09.015.

Zia, Sania, Moazzam Rafiq Khan, Muhammad Asim Shabbir, Abid Aslam Maan, Muhammad Kashif Iqbal Khan, Muhammad Nadeem, Anees Ahmed Khalil, Ahmad Din, and Rana Muhammad Aadil. 2020. “An Inclusive Overview of Advanced Thermal and Nonthermal Extraction Techniques for Bioactive Compounds in Food and Food-Related Matrices.” *Food Reviews International* 00 (00): 1–31. https://doi.org/10.1080/87559129.2020.1772283.

APPENDICES

APPENDIX A. STATISTICAL ANALYSES

Table A.1 RSM results for the experiments containing ethanol acidified with 0.1% Ac ($v\ v^{-1}$) on TMA

Analysis of Variance

Source	DF	Seq SS	Adj MS	F-Value	P-Value
Model	9	49.5139	5.5015	16.86	0.003
Linear	3	6.3455	2.1152	6.48	0.036
Ethanol Concentration	1	2.0784	2.0784	6.37	0.053
Solvent/Solid	1	1.8624	1.8624	5.71	0.062
Time	1	2.4048	2.4048	7.37	0.042
Square	3	42.7137	14.2379	43.62	0.001
Ethanol Concentration*Ethanol Concentration	1	42.2778	42.6659	130.73	0.000
Solvent/Solid*Solvent/Solid	1	0.0733	0.1000	0.31	0.604
Time*Time	1	0.3626	0.3626	1.11	0.340
2-Way Interaction	3	0.4547	0.1516	0.46	0.720
Ethanol Concentration*Solvent/Solid	1	0.3949	0.3949	1.21	0.321
Ethanol Concentration*Time	1	0.0511	0.0511	0.16	0.709
Solvent/Solid*Time	1	0.0087	0.0087	0.03	0.877
Error	5	1.6319	0.3264		
Lack-of-Fit	3	1.5481	0.5160	12.32	0.076
Pure Error	2	0.0837	0.0419		
Total	14	51.1458			

Model Summary

S	R-sq	R-sq(adj)	PRESS	R-sq(pred)
0.571294	96.81%	91.07%	24.9586	51.20%

Coded Coefficients

Term	Coef	SE Coef	95% CI	P-Value
Constant	4.444	0.330	(3.596; 5.292)	0.000
Ethanol Concentration	-0.510	0.202	(-1.029; 0.010)	0.053
Solvent/Solid	0.482	0.202	(-0.037; 1.002)	0.062
Time	0.548	0.202	(0.029; 1.067)	0.042
Ethanol Concentration*Ethanol Concentration	-3.399	0.297	(-4.164; -2.635)	0.000
Solvent/Solid*Solvent/Solid	-0.165	0.297	(-0.929; 0.600)	0.604
Time*Time	-0.313	0.297	(-1.078; 0.451)	0.340
Ethanol Concentration*Solvent/Solid	-0.314	0.286	(-1.048; 0.420)	0.321
Ethanol Concentration*Time	-0.113	0.286	(-0.847; 0.621)	0.709
Solvent/Solid*Time	-0.047	0.286	(-0.781; 0.688)	0.877

Regression Equation in Uncoded Units

Anthocyanin(mg/ g purple basil) = -4.52 + 0.2197 Ethanol Concentration + 0.160 Solvent/Solid
+ 0.0574 Time - 0.002125 Ethanol Concentration*Ethanol Concentration
- 0.00165 Solvent/Solid*Solvent/Solid - 0.000348 Time*Time
- 0.000786 Ethanol Concentration*Solvent/Solid
- 0.000094 Ethanol Concentration*Time
- 0.000156 Solvent/Solid*Time

Optimization Plot

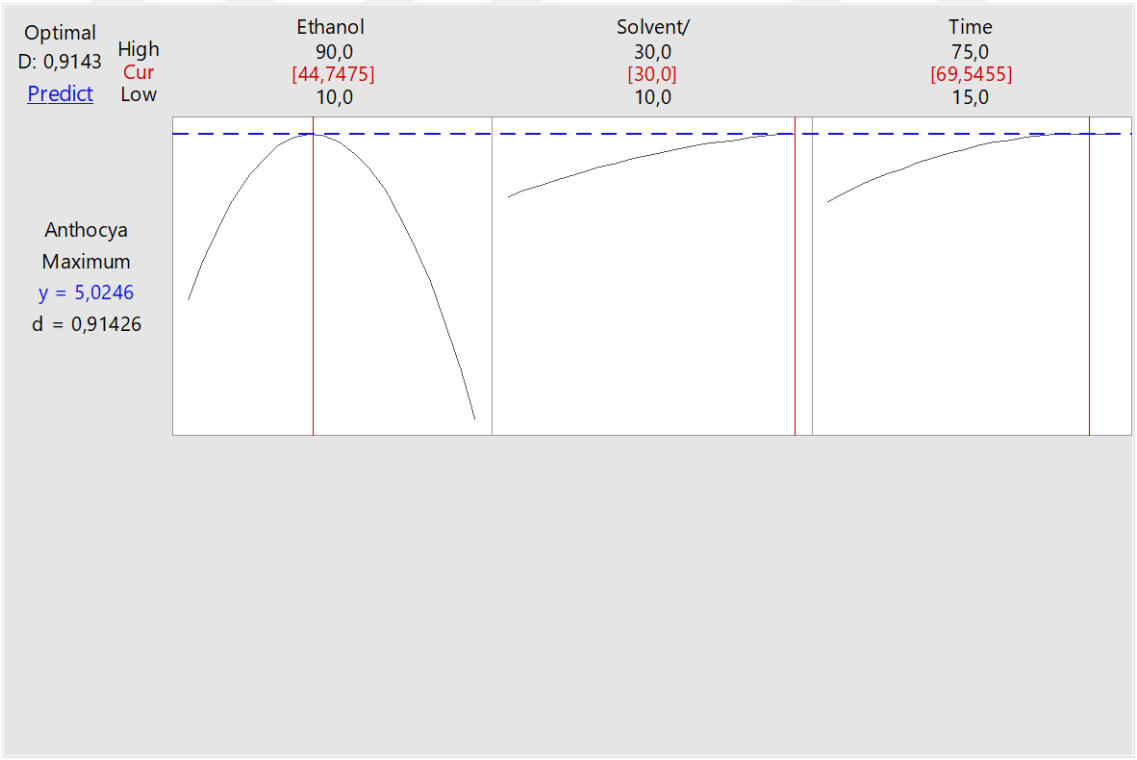

Table A.2 RSM results for the experiments containing ethanol acidified with 0.1% HCl (v v^{-1}) on TMA

Analysis of Variance

Source	DF	Seq SS	Adj MS	F-Value	P-Value
Model	9	42.4094	4.7122	8.46	0.015
Linear	3	8.9282	2.9761	5.34	0.051
Ethanol Concentration	1	5.1495	5.1495	9.25	0.029
Solvent/Solid	1	0.5381	0.5381	0.97	0.371
Time	1	3.2406	3.2406	5.82	0.061
Square	3	32.5317	10.8439	19.47	0.003
Ethanol Concentration*Ethanol Concentration	1	30.3686	31.6678	56.86	0.001
Solvent/Solid*Solvent/Solid	1	1.6334	1.7695	3.18	0.135
Time*Time	1	0.5298	0.5298	0.95	0.374
2-Way Interaction	3	0.9495	0.3165	0.57	0.660
Ethanol Concentration*Solvent/Solid	1	0.9264	0.9264	1.66	0.254
Ethanol Concentration*Time	1	0.0034	0.0034	0.01	0.941
Solvent/Solid*Time	1	0.0197	0.0197	0.04	0.858
Error	5	2.7846	0.5569		
Lack-of-Fit	3	1.2034	0.4011	0.51	0.716
Pure Error	2	1.5812	0.7906		
Total	14	45.1940			

Model Summary

S	R-sq	R-sq(adj)	PRESS	R-sq(pred)
0.746272	93.84%	82.75%	22.8116	49.53%

Coded Coefficients

Term	Coef	SE Coef	95% CI	P-Value
Constant	4.658	0.431	(3.550; 5.766)	0.000
Ethanol Concentration	-0.802	0.264	(-1.481; -0.124)	0.029
Solvent/Solid	0.259	0.264	(-0.419; 0.938)	0.371
Time	0.636	0.264	(-0.042; 1.315)	0.061
Ethanol Concentration*Ethanol Concentration	-2.929	0.388	(-3.927; -1.930)	0.001
Solvent/Solid*Solvent/Solid	-0.692	0.388	(-1.691; 0.306)	0.135
Time*Time	-0.379	0.388	(-1.377; 0.620)	0.374
Ethanol Concentration*Solvent/Solid	-0.481	0.373	(-1.440; 0.478)	0.254
Ethanol Concentration*Time	-0.029	0.373	(-0.988; 0.930)	0.941
Solvent/Solid*Time	-0.070	0.373	(-1.029; 0.889)	0.858

Regression Equation in Uncoded Units

Anthocyanin(mg/ g purple basil)	=	-5.48 + 0.1881 Ethanol Concentration + 0.374 Solvent/Solid + 0.0650 Time- 0.001830 Ethanol Concentration*Ethanol Concentration - 0.00692 Solvent/Solid*Solvent/Solid - 0.000421 Time*Time - 0.001203 Ethanol Concentration*Solvent/Solid - 0.000024 Ethanol Concentration*Time - 0.00023 Solvent/Solid*Time

Optimization Plot

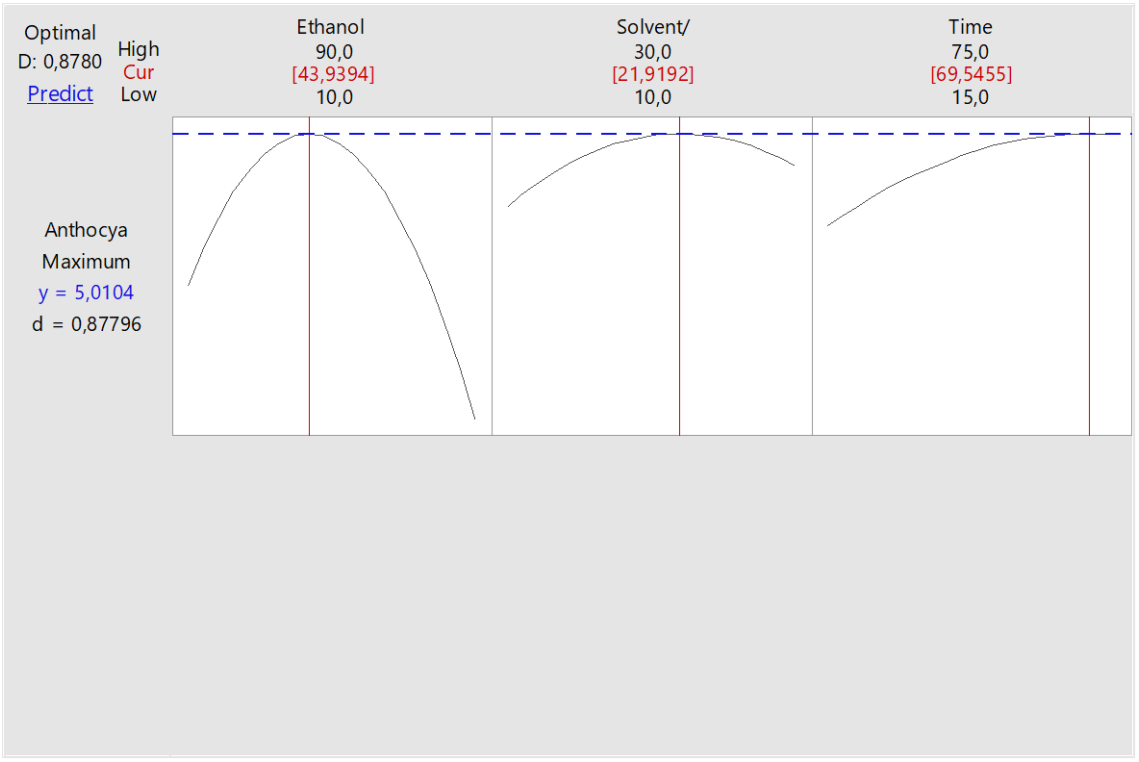

Table A.3 RSM results for the experiments containing ethanol acidified with 0.1% Ac (v v^{-1}) on Increase in Green Intensity

Analysis of Variance

Source	DF	Seq SS	Adj MS	F-Value	P-Value
Model	9	5.41278	0.60142	11.41	0.008
Linear	3	3.54064	1.18021	22.39	0.003
Ethanol Concentration	1	3.40615	3.40615	64.61	0.000
Solvent/Solid	1	0.09064	0.09064	1.72	0.247
Time	1	0.04385	0.04385	0.83	0.404
Square	3	1.64393	0.54798	10.39	0.014
Ethanol Concentration*Ethanol Concentration	1	1.62773	1.62596	30.84	0.003
Solvent/Solid*Solvent/Solid	1	0.01519	0.01450	0.28	0.622
Time*Time	1	0.00101	0.00101	0.02	0.895
2-Way Interaction	3	0.22821	0.07607	1.44	0.335
Ethanol Concentration*Solvent/Solid	1	0.09547	0.09547	1.81	0.236
Ethanol Concentration*Time	1	0.04827	0.04827	0.92	0.383
Solvent/Solid*Time	1	0.08447	0.08447	1.60	0.261
Error	5	0.26361	0.05272		
Lack-of-Fit	3	0.23246	0.07749	4.97	0.172
Pure Error	2	0.03116	0.01558		
Total	14	5.67639		11.41	0.008

Model Summary

S	R-sq	R-sq(adj)	PRESS	R-sq(pred)
0.229614	95.36%	87.00%	3.78942	33.24%

Coded Coefficients

Term	Coef	SE Coef	95% CI	P-Value
Constant	2.119	0.133	(1.778; 2.460)	0.000
Ethanol Concentration	0.653	0.0812	(0.4438; 0.8612)	0.000
Solvent/Solid	0.106	0.0812	(-0.1022; 0.3151)	0.247
Time	-0.074	0.0812	(-0.2827; 0.1346)	0.404
Ethanol Concentration*Ethanol Concentration	-0.664	0.119	(-0.971; -0.356)	0.003
Solvent/Solid*Solvent/Solid	-0.063	0.119	(-0.370; 0.244)	0.622
Time*Time	0.017	0.119	(-0.291; 0.324)	0.895
Ethanol Concentration*Solvent/Solid	0.154	0.115	(-0.141; 0.450)	0.236
Ethanol Concentration*Time	-0.110	0.115	(-0.405; 0.185)	0.383
Solvent/Solid*Time	-0.145	0.115	(-0.440; 0.150)	0.261

Regression Equation in Uncoded Units

Increase in Green Intensity	=	-0.305 + 0.0542 Ethanol Concentration + 0.0382 Solvent/Solid + 0.0101 Time- 0.000415 Ethanol Concentration*Ethanol Concentration - 0.00063 Solvent/Solid*Solvent/Solid + 0.000018 Time*Time + 0.000386 Ethanol Concentration*Solvent/Solid - 0.000092 Ethanol Concentration*Time - 0.000484 Solvent/Solid*Time

Optimization Plot

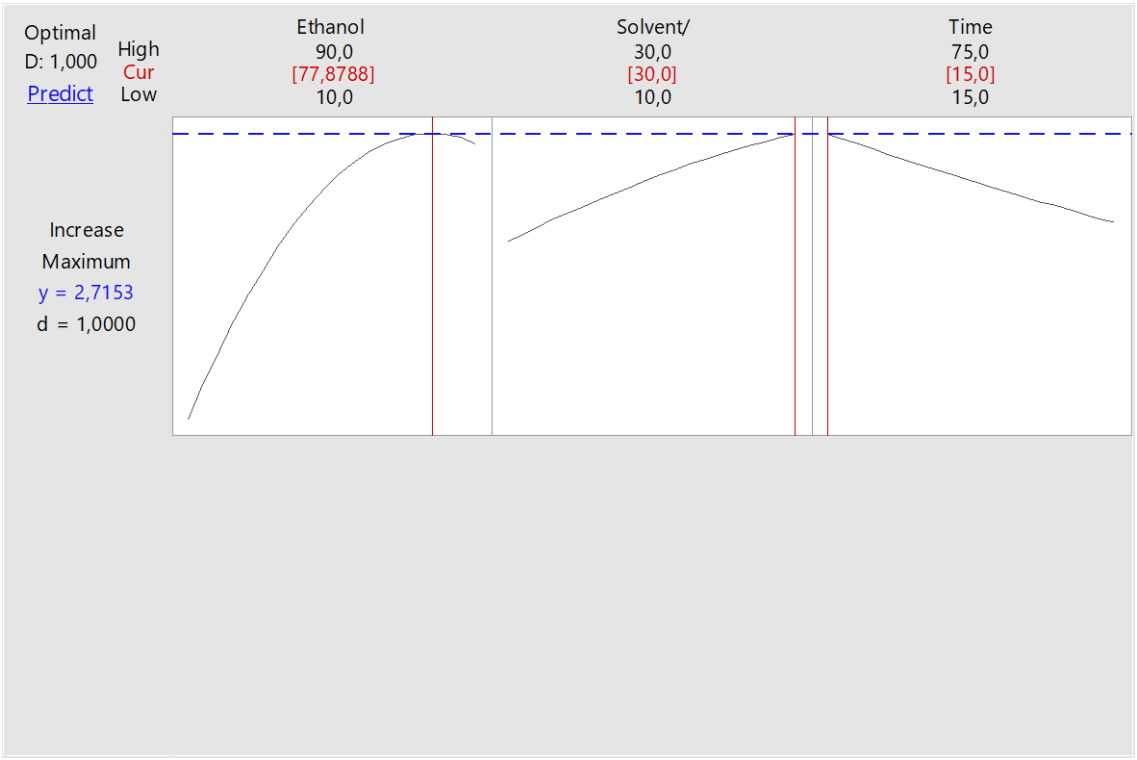

Table A.4 RSM results for the experiments containing ethanol acidified with 0.1% HCl (v v^{-1}) on Increase in Green Intensity

Analysis of Variance

Source	DF	Seq SS	Adj MS	F-Value	P-Value
Model	9	8.43354	0.93706	19.63	0.002
Linear	3	7.89562	2.63187	55.13	0.000
Ethanol Concentration	1	7.52637	7.52637	157.64	0.000
Solvent/Solid	1	0.36915	0.36915	7.73	0.039
Time	1	0.00011	0.00011	0.00	0.964
Square	3	0.51416	0.17139	3.59	0.101
Ethanol Concentration*Ethanol Concentration	1	0.40863	0.36865	7.72	0.039
Solvent/Solid*Solvent/Solid	1	0.00304	0.00634	0.13	0.731
Time*Time	1	0.10249	0.10249	2.15	0.203
2-Way Interaction	3	0.02376	0.00792	0.17	0.915
Ethanol Concentration*Solvent/Solid	1	0.02360	0.02360	0.49	0.513
Ethanol Concentration*Time	1	0.00003	0.00003	0.00	0.982
Solvent/Solid*Time	1	0.00014	0.00014	0.00	0.960
Error	5	0.23872	0.04774		
Lack-of-Fit	3	0.19802	0.06601	3.24	0.244
Pure Error	2	0.04069	0.02035		
Total	14	8.67226			

Model Summary

S	R-sq	R-sq(adj)	PRESS	R-sq(pred)
0.218502	97.25%	92.29%	3.25992	62.41%

Coded Coefficients

Term	Coef	SE Coef	95% CI	P-Value
Constant	2.165	0.126	(1.841; 2.489)	0.000
Ethanol Concentration	0.970	0.0773	(0.7714; 1.1685)	0.000
Solvent/Solid	0.215	0.0773	(0.0162; 0.4134)	0.039
Time	0.004	0.0773	(-0.1950; 0.2022)	0.964
Ethanol Concentration*Ethanol Concentration	-0.316	0.114	(-0.608; -0.024)	0.039
Solvent/Solid*Solvent/Solid	0.041	0.114	(-0.251; 0.334)	0.731
Time*Time	0.167	0.114	(-0.126; 0.459)	0.203
Ethanol Concentration*Solvent/Solid	0.077	0.109	(-0.204; 0.358)	0.513
Ethanol Concentration*Time	-0.003	0.109	(-0.283; 0.278)	0.982
Solvent/Solid*Time	0.006	0.109	(-0.275; 0.287)	0.960

Regression Equation in Uncoded Units

Increase in Green Intensity	=	0.769 + 0.0403 Ethanol Concentration - 0.0056 Solvent/Solid - 0.0168 Time- 0.000197 Ethanol Concentration*Ethanol Concentration + 0.00041 Solvent/Solid*Solvent/Solid + 0.000185 Time*Time + 0.000192 Ethanol Concentration*Solvent/Solid - 0.000002 Ethanol Concentration*Time + 0.000019 Solvent/Solid*Time

Optimization Plot

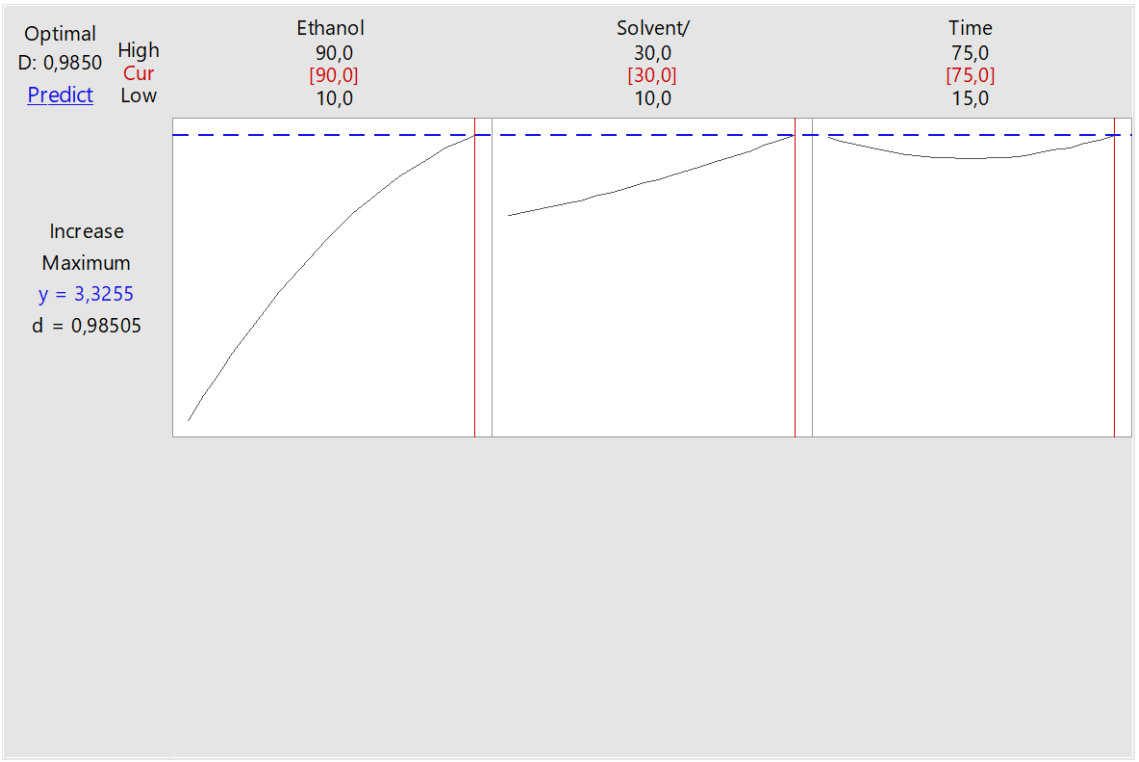

Table A.5 Optimization plot of the experiments containing ethanol acidified with 0.1% Ac (v v^{-1}) for multiple responses (Anthocyanin and Increase in Green Intensity)

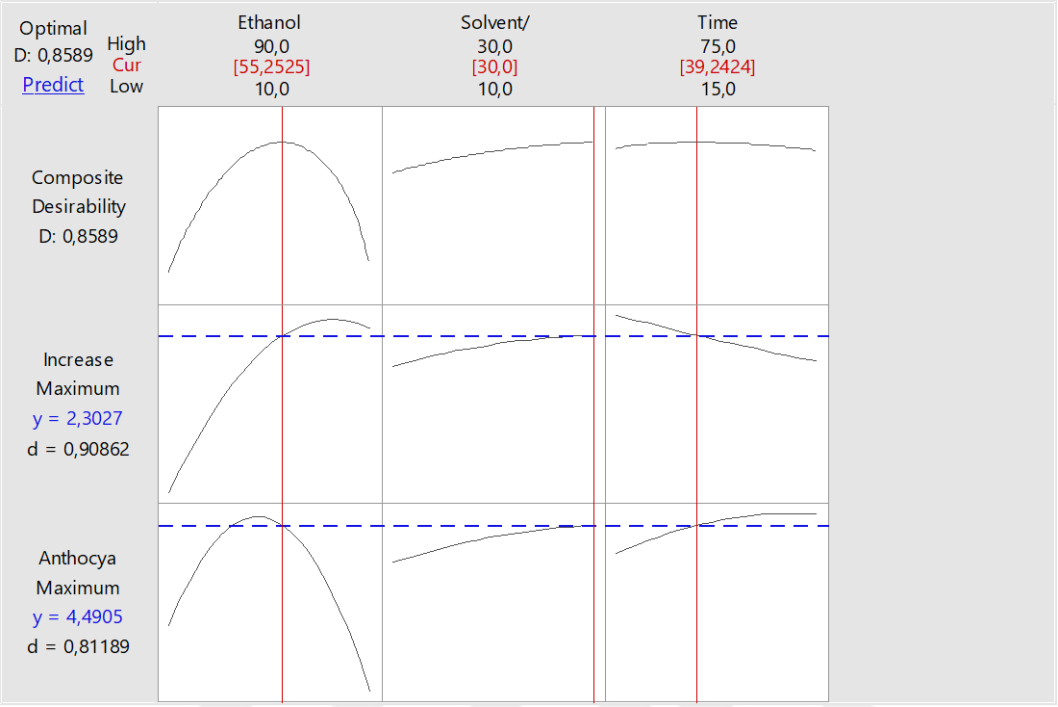

Table A.6 Optimization plot of the experiments containing ethanol acidified with 0.1% HCl (v v^{-1}) for multiple responses (Anthocyanin and Increase in Green Intensity)

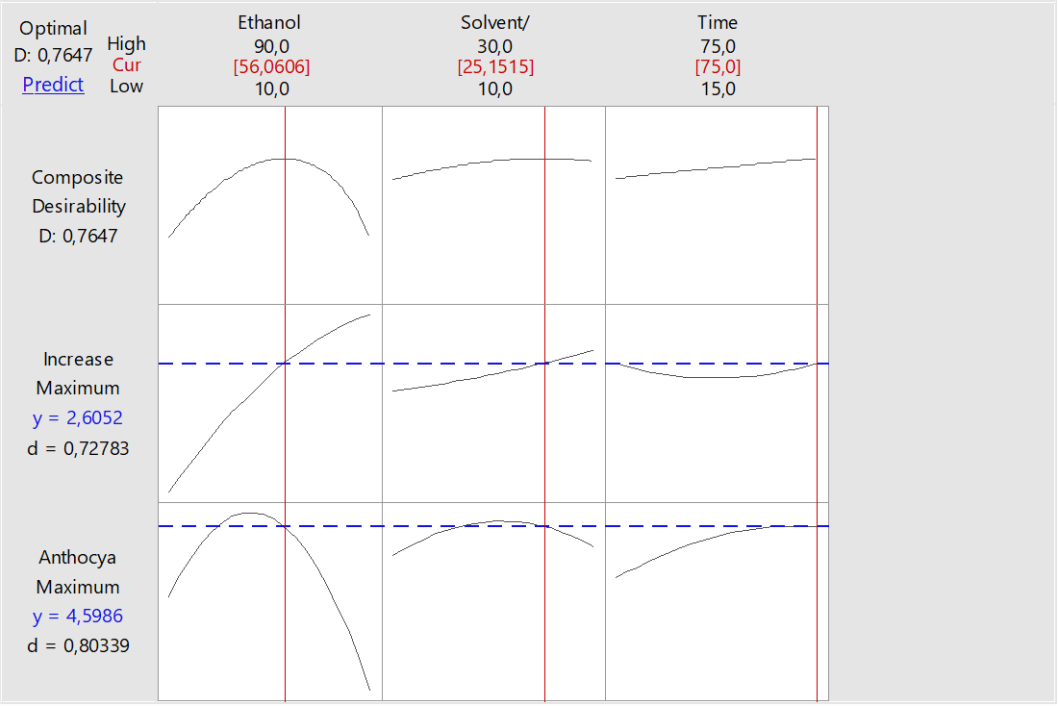

Table A.7 One-way ANOVA and Tukey's comparisons test for TMA results in different optimized extraction conditions

Method

Null hypothesis	All means are equal
Alternative hypothesis	Not all means are equal
Significance level	α = 0.05

Equal variances were assumed for the analysis.

Factor Information

Factor	Levels	Values
Extraction Conditions	4	55.25(0.1 % Ac)-30-39.24; 44.75(0.1%Ac)-30-69.55; 56.06(0.1 % HCl)-25.15-75; 43.94(0.1%HCl)-21.92-69.55

Analysis of Variance

Source	DF	Seq SS	Contribution	Adj SS	Adj MS	F-Value	P-Value
Extraction Conditions	3	1.7511	80.85%	1.7511	0.58371	11.26	0.003
Error	8	0.4149	19.15%	0.4149	0.05186		
Total	11	2.1660	100.00%				

Model Summary

S	R-sq	R-sq(adj)	PRESS	R-sq(pred)
0.227722	80.85%	73.66%	0.933430	56.91%

Means

Extraction Conditions	N	Mean	StDev	95% CI
55.25(0.1% Ac)-30-39.24	3	4.834	0.175	(4.531; 5.137)
44.75(0.1% Ac)-30-69.55	3	5.5017	0.1363	(5.1985; 5.8049)
56.06(0.1% HCl)-25.15-75	3	4.471	0.278	(4.168; 4.774)
43.94(0.1% HCl)-21.92-69.55	3	5.157	0.284	(4.854; 5.460)

Pooled StDev = 0.227722

Tukey Pairwise Comparisons
Grouping Information Using the Tukey Method and 95% Confidence

Extraction Conditions	N	Mean	Grouping		
44.75(0.1% Ac)-30-69.55	3	5.5017	A		
43.94(0.1% HCl)-21.92-69.55	3	5.157	A	B	
55.25(0.1% Ac)-30-39.24	3	4.834		B	C
56.06(0.1% HCl)-25.15-75	3	4.471			C

Means that do not share a letter are significantly different.

Table A.8 One-way ANOVA and Tukey's comparisons test for PPC results in different optimized extraction conditions

Method

Null hypothesis	All means are equal
Alternative hypothesis	Not all means are equal
Significance level	$\alpha = 0.05$

Equal variances were assumed for the analysis.

Factor Information

Factor	Levels	Values
Extraction Conditions	4	55.25(0.1 % Ac)-30-39.24; 44.75(0.1%Ac)-30-69.55; 56.06(0.1 % HCl)-25.15-75; 43.94(0.1%HCl)-21.92-69.55

Analysis of Variance

Source	DF	Seq SS	Contribution	Adj SS	Adj MS	F-Value
Extraction Conditions	3	450.1	79.18%	450.1	150.02	10.14
Error	8	118.4	20.82%	118.4	14.80	
Total	11	568.4	100.00%			

Model Summary

S	R-sq	R-sq(adj)	PRESS	R-sq(pred)
3.84671	79.18%	71.37%	266.349	53.14%

Means

Extraction Conditions	N	Mean	StDev	95% CI
55.25(0.1% Ac)-30-39.24	3	68.07	3.17	(62.95; 73.19)
44.75(0.1% Ac)-30-69.55	3	52.72	4.76	(47.59; 57.84)
56.06(0.1% HCl)-25.15-75	3	53.48	1.77	(48.36; 58.60)
43.94(0.1% HCl)-21.92-69.55	3	57.58	4.83	(52.45; 62.70)

Pooled StDev = 3.84671

Tukey Pairwise Comparisons
Grouping Information Using the Tukey Method and 95% Confidence

Extraction Conditions	N	Mean	Grouping	
55.25(0.1% Ac)-30-39.24	3	68.07	A	
43.94(0.1% HCl)-21.92-69.55	3	57.58		B
56.06(0.1% HCl)-25.15-75	3	53.48		B
44.75(0.1% Ac)-30-69.55	3	52.72		B

Means that do not share a letter are significantly different.

Table A.9 One-way ANOVA and Tukey's comparisons test for TPC results in different optimized extraction conditions

Method

Null hypothesis	All means are equal
Alternative hypothesis	Not all means are equal
Significance level	α = 0.05

Equal variances were assumed for the analysis.

Factor Information

Factor	Levels	Values
Extraction Conditions	4	55.25(0.1 % Ac)-30-39.24; 44.75(0.1%Ac)-30-69.55; 56.06(0.1 % HCl)-25.15-75; 43.94(0.1%HCl)-21.92-69.55

Analysis of Variance

Source	DF	Seq SS	Contribution	Adj SS	Adj MS	F-Value	P-Value
Extraction Conditions	3	72.87	80.87%	72.87	24.288	11.27	0.003
Error	8	17.24	19.13%	17.24	2.155		
Total	11	90.10	100.00%				

Model Summary

S	R-sq	R-sq(adj)	PRESS	R-sq(pred)
1.46796	80.87%	73.69%	38.7881	56.95%

Means

Extraction Conditions	N	Mean	StDev	95% CI
55.25(0.1% Ac)-30-39.24	3	28.788	1.539	(26.834; 30.743)
44.75(0.1% Ac)-30-69.55	3	32.795	0.316	(30.841; 34.750)
56.06(0.1% HCl)-25.15-75	3	26.55	2.39	(24.60; 28.51)
43.94(0.1% HCl)-21.92-69.55	3	31.771	0.663	(29.816; 33.725)

Pooled StDev = 1.46796

Tukey Pairwise Comparisons
Grouping Information Using the Tukey Method and 95% Confidence

Extraction Conditions	N	Mean	Grouping		
44.75(0.1% Ac)-30-69.55	3	32.795	A		
43.94(0.1% HCl)-21.92-69.55	3	31.771	A	B	
55.25(0.1% Ac)-30-39.24	3	28.788		B	C
56.06(0.1% HCl)-25.15-75	3	26.55			C

Means that do not share a letter are significantly different.

Table A.10 One-way ANOVA and Tukey's comparisons test for ABTS results in different optimized extraction conditions

Method

Null hypothesis	All means are equal
Alternative hypothesis	Not all means are equal
Significance level	α = 0.05

Equal variances were assumed for the analysis.

Factor Information

Factor	Levels	Values
Extraction Conditions	4	55.25(0.1 % Ac)-30-39.24; 44.75(0.1%Ac)-30-69.55; 56.06(0.1 % HCl)-25.15-75; 43.94(0.1%HCl)-21.92-69.55

Analysis of Variance

Source	DF	Seq SS	Contribution	Adj SS	Adj MS	F-Value	P-Value
Extraction Conditions	3	356.46	83.20%	356.46	118.820	13.20	0.002
Error	8	71.99	16.80%	71.99	8.999		
Total	11	428.45	100.00%				

Model Summary

S	R-sq	R-sq(adj)	PRESS	R-sq(pred)
2.99979	83.20%	76.90%	161.977	62.19%

Means

Extraction Conditions	N	Mean	StDev	95% CI
55.25(0.1% Ac)-30-39.24	3	55.849	1.708	(51.856; 59.843)
44.75(0.1% Ac)-30-69.55	3	69.59	3.27	(65.59; 73.58)
56.06(0.1% HCl)-25.15-75	3	61.693	0.676	(57.700; 65.687)
43.94(0.1% HCl)-21.92-69.55	3	68.01	4.68	(64.01; 72.00)

Pooled StDev = 2.99979

Tukey Pairwise Comparisons
Grouping Information Using the Tukey Method and 95% Confidence

Extraction Conditions	N	Mean	Grouping		
44.75(0.1% Ac)-30-69.55	3	69.59	A		
56.06(0.1% HCl)-25.15-75	3	68.01	A	B	
43.94(0.1% HCl)-21.92-69.55	3	61.693		B	C
55.25(0.1% Ac)-30-39.24	3	55.849			C

Means that do not share a letter are significantly different.

Table A.11 One-way ANOVA and Tukey's comparisons test for DPPH results in different optimized extraction conditions

Method

Null hypothesis	All means are equal
Alternative hypothesis	Not all means are equal
Significance level	$\alpha = 0.05$

Equal variances were assumed for the analysis.

Factor Information

Factor	Levels	Values
Extraction Conditions	4	55.25(0.1 % Ac)-30-39.24; 44.75(0.1%Ac)-30-69.55; 56.06(0.1 % HCl)-25.15-75; 43.94(0.1%HCl)-21.92-69.55

Analysis of Variance

Source	DF	Seq SS	Contribution	Adj SS	Adj MS	F-Value	P-Value
Extraction Conditions	3	98.41	86.04%	98.41	32.804	16.44	0.001
Error	8	15.96	13.96%	15.96	1.995		
Total	11	114.38	100.00%				

Model Summary

S	R-sq	R-sq(adj)	PRESS	R-sq(pred)
1.41258	86.04%	80.81%	35.9169	68.60%

Means

Extraction Conditions	N	Mean	StDev	95% CI
55.25(0.1% Ac)-30-39.24	3	16.800	1.080	(14.920; 18.681)
44.75(0.1% Ac)-30-69.55	3	19.984	0.848	(18.103; 21.865)
56.06(0.1% HCl)-25.15-75	3	19.27	2.04	(17.39; 21.15)
43.94(0.1% HCl)-21.92-69.55	3	24.709	1.397	(22.828; 26.590)

Pooled StDev = 1.41258

Tukey Pairwise Comparisons
Grouping Information Using the Tukey Method and 95% Confidence

Extraction Conditions	N	Mean	Grouping
43.94(0.1% HCl)-21.92-69.55	3	24.709	A
44.75(0.1% Ac)-30-69.55	3	19.984	B
56.06(0.1% HCl)-25.15-75	3	19.27	B
55.25(0.1% Ac)-30-39.24	3	16.800	B

Means that do not share a letter are significantly different.

Table A.12 One-way ANOVA and Tukey's comparisons test for K values of 10% PCL (w v^{-1}) solution prepared by different PBE concentrations % (w v^{-1})

Method

Null hypothesis	All means are equal
Alternative hypothesis	Not all means are equal
Significance level	$\alpha = 0.05$

Equal variances were assumed for the analysis.

Factor Information

Factor	Levels	Values
PBE Concentration	4	10 % PCL & 0 % PBE; 10 % PCL & 0.2 % PBE; 10 % PCL & 0.4 % PBE; 10 % PCL & 0.6 % PBE

Analysis of Variance

Source	DF	Adj SS	Adj MS	F-Value	P-Value
PBE Concentration	3	0.05123	0.017076	11.43	0.003
Error	8	0.01195	0.001494		
Total	11	0.06318			

Model Summary

S	R-sq	R-sq(adj)	R-sq(pred)
0.0386488	81.09%	73.99%	57.44%

Means

Sample Explanations	N	Mean	StDev	95% CI
10 % PCL & 0 % PBE	3	0.5914	0.0452	(0.5399; 0.6428)
10 % PCL & 0.2 % PBE	3	0.6895	0.0228	(0.6380; 0.7409)
10 % PCL & 0.4 % PBE	3	0.7002	0.0217	(0.6487; 0.7516)
10 % PCL & 0.6 % PBE	3	0.7751	0.0542	(0.7237; 0.8266)

Pooled StDev = 0.0386488

Tukey Pairwise Comparisons
Grouping Information Using the Tukey Method and 95% Confidence

Sample Explanations	N	Mean	Grouping	
10 % PCL & 0.6 % PBE	3	0.7751	A	
10 % PCL & 0.4 % PBE	3	0.7002	A	
10 % PCL & 0.2 % PBE	3	0.6895	A	B
10 % PCL & 0 % PBE	3	0.5914		B

Means that do not share a letter are significantly different.

Table A.13 One-way ANOVA and Tukey's comparisons test for n values of 10% PCL (w v^{-1}) solution prepared by different PBE concentrations % (w v^{-1})

Method

Null hypothesis	All means are equal
Alternative hypothesis	Not all means are equal
Significance level	$\alpha = 0.05$

Equal variances were assumed for the analysis.

Factor Information

Factor	Levels	Values
PBE Concentration	4	10 % PCL & 0 % PBE; 10 % PCL & 0.2 % PBE; 10 % PCL & 0.4 % PBE; 10 % PCL & 0.6 % PBE

Analysis of Variance

Source	DF	Adj SS	Adj MS	F-Value	P-Value
PBE Concentration	3	0.006413	0.002138	1.71	0.242
Error	8	0.010018	0.001252		
Total	11	0.016431			

Model Summary

S	R-sq	R-sq(adj)	R-sq(pred)
0.0353874	39.03%	16.16%	0.00%

Means

Sample Explanations	N	Mean	StDev	95% CI
10 % PCL & 0 % PBE	3	0.8253	0.0579	(0.7782; 0.8724)
10 % PCL & 0.2 % PBE	3	0.8689	0.0378	(0.8218; 0.9160)
10 % PCL & 0.4 % PBE	3	0.87177	0.01477	(0.82465; 0.91888)
10 % PCL & 0.6 % PBE	3	0.88760	0.00392	(0.84049; 0.93471)

Pooled StDev = 0.0353874

Tukey Pairwise Comparisons
Grouping Information Using the Tukey Method and 95% Confidence

Sample Explanations	N	Mean	Grouping
10 % PCL & 0.6 % PBE	3	0.88760	A
10 % PCL & 0.4 % PBE	3	0.87177	A
10 % PCL & 0.2 % PBE	3	0.8689	A
10 % PCL & 0 % PBE	3	0.8253	A

Means that do not share a letter are significantly different.

Table A.14 One-way ANOVA and Tukey's comparisons test for apparent viscosity values of 10% PCL (w v^{-1}) solution prepared by different PBE concentrations % (w v^{-1})

Method

Null hypothesis	All means are equal
Alternative hypothesis	Not all means are equal
Significance level	α = 0.05

Equal variances were assumed for the analysis.

Factor Information

Factor	Levels	Values
PBE Concentration	4	10 % PCL & 0 % PBE; 10 % PCL & 0.2 % PBE; 10 % PCL & 0.4 % PBE; 10 % PCL & 0.6 % PBE

Analysis of Variance

Source	DF	Adj SS	Adj MS	F-Value	P-Value
PBE Concentration	3	0.05773	0.019245	5.71	0.022
Error	8	0.02695	0.003368		
Total	11	0.08468			

Model Summary

S	R-sq	R-sq(adj)	R-sq(pred)
0.0580364	68.18%	56.25%	28.40%

Means

Sample Explanations	N	Mean	StDev	95% CI
10 % PCL & 0 % PBE	3	0.2994	0.0823	(0.2221; 0.3767)
10 % PCL & 0.2 % PBE	3	0.4115	0.0715	(0.3342; 0.4887)
10 % PCL & 0.4 % PBE	3	0.4183	0.0271	(0.3411; 0.4956)
10 % PCL & 0.6 % PBE	3	0.4938	0.0291	(0.4165; 0.5710)

Pooled StDev = 0.0580364

Tukey Pairwise Comparisons
Grouping Information Using the Tukey Method and 95% Confidence

Sample Explanations	N	Mean	Grouping	
10 % PCL & 0.6 % PBE	3	0.4938	A	
10 % PCL & 0.4 % PBE	3	0.4183	A	B
10 % PCL & 0.2 % PBE	3	0.4115	A	B
10 % PCL & 0 % PBE	3	0.2994		B

Means that do not share a letter are significantly different.

Table A.15 One-way ANOVA: Fiber Diameter (nm) vs Experiment Conditions for 10% PCL (w v^{-1}) & 0% PBE(w v^{-1})

Method

Null hypothesis	All means are equal
Alternative hypothesis	Not all means are equal
Significance level	$\alpha = 0.05$

Equal variances were assumed for the analysis.

Factor Information

Factor	Levels	Values
Experiment	4	1(V=20 kV; Q=0.5 ml/h); 2(V=25 kV; Q=0.5 ml/h); 3(V=20 kV; Q=0.4 ml/h); 4(V=25 kV; Q=0.4 ml/h)

Analysis of Variance

Source	DF	Adj SS	Adj MS	F-Value	P-Value
Experiment	3	81135	27045	9.56	0.000
Error	236	667722	2829		
Total	239	748856			

Model Summary

S	R-sq	R-sq(adj)	R-sq(pred)
53.1914	10.83%	9.70%	7.79%

Means

Experiment	N	Mean	StDev	95% CI
1(V=20 kV; Q=0.5 ml/h)	60	111.99	52.16	(98.46; 125.52)
2(V=25 kV; Q=0.5 ml/h)	60	123.82	48.22	(110.29; 137.35)
3(V=20 kV; Q=0.4 ml/h)	60	145.92	50.05	(132.39; 159.45)
4(V=25 kV; Q=0.4 ml/h)	60	159.06	61.37	(145.53; 172.59)

Pooled StDev = 53.1914

Tukey Pairwise Comparisons
Grouping Information Using the Tukey Method and 95% Confidence

Experiment	N	Mean	Grouping		
4(V=25 kV; Q=0.4 ml/h)	60	159.06	A		
3(V=20 kV; Q=0.4 ml/h)	60	145.92	A	B	
2(V=25 kV; Q=0.5 ml/h)	60	123.82		B	C
1(V=20 kV; Q=0.5 ml/h)	60	111.99			C

Means that do not share a letter are significantly different.

Table A.16 One-way ANOVA: Fiber Diameter (nm) vs Experiment Conditions for 10% PCL (w v^{-1}) & 0.2% PBE (w v^{-1})

Method

Null hypothesis	All means are equal
Alternative hypothesis	Not all means are equal
Significance level	$\alpha = 0.05$

Equal variances were assumed for the analysis.

Factor Information

Factor	Levels	Values
Experiment	4	1(V=20 kV; Q=0.5 ml/h); 2(V=25 kV; Q=0.5 ml/h); 3(V=20 kV; Q=0.4 ml/h); 4(V=25 kV; Q=0.4 ml/h)

Analysis of Variance

Source	DF	Adj SS	Adj MS	F-Value	P-Value
Experiment	3	18347	6116	0.90	0.444
Error	236	1611443	6828		
Total	239	1629790			

Model Summary

S	R-sq	R-sq(adj)	R-sq(pred)
82.6326	1.13%	0.00%	0.00%

Means

Experiment	N	Mean	StDev	95% CI
1(V=20 kV; Q=0.5 ml/h)	60	172.55	76.58	(151.53; 193.56)
2(V=25 kV; Q=0.5 ml/h)	60	195.3	91.4	(174.2; 216.3)
3(V=20 kV; Q=0.4 ml/h)	60	178.97	67.65	(157.96; 199.99)
4(V=25 kV; Q=0.4 ml/h)	60	188.7	92.3	(167.7; 209.8)

Pooled StDev = 82.6326

Tukey Pairwise Comparisons
Grouping Information Using the Tukey Method and 95% Confidence

Experiment	N	Mean	Grouping
2(V=25 kV; Q=0.5 ml/h)	60	195.3	A
4(V=25 kV; Q=0.4 ml/h)	60	188.7	A
3(V=20 kV; Q=0.4 ml/h)	60	178.97	A
1(V=20 kV; Q=0.5 ml/h)	60	172.55	A

Means that do not share a letter are significantly different.

Table A.17 One-way ANOVA: Fiber Diameter (nm) vs Experiment Conditions for 10% PCL (w v^{-1}) & 0.4% PBE (w v^{-1})

Method

Null hypothesis	All means are equal
Alternative hypothesis	Not all means are equal
Significance level	$\alpha = 0.05$

Equal variances were assumed for the analysis.

Factor Information

Factor	Levels	Values
Experiment	4	1(V=20 kV; Q=0.5 ml/h); 2(V=25 kV; Q=0.5 ml/h); 3(V=20 kV; Q=0.4 ml/h); 4(V=25 kV; Q=0.4 ml/h)

Analysis of Variance

Source	DF	Adj SS	Adj MS	F-Value	P-Value
Experiment	3	47901	15967	2.52	0.059
Error	236	1497891	6347		
Total	239	1545792			

Model Summary

S	R-sq	R-sq(adj)	R-sq(pred)
79.6680	3.10%	1.87%	0.00%

Means

Experiment	N	Mean	StDev	95% CI
1(V=20 kV; Q=0.5 ml/h)	60	173.7	79.9	(153.5; 194.0)
2(V=25 kV; Q=0.5 ml/h)	60	195.2	102.3	(174.9; 215.5)
3(V=20 kV; Q=0.4 ml/h)	60	178.59	52.92	(158.33; 198.86)
4(V=25 kV; Q=0.4 ml/h)	60	209.46	75.76	(189.20; 229.73)

Pooled StDev = 79.6680

Tukey Pairwise Comparisons
Grouping Information Using the Tukey Method and 95% Confidence

Experiment	N	Mean	Grouping
4(V=25 kV; Q=0.4 ml/h)	60	209.46	A
2(V=25 kV; Q=0.5 ml/h)	60	195.2	A
3(V=20 kV; Q=0.4 ml/h)	60	178.59	A
1(V=20 kV; Q=0.5 ml/h)	60	173.7	A

Means that do not share a letter are significantly different

Table A.18 One-way ANOVA: Fiber Diameter (nm) vs Experiment Conditions for 10% PCL (w v^{-1}) & 0.6% PBE (w v^{-1})

Method

Null hypothesis	All means are equal
Alternative hypothesis	Not all means are equal
Significance level	$\alpha = 0.05$

Equal variances were assumed for the analysis.

Factor Information

Factor	Levels	Values
Experiment	4	1(V=20 kV; Q=0.5 ml/h); 2(V=25 kV; Q=0.5 ml/h); 3(V=20 kV; Q=0.4 ml/h); 4(V=25 kV; Q=0.4 ml/h)

Analysis of Variance

Source	DF	Adj SS	Adj MS	F-Value	P-Value
Experiment	3	127199	42400	4.32	0.005
Error	236	2317317	9819		
Total	239	2444516			

Model Summary

S	R-sq	R-sq(adj)	R-sq(pred)
99.0916	5.20%	4.00%	1.96%

Means

Experiment	N	Mean	StDev	95% CI
1(V=20 kV; Q=0.5 ml/h)	60	253.4	80.9	(228.2; 278.6)
2(V=25 kV; Q=0.5 ml/h)	60	225.4	83.2	(200.2; 250.6)
3(V=20 kV; Q=0.4 ml/h)	60	235.4	92.5	(210.2; 260.6)
4(V=25 kV; Q=0.4 ml/h)	60	285.9	131.4	(260.7; 311.1)

Pooled StDev = 99.0916

Tukey Pairwise Comparisons
Grouping Information Using the Tukey Method and 95% Confidence

Experiment	N	Mean	Grouping	
4(V=25 kV; Q=0.4 ml/h)	60	285.9	A	
1(V=20 kV; Q=0.5 ml/h)	60	253.4	A	B
1(V=20 kV; Q=0.5 ml/h)	60	235.4		B
2(V=25 kV; Q=0.5 ml/h)	60	225.4		B

Means that do not share a letter are significantly different.

Table A.19 One-way ANOVA: Fiber Diameter (nm) Electrospun at V=20 kV; Q=0.5 mL h^{-1} vs 10% PCL (w v^{-1}) for different PBE% (w v^{-1}) Concentrations

Method

Null hypothesis	All means are equal
Alternative hypothesis	Not all means are equal
Significance level	$\alpha = 0.05$

Equal variances were assumed for the analysis.

Factor Information

Factor	Levels	Values
PBE Concentration	4	10 % PCL & 0 % PBE; 10 % PCL & 0.2 % PBE; 10 % PCL & 0.4 % PBE; 10 % PCL & 0.6 % PBE

Analysis of Variance

Source	DF	Adj SS	Adj MS	F-Value	P-Value
PBE Concentration	3	605267	201756	37.52	0.000
Error	236	1268955	5377		
Total	239	1874222			

Model Summary

S	R-sq	R-sq(adj)	R-sq(pred)
73.3275	32.29%	31.43%	29.98%

Means

PBE Concentration	N	Mean	StDev	95% CI
10 % PCL & 0 % PBE	60	111.99	52.16	(93.34; 130.64)
10 % PCL & 0.2 % PBE	60	172.55	76.58	(153.90; 191.19)
10 % PCL & 0.4 % PBE	60	173.7	79.9	(155.1; 192.4)
10 % PCL & 0.6 % PBE	60	253.4	80.9	(234.7; 272.0)

Pooled StDev = 73.3275

Tukey Pairwise Comparisons
Grouping Information Using the Tukey Method and 95% Confidence

PBE Concentration	N	Mean	Grouping		
10 % PCL & 0.6 % PBE	60	253.4	A		
10 % PCL & 0.4 % PBE	60	173.7		B	
10 % PCL & 0.2 % PBE	60	172.55		B	
10 % PCL & 0 % PBE	60	111.99			C

Means that do not share a letter are significantly different

Table A.20 One-way ANOVA: Fiber Diameter (nm) Electrospun at V=25 kV; Q=0.5 mL h^{-1} vs 10% PCL (w v^{-1}) for different PBE % (w v^{-1}) Concentrations

Method

Null hypothesis	All means are equal
Alternative hypothesis	Not all means are equal
Significance level	$\alpha = 0.05$

Equal variances were assumed for the analysis.

Factor Information

Factor	Levels	Values
PBE Concentration	4	10 % PCL & 0 % PBE; 10 % PCL & 0.2 % PBE; 10 % PCL & 0.4 % PBE; 10 % PCL & 0.6 % PBE

Analysis of Variance

Source	DF	Adj SS	Adj MS	F-Value	P-Value
PBE Concentration	3	335239	111746	15.93	0.000
Error	236	1655859	7016		
Total	239	1991098			

Model Summary

S	R-sq	R-sq(adj)	R-sq(pred)
83.7637	16.84%	15.78%	13.99%

Means

PBE Concentration	N	Mean	StDev	95% CI
10 % PCL & 0 % PBE	60	123.82	48.22	(102.51; 145.12)
10 % PCL & 0.2 % PBE	60	195.3	91.4	(174.0; 216.6)
10 % PCL & 0.4 % PBE	60	195.2	102.3	(173.9; 216.5)
10 % PCL & 0.6 % PBE	60	225.4	83.2	(204.1; 246.7)

Pooled StDev = 83.7637

Tukey Pairwise Comparisons
Grouping Information Using the Tukey Method and 95% Confidence

PBE Concentration	N	Mean	Grouping
10 % PCL & 0.6 % PBE	60	225.4	A
10 % PCL & 0.4 % PBE	60	195.3	A
10 % PCL & 0.2 % PBE	60	195.2	A
10 % PCL & 0 % PBE	60	123.82	B

Means that do not share a letter are significantly different

Table A.21 One-way ANOVA: Fiber Diameter (nm) Electrospun at V=20 kV; Q=0.4 mL h^{-1} vs 10% PCL (w v^{-1}) for different PBE % (w v^{-1}) Concentrations

Method

Null hypothesis	All means are equal
Alternative hypothesis	Not all means are equal
Significance level	$\alpha = 0.05$

Equal variances were assumed for the analysis.

Factor Information

Factor	Levels	Values
PBE Concentration	4	10 % PCL & 0 % PBE; 10 % PCL & 0.2 % PBE; 10 % PCL & 0.4 % PBE; 10 % PCL & 0.6 % PBE

Analysis of Variance

Source	DF	Adj SS	Adj MS	F-Value	P-Value
PBE Concentration	3	248597	82866	17.98	0.000
Error	236	1087409	4608		
Total	239	1336006			

Model Summary

S	R-sq	R-sq(adj)	R-sq(pred)
67.8798	18.61%	17.57%	15.83%

Means

PBE Concentration	N	Mean	StDev	95% CI
10 % PCL & 0 % PBE	60	145.92	50.05	(128.65; 163.18)
10 % PCL & 0.2 % PBE	60	178.97	67.65	(161.71; 196.24)
10 % PCL & 0.4 % PBE	60	178.59	52.92	(161.33; 195.86)
10 % PCL & 0.6 % PBE	60	235.4	92.5	(218.1; 252.7)

Pooled StDev = 67.8798

Tukey Pairwise Comparisons
Grouping Information Using the Tukey Method and 95% Confidence

PBE Concentration	N	Mean	Grouping		
10 % PCL & 0.6 % PBE	60	235.4	A		
10 % PCL & 0.2 % PBE	60	178.97		B	
10 % PCL & 0.4 % PBE	60	178.59		B	
10 % PCL & 0 % PBE	60	145.92			C

Means that do not share a letter are significantly different

Table A.22 One-way ANOVA: Fiber Diameter (nm) Electrospun at V=25 kV; Q=0.4 mL h^{-1} vs 10% PCL (w v^{-1}) for different PBE % (w v^{-1}) Concentrations

Method

Null hypothesis	All means are equal
Alternative hypothesis	Not all means are equal
Significance level	$\alpha = 0.05$

Equal variances were assumed for the analysis.

Factor Information

Factor	Levels	Values
PBE Concentration	4	10 % PCL & 0 % PBE; 10 % PCL & 0.2 % PBE; 10 % PCL & 0.4 % PBE; 10 % PCL & 0.6 % PBE

Analysis of Variance

Source	DF	Adj SS	Adj MS	F-Value	P-Value
PBE Concentration	3	528637	176212	19.97	0.000
Error	236	2082149	8823		
Total	239	2610786			

Model Summary

S	R-sq	R-sq(adj)	R-sq(pred)
93.9290	20.25%	19.23%	17.52%

Means

PBE Concentration	N	Mean	StDev	95% CI
10 % PCL & 0 % PBE	60	159.06	61.37	(135.17; 182.95)
10 % PCL & 0.2 % PBE	60	188.7	92.3	(164.9; 212.6)
10 % PCL & 0.4 % PBE	60	209.46	75.76	(185.57; 233.35)
10 % PCL & 0.6 % PBE	60	285.9	131.4	(262.0; 309.8)

Pooled StDev = 93.9290

Tukey Pairwise Comparisons
Grouping Information Using the Tukey Method and 95% Confidence

PBE Concentration	N	Mean	Grouping		
10 % PCL & 0.6 % PBE	60	285.9	A		
10 % PCL & 0.4 % PBE	60	209.46		B	
10 % PCL & 0.2 % PBE	60	188.7		B	C
10 % PCL & 0 % PBE	60	159.06			C

Means that do not share a letter are significantly differen

Table A.23 One-way ANOVA: Film Thickness (μm) vs Experiment Conditions for 10% PCL (w v^{-1}) & 0% PBE (w v^{-1})

Method

Null hypothesis	All means are equal
Alternative hypothesis	Not all means are equal
Significance level	α = 0.05

Equal variances were assumed for the analysis.

Factor Information

Factor	Levels	Values
Experiment	4	1(V=20 kV; Q=0.5 ml/h); 2(V=25 kV; Q=0.5 ml/h); 3(V=20 kV; Q=0.4 ml/h); 4(V=25 kV; Q=0.4 ml/h)

Analysis of Variance

Source	DF	Adj SS	Adj MS	F-Value	P-Value
Experiment	3	7906	2635.3	3.40	0.028
Error	36	27932	775.9		
Total	39	35837			

Model Summary

S	R-sq	R-sq(adj)	R-sq(pred)
27.8545	22.06%	15.57%	3.78%

Means

Experiment	N	Mean	StDev	95% CI
1(V=20 kV; Q=0.5 ml/h)	10	117.40	26.91	(99.54; 135.26)
2(V=25 kV; Q=0.5 ml/h)	10	142.70	40.12	(124.8; 160.6)
3(V=20 kV; Q=0.4 ml/h)	10	122.10	14.40	(104.24; 139.96)
4(V=25 kV; Q=0.4 ml/h)	10	151.30	23.71	(133.44; 169.16)

Pooled StDev = 27.8545

Tukey Pairwise Comparisons
Grouping Information Using the Tukey Method and 95% Confidence

Experiment	N	Mean	Grouping	
4(V=25 kV; Q=0.4 ml/h)4	10	151.30	A	
2(V=25 kV; Q=0.5 ml/h)	10	142.70	A	B
3(V=20 kV; Q=0.4 ml/h)	10	122.10	A	B
1(V=20 kV; Q=0.5 ml/h)	10	117.40		B

Means that do not share a letter are significantly different

Table A.24 One-way ANOVA: Film Thickness (μm) vs Experiment Conditions for 10% PCL (w v^{-1}) & 0.2% PBE (w v^{-1})

Method

Null hypothesis	All means are equal
Alternative hypothesis	Not all means are equal
Significance level	α = 0.05

Equal variances were assumed for the analysis.

Factor Information

Factor	Levels	Values
Experiment	4	1(V=20 kV; Q=0.5 ml/h); 2(V=25 kV; Q=0.5 ml/h); 3(V=20 kV; Q=0.4 ml/h); 4(V=25 kV; Q=0.4 ml/h)

Analysis of Variance

Source	DF	Adj SS	Adj MS	F-Value	P-Value
Experiment	3	5555	1851.8	2.86	0.051
Error	36	23350	648.6		
Total	39	28905			

Model Summary

S	R-sq	R-sq(adj)	R-sq(pred)
25.4676	19.22%	12.49%	0.27%

Means

Experiment	N	Mean	StDev	95% CI
1(V=20 kV; Q=0.5 ml/h)	10	92.00	37.22	(75.67; 108.33)
2(V=25 kV; Q=0.5 ml/h)	10	121.90	18.22	(105.57; 138.23)
3(V=20 kV; Q=0.4 ml/h)	10	103.70	29.07	(87.37; 120.03)
4(V=25 kV; Q=0.4 ml/h)	10	117.50	5.68	(101.17; 133.83)

Pooled StDev = 25.4676

Tukey Pairwise Comparisons
Grouping Information Using the Tukey Method and 95% Confidence

Experiment	N	Mean	Grouping
2(V=25 kV; Q=0.5 ml/h)	10	121.90	A
4(V=25 kV; Q=0.4 ml/h)	10	117.50	A
3(V=20 kV; Q=0.4 ml/h)	10	103.70	A
1(V=20 kV; Q=0.5 ml/h)	10	92.00	A

Means that do not share a letter are significantly different.

Table A.25 One-way ANOVA: Film Thickness (μm) vs Experiment Conditions for 10% PCL(w v^{-1}) & 0.4% PBE (w v^{-1})

Method

Null hypothesis	All means are equal
Alternative hypothesis	Not all means are equal
Significance level	α = 0.05

Equal variances were assumed for the analysis.

Factor Information

Factor	Levels	Values
Experiment	4	1(V=20 kV; Q=0.5 ml/h); 2(V=25 kV; Q=0.5 ml/h); 3(V=20 kV; Q=0.4 ml/h); 4(V=25 kV; Q=0.4 ml/h)

Analysis of Variance

Source	DF	Adj SS	Adj MS	F-Value	P-Value
Experiment	3	12351	4117.2	10.43	0.000
Error	36	14217	394.9		
Total	39	26568			

Model Summary

S	R-sq	R-sq(adj)	R-sq(pred)
19.8722	46.49%	42.03%	33.94%

Means

Experiment	N	Mean	StDev	95% CI
1(V=20 kV; Q=0.5 ml/h)	10	83.30	12.57	(70.56; 96.04)
2(V=25 kV; Q=0.5 ml/h)	10	132.40	26.98	(119.66; 145.14)
3(V=20 kV; Q=0.4 ml/h)	10	108.80	15.05	(96.06; 121.54)
4(V=25 kV; Q=0.4 ml/h)	10	114.40	21.61	(101.66; 127.14)

Pooled StDev = 19.8722

Tukey Pairwise Comparisons
Grouping Information Using the Tukey Method and 95% Confidence

Experiment	N	Mean	Grouping	
2(V=25 kV; Q=0.5 ml/h	10	132.40	A	
4(V=25 kV; Q=0.4 ml/h)	10	114.40	A	
3(V=20 kV; Q=0.4 ml/h)	10	108.80	A	
1(V=20 kV; Q=0.5 ml/h)	10	83.30		B

Means that do not share a letter are significantly different.

Table A.26 One-way ANOVA: Film Thickness (μm) vs Experiment Conditions for 10% PCL (w v^{-1}) & 0.6% PBE (w v^{-1})

Method

Null hypothesis	All means are equal
Alternative hypothesis	Not all means are equal
Significance level	α = 0.05

Equal variances were assumed for the analysis.

Factor Information

Factor	Levels	Values
Experiment	4	1(V=20 kV; Q=0.5 ml/h); 2(V=25 kV; Q=0.5 ml/h); 3(V=20 kV; Q=0.4 ml/h); 4(V=25 kV; Q=0.4 ml/h)

Analysis of Variance

Source	DF	Adj SS	Adj MS	F-Value	P-Value
Experiment	3	67409	22470	14.40	0.000
Error	36	56164	1560		
Total	39	123573			

Model Summary

S	R-sq	R-sq(adj)	R-sq(pred)
39.4983	54.55%	50.76%	43.89%

Means

Experiment	N	Mean	StDev	95% CI
1(V=20 kV; Q=0.5 ml/h)	10	92.80	12.68	(67.47; 118.13)
2(V=25 kV; Q=0.5 ml/h)	10	192.50	57.78	(167.17; 217.83)
3(V=20 kV; Q=0.4 ml/h)	10	95.60	19.59	(70.27; 120.93)
4(V=25 kV; Q=0.4 ml/h)	10	146.80	48.55	(121.47; 172.13)

Pooled StDev = 39.4983

Tukey Pairwise Comparisons
Grouping Information Using the Tukey Method and 95% Confidence

Experiment	N	Mean	Grouping	
2(V=25 kV; Q=0.5 ml/h)	10	192.50	A	
4(V=25 kV; Q=0.4 ml/h)	10	146.80	A	
3(V=20 kV; Q=0.4 ml/h)	10	95.60		B
1(V=20 kV; Q=0.5 ml/h)	10	92.80		B

Means that do not share a letter are significantly different.

Table A.27 One-way ANOVA: Film Thickness (μm) Electrospun at V=20 kV; Q=0.5 mL h^{-1} vs 10% PCL (w v^{-1}) for different PBE % (w v^{-1}) Concentrations

Method

Null hypothesis	All means are equal
Alternative hypothesis	Not all means are equal
Significance level	α = 0.05

Equal variances were assumed for the analysis.

Factor Information

Factor	Levels	Values
PBE Concentration	4	10 % PCL & 0 % PBE; 10 % PCL & 0.2 % PBE; 10 % PCL & 0.4 % PBE; 10 % PCL & 0.6 % PBE

Analysis of Variance

Source	DF	Adj SS	Adj MS	F-Value	P-Value
PBE Concentration	3	6449	2149.8	3.54	0.024
Error	36	21854	607.1		
Total	39	28303			

Model Summary

S	R-sq	R-sq(adj)	R-sq(pred)
24.6386	22.79%	16.35%	4.67%

Means

PBE Concentration	N	Mean	StDev	95% CI
10 % PCL & 0 % PBE	10	117.40	26.91	(101.60; 133.20)
10 % PCL & 0.2 % PBE	10	92.80	12.68	(77.00; 108.60)
10 % PCL & 0.4 % PBE	10	92.00	37.22	(76.20; 107.80)
10 % PCL & 0.6 % PBE	10	83.30	12.57	(67.50; 99.10)

Pooled StDev = 24.6386

Tukey Pairwise Comparisons
Grouping Information Using the Tukey Method and 95% Confidence

PBE Concentration	N	Mean	Grouping	
10 % PCL & 0 % PBE	10	117.40	A	
10 % PCL & 0.6 % PBE	10	92.80	A	B
10 % PCL & 0.2 % PBE	10	92.00	A	B
10 % PCL & 0.4 % PBE	10	83.30		B

Means that do not share a letter are significantly different.

Table A.28 One-way ANOVA: Film Thickness (μm) Electrospun at V=25 kV; Q=0.5 mL h^{-1} vs 10% PCL (w v^{-1}) for different PBE % (w v^{-1}) Concentrations

Method

Null hypothesis	All means are equal
Alternative hypothesis	Not all means are equal
Significance level	$\alpha = 0.05$

Equal variances were assumed for the analysis.

Factor Information

Factor	Levels	Values
PBE Concentration	4	10 % PCL & 0 % PBE; 10 % PCL & 0.2 % PBE; 10 % PCL & 0.4 % PBE; 10 % PCL & 0.6 % PBE

Analysis of Variance

Source	DF	Adj SS	Adj MS	F-Value	P-Value
PBE Concentration	3	29313	9771	6.50	0.001
Error	36	54076	1502		
Total	39	83389			

Model Summary

S	R-sq	R-sq(adj)	R-sq(pred)
38.7570	35.15%	29.75%	19.94%

Means

PBE Concentration	N	Mean	StDev	95% CI
10 % PCL & 0 % PBE	10	142.70	40.12	(117.84; 167.56)
10 % PCL & 0.2 % PBE	10	121.90	18.22	(97.04; 146.76)
10 % PCL & 0.4 % PBE	10	132.40	26.98	(107.54; 157.26)
10 % PCL & 0.6 % PBE	10	192.50	57.78	(167.64; 217.36)

Pooled StDev = 38.7570

Tukey Pairwise Comparisons
Grouping Information Using the Tukey Method and 95% Confidence

PBE Concentration	N	Mean	Grouping	
10 % PCL & 0.6 % PBE	10	192.50	A	
10 % PCL & 0 % PBE	10	142.70		B
10 % PCL & 0.4 % PBE	10	132.40		B
10 % PCL & 0.2 % PBE	10	121.90		B

Means that do not share a letter are significantly different.

Table A.29 One-way ANOVA: Film Thickness (μm) Electrospun at V=20 kV; Q=0.4 mL h^{-1} vs 10% PCL (w v^{-1}) for different PBE % (w v^{-1}) Concentrations

Method

Null hypothesis	All means are equal
Alternative hypothesis	Not all means are equal
Significance level	$\alpha = 0.05$

Equal variances were assumed for the analysis.

Factor Information

Factor	Levels	Values
PBE Concentration	4	10 % PCL & 0 % PBE; 10 % PCL & 0.2 % PBE; 10 % PCL & 0.4 % PBE; 10 % PCL & 0.6 % PBE

Analysis of Variance

Source	DF	Adj SS	Adj MS	F-Value	P-Value
PBE Concentration	3	3709	1236.3	2.97	0.044
Error	36	14963	415.6		
Total	39	18672			

Model Summary

S	R-sq	R-sq(adj)	R-sq(pred)
20.3872	19.86%	13.19%	1.07%

Means

PBE Concentration	N	Mean	StDev	95% CI
10 % PCL & 0 % PBE	10	122.10	14.40	(109.02; 135.18)
10 % PCL & 0.2% PBE	10	103.70	29.07	(90.62; 116.78)
10 % PCL & 0.4 % PBE	10	108.80	15.05	(95.72; 121.88)
10 % PCL & 0.6 % PBE	10	95.60	19.59	(82.52; 108.68)

Pooled StDev = 20.3872

Tukey Pairwise Comparisons
Grouping Information Using the Tukey Method and 95% Confidence

PBE Concentration	N	Mean	Grouping	
10 % PCL & 0 % PBE	10	122.10	A	
10 % PCL & 0.4 % PBE	10	108.80	A	B
10 % PCL & 0.2 % PBE	10	103.70	A	B
10 % PCL & 0.6 % PBE	10	95.60		B

Means that do not share a letter are significantly different.

Table A.30 One-way ANOVA: Film Thickness (μm) Electrospun at V=25 kV; Q=0.4 mL h^{-1} vs 10 % PCL (w v^{-1}) for different PBE % (w v^{-1}) Concentrations

Method

Null hypothesis	All means are equal
Alternative hypothesis	Not all means are equal
Significance level	$\alpha = 0.05$

Equal variances were assumed for the analysis.

Factor Information

Factor	Levels	Values
PBE Concentration	4	10 % PCL & 0 % PBE; 10 % PCL & 0.2 % PBE; 10 % PCL & 0.4 % PBE; 10 % PCL & 0.6 % PBE

Analysis of Variance

Source	DF	Adj SS	Adj MS	F-Value	P-Value
PBE Concentration	3	11105	3701.8	4.33	0.010
Error	36	30769	854.7		
Total	39	41874			

Model Summary

S	R-sq	R-sq(adj)	R-sq(pred)
29.2350	26.52%	20.40%	9.29%

Means

PBE Concentration	N	Mean	StDev	95% CI
10 % PCL & 0 % PBE	10	151.30	23.71	(132.55; 170.05)
10 % PCL & 0.2% PBE	10	117.50	5.68	(98.75; 136.25)
10 % PCL & 0.4 % PBE	10	114.40	21.61	(95.65; 133.15)
10 % PCL & 0.6 % PBE	10	146.8	48.5	(128.1; 165.5)

Pooled StDev = 29.2350

Tukey Pairwise Comparisons
Grouping Information Using the Tukey Method and 95% Confidence

PBE Concentration	N	Mean	Grouping	
10 % PCL & 0 % PBE	10	151.30	A	
10 % PCL & 0.6 % PBE	10	146.8	A	B
10 % PCL & 0.2 % PBE	10	117.50	A	B
10 % PCL & 0.4 % PBE	10	114.40		B

Means that do not share a letter are significantly different.

Table A.31 One-way ANOVA and Tukey's comparisons test for Tensile Strength (MPa) values of 10 % PCL (w v^{-1}) solution prepared by different PBE concentrations % (w v^{-1}) Electrospun at V=20 kV; Q=0.4 mL h^{-1}

Method

Null hypothesis	All means are equal
Alternative hypothesis	Not all means are equal
Significance level	$\alpha = 0.05$

Equal variances were assumed for the analysis.

Factor Information

Factor	Levels	Values
PBE Concentration	3	10 % PCL & 0 % PBE; 10 % PCL & 0.4 % PBE; 10 % PCL & 0.6 % PBE

Analysis of Variance

Source	DF	Adj SS	Adj MS	F-Value	P-Value
PBE Concentration	2	23.76	11.879	4.34	0.026
Error	21	57.48	2.737		
Total	23	81.24			

Model Summary

S	R-sq	R-sq(adj)	R-sq(pred)
1.65438	29.25%	22.51%	7.59%

Means

PBE Concentration	N	Mean	StDev	95% CI
10 % PCL & 0 % PBE	8	4.90	2.67	(3.69; 6.12)
10 % PCL & 0.4 % PBE	8	3.80	0.99	(2.59; 5.02)
10 % PCL & 0.6 % PBE	8	2.47	0.34	(1.25; 3.68)

Pooled StDev = 1.65438

Tukey Pairwise Comparisons
Grouping Information Using the Tukey Method and 95% Confidence

PBE Concentration	N	Mean	Grouping	
10 % PCL & 0 % PBE	8	4.90	A	
10 % PCL & 0.4 % PBE	8	3.80	A	B
10 % PCL & 0.6 % PBE	8	2.47		B

Means that do not share a letter are significantly different.

Table A.32 One-way ANOVA and Tukey's comparisons test for Elongation at Break (%) values of 10 % PCL (w v^{-1}) solution prepared by different PBE concentrations % (w v^{-1}) Electrospun at V=20 kV; Q=0.4 mL h^{-1}

Method

Null hypothesis	All means are equal
Alternative hypothesis	Not all means are equal
Significance level	$\alpha = 0.05$

Equal variances were assumed for the analysis.

Factor Information

Factor	Levels	Values
PBE Concentration	3	10 % PCL & 0 % PBE; 10 % PCL & 0.4 % PBE; 10 % PCL & 0.6 % PBE

Analysis of Variance

Source	DF	Adj SS	Adj MS	F-Value	P-Value
PBE Concentration	2	4288	2144.2	6.59	0.006
Error	21	6837	325.6		
Total	23	11126			

Model Summary

S	R-sq	R-sq(adj)	R-sq(pred)
18.0439	38.55%	32.69%	19.73%

Means

PBE Concentration	N	Mean	StDev	95% CI
10 % PCL & 0 % PBE	8	55.46	11.29	(42.19; 68.73)
10 % PCL & 0.4 % PBE	8	82.26	21.79	(69.00; 95.53)
10 % PCL & 0.6 % PBE	8	85.15	19.36	(71.88; 98.41)

Pooled StDev = 18.0439

Tukey Pairwise Comparisons
Grouping Information Using the Tukey Method and 95% Confidence

PBE Concentration	N	Mean	Grouping	
10 % PCL & 0.6 % PBE	8	85.15	A	
10 % PCL & 0.4 % PBE	8	82.26	A	
10 % PCL & 0 % PBE	8	55.46		B

Means that do not share a letter are significantly different.

Table A.33 One-way ANOVA and Tukey's comparisons test for Young's Modulus values of 10 % PCL (w v^{-1}) solution prepared by different PBE concentrations % (w v^{-1}) Electrospun at V=20 kV; Q=0.4 mL h^{-1}

Method

Null hypothesis	All means are equal
Alternative hypothesis	Not all means are equal
Significance level	α = 0.05

Equal variances were assumed for the analysis.

Factor Information

Factor	Levels	Values
PBE Concentration	3	10 % PCL & 0 % PBE; 10 % PCL & 0.4 % PBE; 10 % PCL & 0.6 % PBE

Analysis of Variance

Source	DF	Adj SS	Adj MS	F-Value	P-Value
PBE Concentration	2	0.005589	0.002794	3.22	0.060
Error	21	0.018229	0.000868		
Total	23	0.023818			

Model Summary

S	R-sq	R-sq(adj)	R-sq(pred)
0.0294630	23.46%	16.17%	0.03%

Means

PBE Concentration	N	Mean	StDev	95% CI
10 % PCL & 0 % PBE	8	0.11	0.05	(0.09; 0.14)
10 % PCL & 0.4 % PBE	8	0.09	0.01	(0.07; 0.11)
10 % PCL & 0.6 % PBE	8	0.08	0.01	(0.06; 0.10)

Pooled StDev = 0.0294630

Tukey Pairwise Comparisons
Grouping Information Using the Tukey Method and 95% Confidence

PBE Concentration	N	Mean	Grouping
10 % PCL & 0 % PBE	8	0.11	A
10 % PCL & 0.4 % PBE	8	0.09	A
10 % PCL & 0.6 % PBE	8	0.08	A

Means that do not share a letter are significantly different.

APPENDIX B. CALIBRATION CURVES

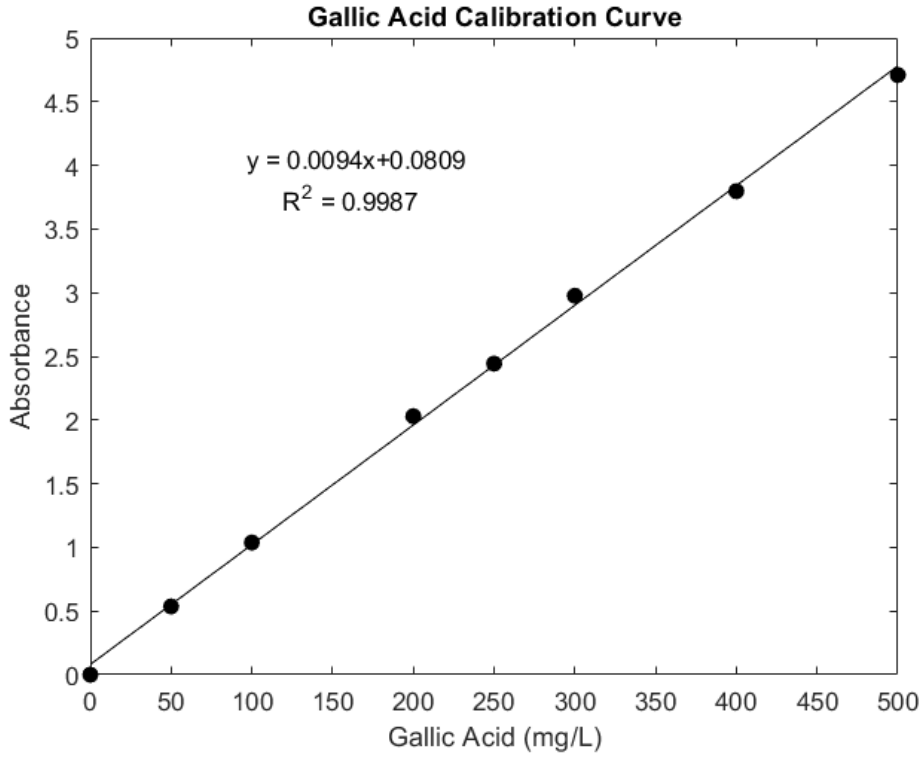

Figure B.1 Gallic Acid Calibration Curve

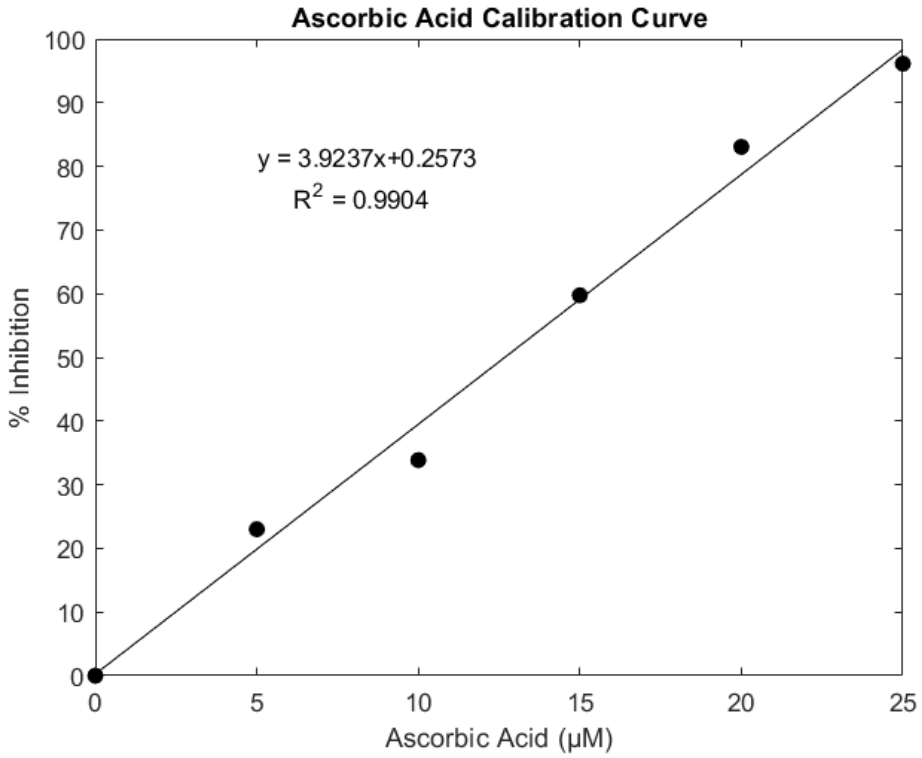

Figure B.2 Ascorbic Acid Calibration Curve

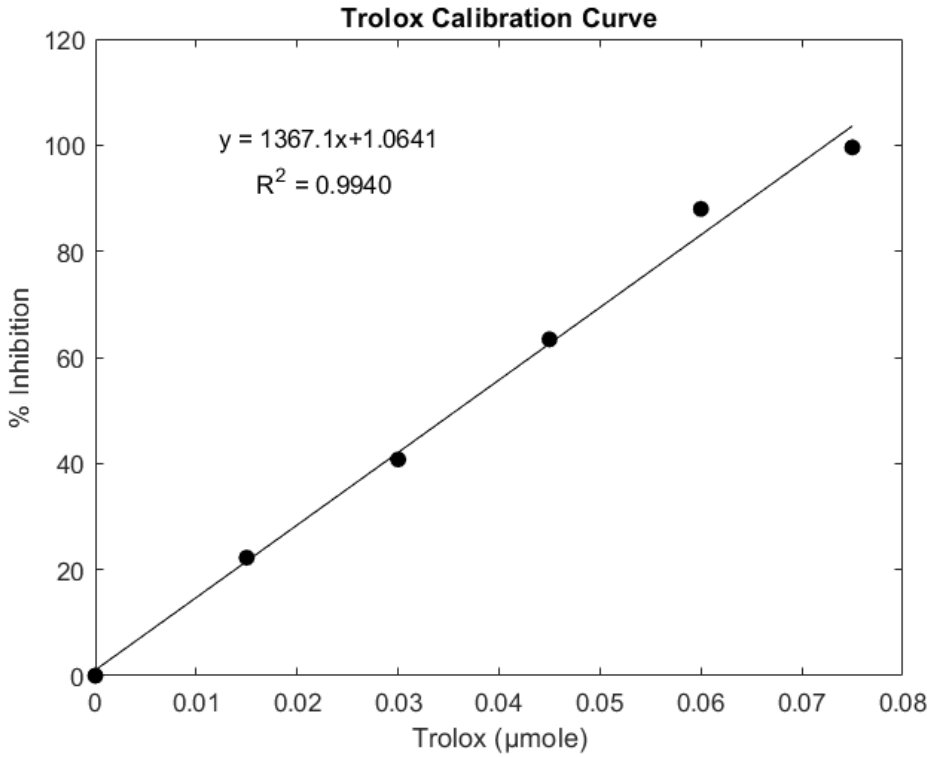

Figure B.3 Trolox Calibration Curve

APPENDIX C. COLOR CHANGE (ΔE) CALCULATIONS

Table C.1 Color change (ΔE) values at pH 2-10 for 10% PCL (w v^{-1}) films containing 0% (w v^{-1}) PBE (V=25 kV; Q=0.5 mL h^{-1})

pH	2	3	4	5	6	7	8	9	10
1	0.27±0.03	0.99±0.59	0.66±0.29	1.10±0.61	0.94±0.31	0.43±0.14	0.59±0.14	0.35±0.04	1.14±1.32
2		0.84±0.54	0.56±0.39	1.18±0.79	0.84±0.18	0.35±0.08	0.50±0.01	0.49±0.06	1.22±1.46
3			0.70±0.38	1.60±1.91	0.33±0.01	0.68±0.39	0.48±0.35	1.28±0.49	1.92±2.18
4				1.10±1.26	0.43±0.41	0.39±0.24	0.32±0.08	0.97±0.38	1.61±1.28
5					1.40±1.83	1.21±1.17	1.21±1.44	1.20±0.23	0.59±0.12
6						0.57±0.21	0.37±0.20	1.25±0.21	1.90±1.87
7							0.24±0.03	0.69±0.01	1.39±1.60
8								0.88±0.02	1.54±1.69
9									1.20±0.91

Table C.2 Color change (ΔE) values at pH 2-10 for 10 %PCL (w v^{-1}) films containing 0.2% (w v^{-1}) PBE (V=20 kV; Q=0.5 mL h^{-1})

pH	2	3	4	5	6	7	8	9	10
1	0.90±0.08	2.67±0.32	4.71±0.74	9.06±1.23	11.67±2.12	12.03±1.27	13.48±1.59	14.27±1.45	15.20±2.13
2		1.80±0.37	3.84±0.70	8.24±1.30	10.85±2.19	11.16±1.34	12.63±1.67	13.43±1.51	14.36±2.19
3			2.12±1.01	6.60±1.12	9.23±2.00	9.46±0.93	10.92±1.30	11.76±1.21	12.68±1.86
4				4.51±2.13	7.14±3.05	7.40±1.94	8.90±2.41	9.66±2.25	10.63±2.96
5					2.70±0.87	3.72±0.12	5.16±0.89	5.36±0.16	6.57±1.18
6						2.75±0.69	3.49±1.06	2.93±0.38	4.28±0.84
7							2.07±1.04	2.93±0.31	3.78±1.10
8								2.20±1.12	2.09±0.42
9									1.66±1.60

Table C.3 Color change (ΔE) values at pH 2-10 for 10% PCL (w v^{-1}) films containing 0.2% (w v^{-1}) PBE (V=25 kV; Q=0.5 mL h^{-1})

pH	2	3	4	5	6	7	8	9	10
1	1.72±1.03	2.61±0.28	4.80±0.39	8.98±1.59	11.11±1.54	12.31±2.16	13.65±1.91	15.99±2.02	16.80±3.06
2		1.36±1.01	3.26±0.85	7.45±0.39	9.57±0.33	10.68±1.01	12.00±0.80	14.35±0.90	15.20±2.02
3			2.39±0.82	6.58±2.04	8.70±1.96	9.76±2.51	11.08±2.20	13.46±2.35	14.37±3.47
4				4.24±1.19	6.37±1.14	7.62±1.70	9.08±1.45	11.37±1.55	12.33±2.61
5					2.15±0.04	3.85±0.63	5.57±0.59	7.46±0.51	8.47±1.46
6						2.56±0.18	4.27±0.35	5.65±0.31	6.74±1.14
7							1.83±0.07	3.88±0.11	5.36±1.44
8								2.76±0.26	4.39±2.18
9									2.20±1.64

Table C.4 Color change (ΔE) values at pH 2-10 for 10% PCL (w v^{-1}) films containing 0.2% (w v^{-1}) PBE (V=20 kV; Q=0.4 mL h^{-1})

pH	2	3	4	5	6	7	8	9	10
1	1.54±0.62	4.60±2.14	5.23±1.69	10.07±4.02	13.35±6.12	15.23±6.52	16.70±7.83	18.09±7.15	18.79±8.46
2		3.17±1.44	3.82±2.49	8.70±4.86	11.98±6.90	13.83±7.31	15.33±8.57	16.76±7.91	17.48±9.32
3			2.90±0.77	5.89±5.83	9.26±7.73	10.95±8.38	12.74±9.26	14.58±8.58	14.67±10.40
4				4.93±2.40	8.24±4.47	10.12±4.96	11.68±6.22	13.11±5.53	13.87±7.09
5					3.52±2.07	5.47±2.81	7.23±3.86	8.55±3.01	9.16±4.87
6						2.21±0.55	3.83±1.74	5.10±0.90	5.90±2.98
7							2.18±0.48	3.52±0.17	4.43±2.80
8								1.91±0.03	3.67±1.78
9									2.77±0.58

Table C.5 Color change (ΔE) values at pH 2-10 for 10% PCL (w v^{-1}) films containing 0.2% (w v^{-1}) PBE (V=25 kV; Q=0.4 mL h^{-1})

pH	2	3	4	5	6	7	8	9	10
1	1.25±0.14	2.12±0.39	4.29±0.89	8.36±0.24	10.82±0.81	12.03±0.92	13.36±1.10	15.44±1.19	16.21±1.53
2		1.10±0.03	3.48±0.13	7.66±0.65	10.14±1.72	11.27±1.60	12.56±1.71	14.69±1.92	15.50±2.26
3			2.48±0.11	6.70±0.71	9.18±1.79	10.21±1.67	11.49±1.78	13.65±1.99	14.49±2.35
4				4.25±0.80	6.74±1.87	7.94±1.61	9.26±1.78	11.32±2.01	12.21±2.29
5					2.51±1.05	4.39±0.54	5.79±0.97	7.39±1.16	8.29±1.31
6						2.95±0.06	4.21±0.53	5.18±0.33	6.00±0.35
7							1.52±0.43	3.53±0.27	4.58±0.70
8								2.57±0.39	3.66±0.88
9									1.55±0.14